

INFORMATION TO USERS

This material was produced from a microfilm copy of the original document. While the most advanced technological means to photograph and reproduce this document have been used, the quality is heavily dependent upon the quality of the original submitted.

The following explanation of techniques is provided to help you understand markings or patterns which may appear on this reproduction.

1. The sign or "target" for pages apparently lacking from the document photographed is "Missing Page(s)". If it was possible to obtain the missing page(s) or section, they are spliced into the film along with adjacent pages. This may have necessitated cutting thru an image and duplicating adjacent pages to insure you complete continuity.
2. When an image on the film is obliterated with a large round black mark, it is an indication that the photographer suspected that the copy may have moved during exposure and thus cause a blurred image. You will find a good image of the page in the adjacent frame.
3. When a map, drawing or chart, etc., was part of the material being photographed the photographer followed a definite method in "sectioning" the material. It is customary to begin photoing at the upper left hand corner of a large sheet and to continue photoing from left to right in equal sections with a small overlap. If necessary, sectioning is continued again — beginning below the first row and continuing on until complete.
4. The majority of users indicate that the textual content is of greatest value, however, a somewhat higher quality reproduction could be made from "photographs" if essential to the understanding of the dissertation. Silver prints of "photographs" may be ordered at additional charge by writing the Order Department, giving the catalog number, title, author and specific pages you wish reproduced.
5. PLEASE NOTE: Some pages may have indistinct print. Filmed as received.

Xerox University Microfilms

300 North Zeeb Road
Ann Arbor, Michigan 48106

74-21,287

KELIHER, Paul Joseph, 1946-

SPIN POLARIZATION TRANSFER REACTIONS: I.
CHEMIONIZATION AND SURFACE ELECTRON EJECTION
BY He(23S). II. A POLARIZED ELECTRON SOURCE.
III. ELECTRON EXCHANGE REACTIONS WITH O₂ AND NO.

Rice University, Ph.D., 1974
Physics, atomic

University Microfilms, A XEROX Company, Ann Arbor, Michigan

RICE UNIVERSITY

SPIN POLARIZATION TRANSFER REACTIONS:

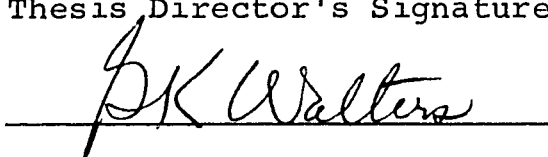
- I. Chemiionization and Surface Electron Ejection by $\text{He}(2^3\text{S})$
- II. A Polarized Electron Source
- III. Electron Exchange Reactions with O_2 and NO

by

Paul Joseph Keliher

A THESIS SUBMITTED
IN PARTIAL FULFILLMENT OF THE
REQUIREMENTS FOR THE DEGREE OF
DOCTOR OF PHILOSOPHY

Thesis Director's Signature:

A handwritten signature in cursive script, appearing to read "P. K. Walters", is written over a horizontal line.

Houston, Texas

May, 1974

To Marcia

ACKNOWLEDGEMENT

I am indebted to many individuals for making this thesis a reality. Dr. G. K. Walters suggested the project to me and over the past four years has allowed me to pursue this research at my own discretion, providing guidance when necessary. Much of the apparatus was designed by Dr. M. V. McCusker. Major Malcolm O'Neill undertook the construction of the apparatus and the initial investigation of the experiment. Since that time, numerous students have contributed to the project especially Bob Gleason who shared the responsibility of the experiment for two years. Dr. F. B. Dunning provided invaluable suggestions at several difficult stages of the investigation, particularly concerning the source of the surface-ejected electron current that was subsequently studied.

Credit is also due to the machinists who build much of the apparatus and in particular Mr. Ed Surles for his interest and skill in creating several vital components. My thanks also go to Mary Comerford who patiently typed and retyped the manuscript on a less than leisurely schedule. I am most grateful however to my wife Marcia who simultaneously encouraged me to complete this work and tolerated my absence for an inordinate period of time.

TABLE OF CONTENTS

	Page
Introduction.....	1
Part I Spin Polarization Transfer Reactions: Chemiionization and Electron Ejection from Surfaces by He(2^3S) Atoms.....	4
Sec. I. Introduction	5
A. Chemiionization	5
B. Electron Ejection from Surfaces	9
Sec. II. Experimental Technique	11
A. Flowing Helium Afterglow	11
B. Electron Extraction	14
C. Mott Scattering	15
Sec. III. Sources of Extracted Electron Current	17
A. Electron Density in the Afterglow	18
1. Electron Removal by RF Heating	18
2. Decay Rates for 2^3S and 2^1S Atoms	19
B. Electron Currents from Surface Ejection by He(2^3S)	22
1. Residual Background Current	22
2. Calculation of Surface Ejection Rate	22
C. Electron Current from Chemiionization	24
1. Ambipolar Diffusion Rate	24
2. Surface Emission by Ions	25
D. Post Extraction Excitation	27
E. Summary	27

	Page
Sec. IV. Optical Pumping	29
A. Properties of the Optical Signal	29
B. Limitations to He 2^3S Polarization	30
Sec. V. Results	33
A. Experimental Conditions	33
B. Correction for the He(2^1S) Density	34
C. Pressure Effects	36
D. Comparison of Two Excitation Sources	38
E. Depolarization Processes	39
1. Polarization Dependence on the He(2^3S) Density	39
2. Polarization Dependence on Reaction Length	40
Sec. VI. Discussion	43
A. Spin Polarization Transfer in Chemi- ionization Reactions	43
1. He(2^3S) with Ar, H ₂ , N ₂ , N ₂ O, CO ₂ , CH ₄ and NH ₃	43
2. He(2^3S) with N ₂ O and CO ₂	48
3. He(2^3S) with CO	49
B. Spin Polarization Transfer in Surface Ejection by He(2^3S) Atoms	51
C. Collisional Depolarization Processes	54
Part II Spin Polarization Transfer Reactions:	
A Polarized Electron Source.....	56
Sec. I. Introduction	57
Sec. II. Experimental Technique	62
A. Overview	62
B. Helium Metastable Sources	62

	Page
C. Optical Pumping	64
D. Extraction of High Currents	66
1. Gas Injection	66
2. Electron Extraction	67
E. Electron Energy Distribution	69
Sec. III. Results	72
A. Efficiency of Electron Extraction	72
B. Energy Spread of the Extracted Beam	74
C. Polarization and Current	76
Sec. IV. Conclusions	79
Part III Spin Polarization Transfer Reactions: Electron Scattering from O ₂ and NO.....	81
Sec. I. Introduction	82
Sec. II. Experimental Technique	86
A. Flowing Gas Reactor	86
B. Calibrations	87
C. Electron Extraction	90
Sec. III. Data Analysis	92
A. Rate Equations for Spin Polarization	93
B. Assumptions and Boundary Conditions	95
Sec. IV. Results	101
Sec. V. Discussion	102
Sec. VI. Conclusion	105
Appendix A. Mass Transport in a Flowing System	106
A. Properties of the Bulk Flow	106
B. Diffusion and Reaction in a Flowing System	109

	Page
Appendix B. Chemiionization Data	115
Appendix C. Measurement of He 2^3S and 2^1S Density by Absorption of $1.08\ \mu$ and $2.06\ \mu$ Resonance Radiation	116
A. Theory: Absorption of a Simple Resonance Line	117
B. Numerical Methods: Absorption by Several Resonance Lines	121
C. Data on Line Widths, Frequency Shifts, and Relative Intensity	124
D. Results	126
Appendix D. Properties of the Optical Signal	131
References	136

INTRODUCTION

The experiments presented in this thesis are the natural extension of several previous investigations in this laboratory concerning the dynamics of atom-atom collision processes, particularly the behavior of the 2^3S metastable state of helium. These studies have exploited the technique of optical pumping to orient the atomic electrons of the 2^3S state thus allowing the exchange of otherwise identical particles to be monitored. Recently Hill et al.¹ demonstrated that spin angular momentum is conserved in the ionizing collision of two He 2^3S atoms. In a separate experiment McCusker et al.²⁻⁴ showed that the above reaction of two metastables as well as electron impact ionization of the metastable state are major ionization processes in helium discharges. This experiment also indicated that an optically pumped helium discharge or its afterglow could be used as an intense source of polarized electron.

The present experiment was designed to extend the capabilities of the previous work by use of a flowing gas reactor, commonly called a flowing afterglow, in which reactions of the 2^3S state with foreign gas atoms and molecules could be isolated from the already complex processes of an active helium discharge. In this way the conservation of spin angular momentum in a broad class of

ionizing reactions with the helium 2^3S state (generally referred to as chemiionization) could be studied and exploited for the development of a practical polarized electron source. During the course of this work it was realized that the flowing afterglow was well suited for measuring the rate of electron spin reversal in the scattering of thermal electrons with various atoms and molecules. As a result this thesis is divided into three parts, each concerning a different aspect of the transfer of spin orientation or polarization:

- I) Chemiionization and electron ejection from surfaces by $He(2^3S)$ atoms
- II) A polarized electron source
- III) Electron scattering from O_2 and NO .

Although the dynamics of the optical pumping process itself was not a major object of study in the present experiment, substantial progress was made toward understanding the effects of the spatial variation of the pumping light passing through the sample of $2S$ atoms that were first observed by Scheerer⁹. These effects are described in Section IV of Part I and explain the difficulties in previous attempts in this laboratory⁷ to measure the rate of collisional mixing of the 2^3P sublevels in He ⁴. We are hopeful that future studies of optical pumping in the near ideal environment of the late afterglow will produce a significant increase in the maximum spin polarization attainable.

The construction and initial operation of the flowing afterglow was done by Malcolm O'Neill who has described the apparatus in great detail in his Master's Thesis. The basic diagnostic technique used throughout this experiment is the spin analysis of electrons extracted from the afterglow. The parallel work by Schearer^{5,6} using optical analysis of spin polarization transfer has further extended the capabilities of the optically pumped, flowing afterglow as a general experimental method for studying reaction dynamics.

SPIN POLARIZATION TRANSFER REACTIONS

PART I:

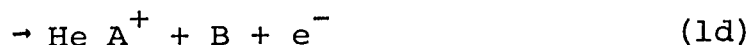
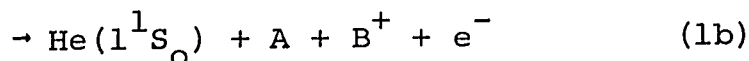
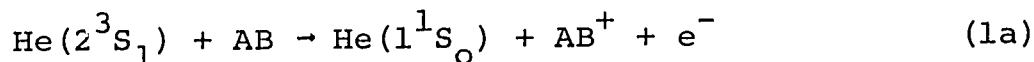
Chemionization and Electron Ejection
from Surfaces by $\text{He}(2^3\text{S})$ Atoms

I. INTRODUCTION

Two reaction mechanisms of the metastable 2^3S_1 state of helium are the chemiionization of other atoms and molecules and the ejection of electrons from surfaces. The present experiment probes the dynamics of these two processes by measuring the degree to which electron spin orientation is transferred from the 2^3S_1 atoms to the free electrons in the final state. We find that spin angular momentum is generally well conserved in a wide variety of reactions studied, indicating that the product electrons do not participate in any long lived intermediate complexes.

A. Chemiionization

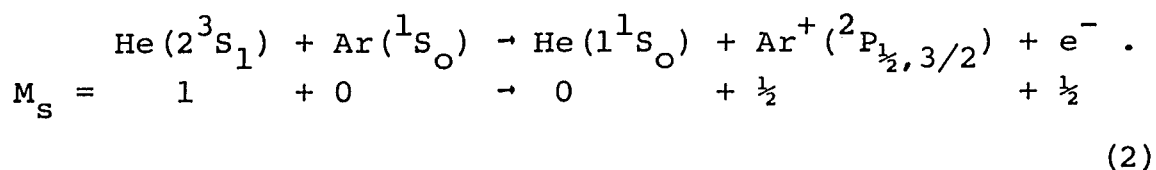
The chemiionization channels available to a molecule (AB) reacting with a helium 2^3S_1 atom are



with only (1a) and (1c) being open for chemiionization of an atom. These reactions are usually referred to as Penning ionization (1a), dissociative ionization (1b), associative ionization (1c), and rearrangement ionization (1d). A number of theoretical approaches to chemiionization reactions have been proposed¹⁰⁻¹³, based respectively on models of orbiting collisions, excitation transfer, and autoionization. The last has proven to be the

most successful for calculating the cross section and electron energy distribution of the $(\text{He}2^3\text{S}_1 + \text{H})$ system¹⁴⁻¹⁶. A special case of the autoionization model is the Auger de-excitation of the 2^3S state suggested by Hotop and Niehaus¹⁷. In this case an electron from AB tunnels to the unfilled $1s$ orbital of He, simultaneously ejecting the $2s$ electron into the continuum.

For the reaction models listed above, except the last, the possibility exists that some reactions proceed via relatively long lived intermediate states prior to the escape of the free electron. This might be indicated by the failure of the z -component of the total electron spin, M_s , to be conserved due to spin-orbit or spin-rotational coupling¹⁸. Consider the possible product spin states, for example, in the Penning ionization of argon by 2^3S_1 atoms that have been oriented in the $m_s = +1$ state,



Any deviation of the initial spin state of the production or electron from $m_s = +\frac{1}{2}$ signifies that spin angular momentum is not conserved in the reaction.

Since the $\text{He } 2^3\text{S}_1$ atoms are not, in practice, all in the $m_s = +1$ state, their spin polarization, P_3 , is defined for purposes of this work by

$$P_3 = \frac{N_+ - N_-}{N_+ + N_0 + N_-} \quad (3)$$

where N_+ , N_0 , and N_- are the populations of the $m_s = +1, 0$, and -1 states. Likewise the polarization of electrons, P_e , is given by

$$P_e = \frac{n_+ - n_-}{n_+ + n_-} \quad (4)$$

where n_+ and n_- are the populations of the $m_s = \pm 1$ states respectively. It can be seen from Eq. (2) that $P_e = P_3$ whenever M_s is completely conserved. More complex reactions that produce ions or neutrals in a spin state other than $S = \frac{1}{2}$ provide an interesting test of the Auger de-excitation model as discussed in Section VI.

In the Penning reaction of $\text{He}(2^3S_1) + \text{He}(2^3S_1)$ conservation of spin angular momentum has been demonstrated qualitatively by several workers, notably Schearer¹⁹ and McCusker² while Hill et al.¹ showed quantitatively that it is fully conserved. Schearer has also demonstrated conservation of both the direction and phase of electron spin in chemiionization reactions of oriented $\text{He}(2^3S)$ atoms with Group II metals^{5,6} by monitoring the polarization of the light emitted by the product ions which are produced in excited states. This method is limited, however, to excited product ions with lifetimes longer than spin-orbit or spin-rotational coupling times which are generally unknown^{20,21}. The N_2 molecule is an example of a system

for which these conditions do not apply²². The polarization of light emitted by the $N_2^+(B^2\Sigma_u)$ state is less than 2% of that measured for the cadmium ions, whereas the results of the present experiment show that spin orientation is completely conserved in the chemiionization of N_2 . Therefore it is difficult to quantitatively assess the conservation of spin orientation by monitoring the light emitted by ions.

The present experiment avoids this uncertainty by measuring the spin polarization of the ejected electrons directly. In a flowing helium afterglow²³⁻²⁵, four essential processes are spatially separated as shown in Fig. 1: 1) production of $He(2^3S_1)$ atoms, 2) optical pumping to the $m_s = +1$ state, 3) injection and chemiionization of a gas (AB), and 4) extraction of electrons to be spin analyzed by Mott scattering. These techniques are described in Section II. In Section III, the various sources of extracted electrons are discussed in detail. Methods of estimating the polarization of the 2^3S state are described in Section IV. The electron polarizations from the chemiionization of Ar, H_2 , N_2O , CO, CO_2 , NH_3 and CH_4 are presented in Section V. The results indicate that spin angular momentum is completely conserved for all of these gases with the possible exception of CO.

B. Electron Ejection from Surfaces

It is shown in Section III that in the absence of a reactant gas (AB) the extracted electron current in these experiments is due to electron ejection by the 2^3S atoms from the surface of the extraction aperture. Although surface ejection is widely used as a detector for metastable particles¹⁰, the yield of electrons per incident particle, γ , and the electron energy distribution, $N(E)$, depend strongly on the condition of the surface and are not well understood for the heavily contaminated surfaces that are often used.

For atomically clean metals, $He(2^3S_1)$ metastables are thought to be resonantly ionized on their approach to the surface so that the resulting γ and $N(E)$ are identical to those for He^+ ions as proposed by Hagstrum²⁶ and Varnerin²⁷ and confirmed by MacLennan²⁸ and Dunning²⁹. The $He\ 2^3S$ atoms and He^+ ions also behave alike for metals covered with an adsorbed monolayer of gas atoms. For both species the yields are reduced and $N(E)$ is shifted to lower energies³⁰⁻³³ when compared to the results for a clean surface. Several plausible mechanisms have been proposed to account for these results³²⁻³⁴.

However, for surfaces that have only been treated with chemical solvents (and therefore heavily contaminated with ill defined species) the γ for 2^3S_1 atoms increases

to values between .6 and 1.0^{29,38,39}. Allison et al.⁴⁰ measured the electron energy distribution for several surface conditions. They suggested that the high yields were due to a two step process of chemiionization of the adsorbed species followed by electron ejection from the substrate by ions produced in the chemiionization reaction. Electrons produced in the first reaction are expected to be polarized if the incident 2^3S atoms are also polarized. Donnally et al.⁴¹ have observed substantial spin polarization of the electrons from contaminated surfaces using a polarized $\text{He}(2^3\text{S})$ atomic beam. We report here in Section V the results from a similar experiment that are in general, but not complete, agreement with those of Donnally et al.

II. EXPERIMENTAL TECHNIQUE

A. Flowing Helium Afterglow

A schematic diagram of the entire experiment is shown in Fig. 1. It consists of a flowing helium afterglow with a provision for extracting electrons and measuring their spin polarization by Mott scattering. The helium gas flows through a 10 cm diameter pyrex tube at typical rates of 38 torr liters/sec and pressures of .125 torr being exhausted by a 500 liter/sec Roots pump. The velocity distribution across the tube is nearly parabolic (as expected for viscous flow) with an average, or bulk flow, velocity of about 4.2×10^3 cm/sec. Pressure and flow rate calibrations are discussed in Part III. The hydrodynamic properties of the flowing gas, especially the effects of a parabolic velocity profile on diffusion and reaction rates, are treated in Appendix A.

Extracted electron currents, for some reactant gases, were found to be sensitive to impurities in the helium stream on the order of 50 to 100 p.p.m. These effects are not observed for helium of 1 and 10 p.p.m. purity used in the present experiments. At low pressures (~ 0.1 torr) some backstreaming of oil from the Roots pump is observed and minimized by the use of low vapor pressure pump oil (10^{-5} torr). Outgassing of the walls was determined not to be significant in this flowing system, which was

Figure 1: Schematic diagram of the experiment
(not to scale).

Figure 2: Detail of gas injector and electron
extractor. The drawing is to scale
except the gas injector ring has been
drawn twice actual size. The ring is
perforated with .010" holes, 12 on the
inside diameter and 28 on the outside
diameter.

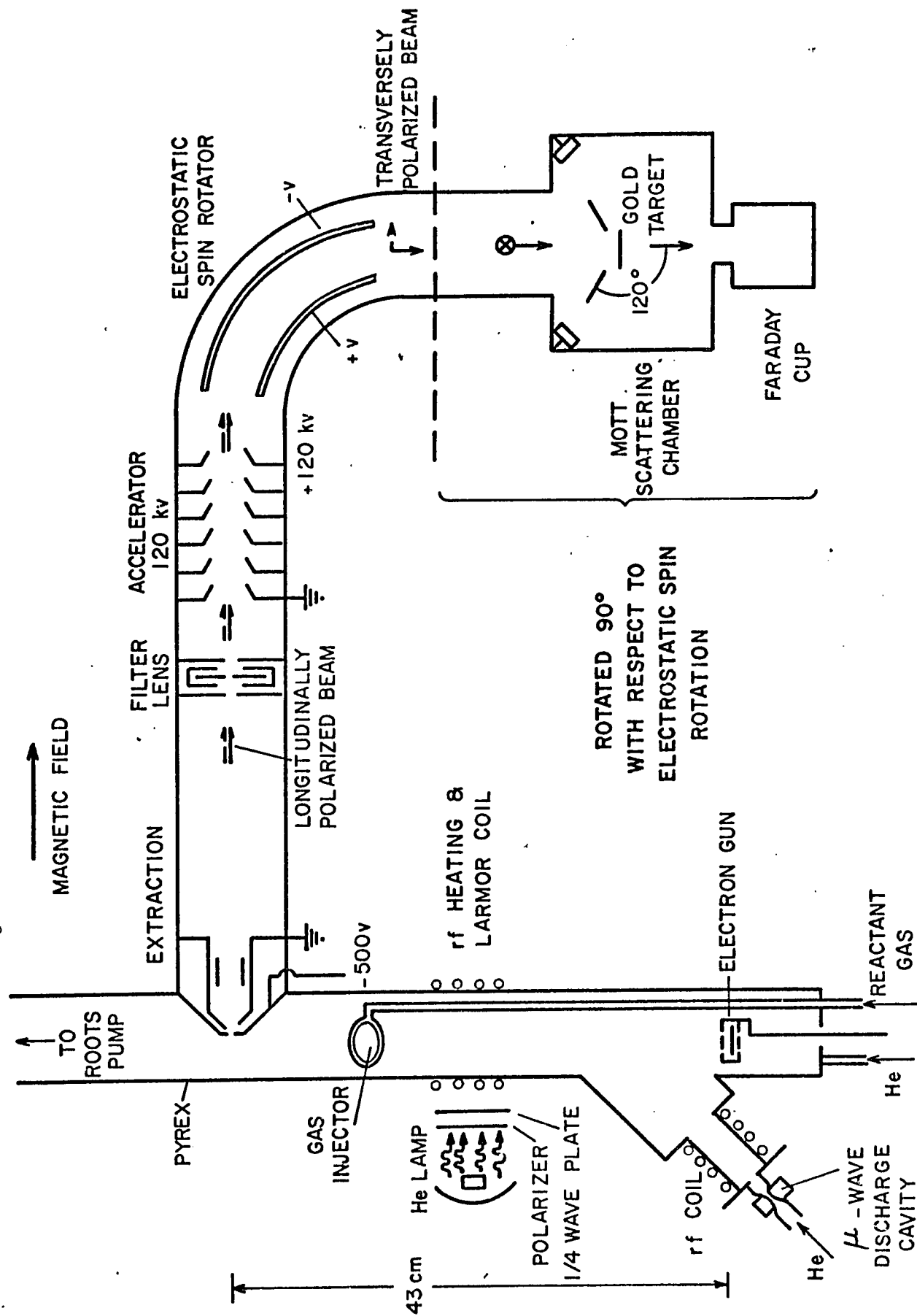


FIGURE 1

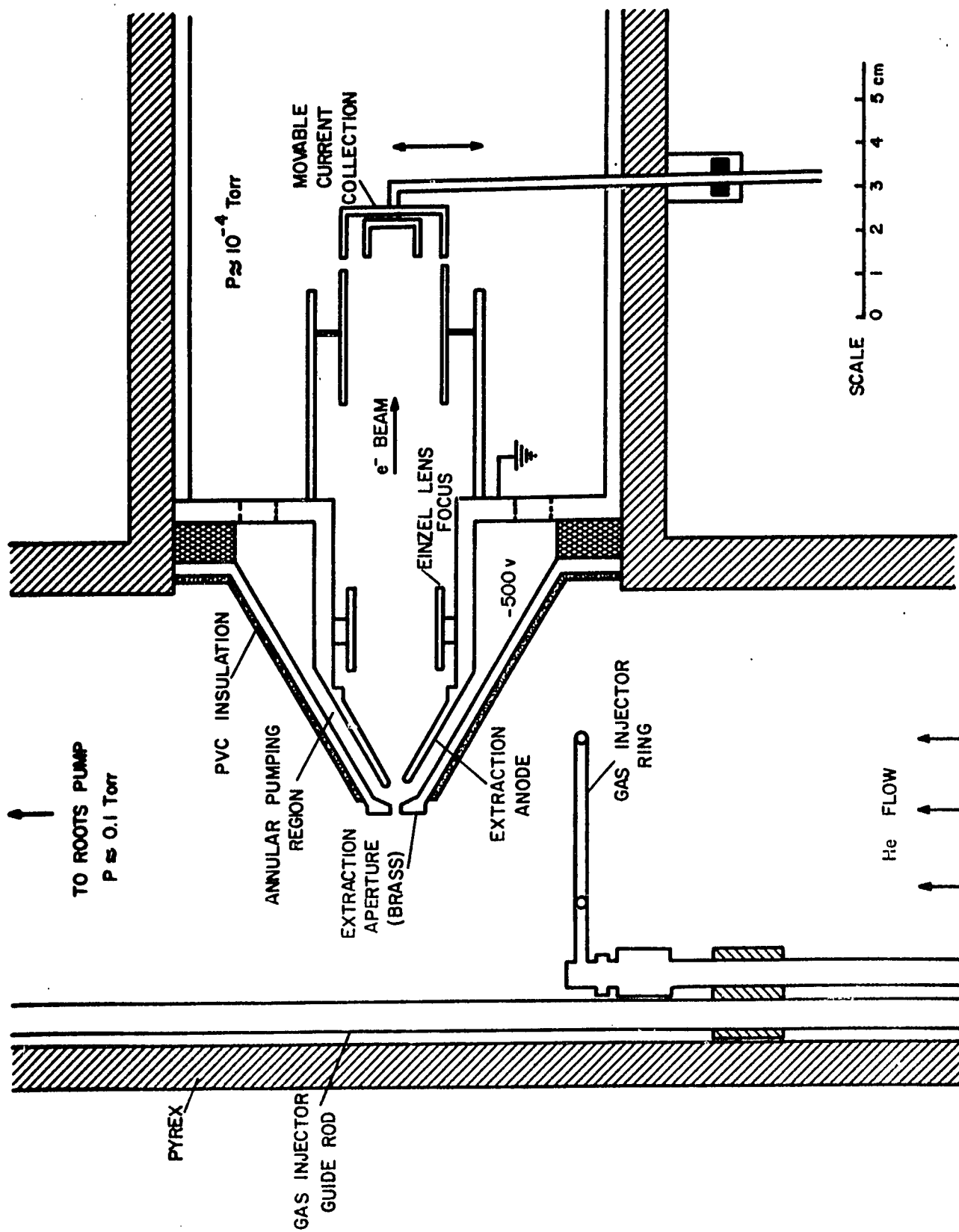


Figure 2

therefore not baked but was pumped to 10^{-6} torr when not in use.

A microwave cavity discharge⁴² and a movable electron gun were used as sources for metastable excitation. Helium gas enters the flow tube through either end of the "Y" shown in Fig. 1 depending on which source is to be used. The microwave discharge is lit in a glass nozzle that passes through the cavity. Both converging-diverging (de Laval) nozzles and simple horn shaped nozzles were used. The metastable densities obtained depend mainly on the position of the cavity along the nozzle and not on the particular shape. The 2^3S density at 30 cm from cavity increases from .2 to $6 \times 10^9 \text{ cm}^{-3}$ with a $1/e$ decay length of 4 to 9.5 cm for pressures of .08 to .15 torr. The electron gun source consisted of a filament between two high transparency ($\sim 97\%$) grids spaced 1 cm apart. The gun was normally operated at 75 V accelerating potential and .12 A of emission current.

Both $\text{He}(2^3S_1)$ and (2^1S_0) metastables are detected in the afterglow. For pressures between .08 and .15 torr, the 2^1S to 2^3S ratio decreases from .07 to .02 for the microwave source and from 0.5 to .2 for the electron gun source when operated at the conditions mentioned above.⁵³ As discussed in the next section, the electron density in the afterglow is so low that the 2^1S_0 metastables are not converted to the 2^3S_1 state by electron exchange as is

common in higher pressure afterglows. Therefore the 2^1S_0 atoms do contribute to any electron production process present in the afterglow and these electrons are necessarily unpolarized. The microwave cavity was used for most of the work reported here because of its lower ratio of 2^1S to 2^3S atoms. The cavity is placed off axis in an attempt to remove $1.08\mu(2^3S-2^3P)$ and $584\text{\AA}(1^1S-2^1P)$ photons from the optical pumping and electron extraction regions⁴³ though the latter may contribute a very small residual background current to be discussed later.

The $\text{He}(2^3S_1)$ atoms are optically pumped to the $m_s = +1$ (or -1) state in the usual manner⁹ by right (or left) circularly polarized 1.08μ resonance radiation from an intense helium discharge lamp. Narrow band interference filters and a PbS photodetector are used to measure the absorption of $1.08\mu(2^3S-2^3P)$ and $2.05\mu(2^1S-2^1P)$ radiation from which the density of the 2^3S and 2^1S atoms can be determined (see Appendix C). Helmholtz coils, six feet in diameter, provide a uniform magnetic field of 5 gauss over the entire flowing afterglow region, thus defining a quantization axis parallel to the pumping light.

In the absence of any reactant gas, the extracted electron current is due to electron ejection from the surface of the extraction aperture by the helium metastables (see Section III). Chemiionization reactions can be studied by injecting a reactant gas into the helium

flow stream through a movable perforated ring. The reaction length is defined by the distance from the gas injector to the extraction aperture and is typically 4 to 15 cm. The positions of the other regions along the flow tube, as measured from extraction aperture, are a) the microwave cavity at 50 cm, b) the electron gun between 40 and 60 cm, and c) the optical pumping lamp extends from 20 to 30 cm.

B. Electron Extraction

Electrons are extracted through a small aperture at the end of a truncated cone, protruding to the center of the flow as shown in Fig. 2. The aperture was machined in a replaceable brass insert so that several geometries could be tested ranging from a canal 1.5 mm diameter by 1.5 mm long to an orifice 2 mm diameter by .2 mm long. The aperture size and the flow tube pressure are limited by the pumping speed available to evacuate the beam tube.

The electron beam energy of 500 eV is achieved by biasing the entire flow tube and extraction aperture negative with respect to the extraction anode. An Einzel lens focuses the beam onto the entrance aperture of a filter lens^{44,45} used for measuring the electron energy distribution. For polarization measurements the filter lens was operated as a simple Einzel lens with a center

aperture 1" in diameter. Measurements of the energy distribution of the beam are discussed in Part II. Beam current is monitored by inserting a movable collector into the beam near the extractor. Mu-metal shields are used to reduce the earth's field near the extractor and also to reduce the 1.5 gauss fringe field produced at the spin rotator by the Helmholtz coils.

C. Mott Scattering

The technique of Mott scattering⁴⁶ used in this experiment has been described by McCusker^{2,4}. The electron beam, which is extracted with longitudinal spin polarization, is first accelerated to 120 keV. The velocity vector is then rotated 90° with respect to the spin vector to obtain a transversely polarized beam⁴⁷. The spin polarization, P_e , is determined from the small azimuthal asymmetry produced by spin-orbit coupling in the elastic scattering of the electrons from a thin gold foil at a scattering angle, θ , of 120°. If N_L and N_R are the number of counts in the left and right detectors, then P_e is given by

$$P_e = \frac{1}{S(\theta)} \frac{X-1}{X+1} ; \quad X = \frac{N_L}{N_R} \quad (5)$$

where $S(\theta)$ is the asymmetry function. $S(\theta)$ has been calculated^{48,49} and measured^{50,51} for 120 keV electrons on gold. Multiple scattering within the gold foil reduces the observed value of $S(\theta)$ from .378 for zero thickness

to .26 for the $193 \pm 5 \mu\text{g}/\text{cm}^2$ foils used here⁵².

All systematic instrumental asymmetries are removed from these measurements by reversing the sense of circularly polarized 1.08 μ optical pumping radiation, thus reversing the direction of electron polarization in the beam. If N , N' are the counts measured for opposite polarizations, then the true P_e is given by Eq. (5) where X is redefined⁴ as $X = (N_L N'_R / N_R N'_L)^{1/2}$. The reported error is the standard deviation of eight separate polarization measurements. The major source of this random error is fluctuation of the electron beam position, thus changing the effective solid angles of the 2 detectors.

III. SOURCES OF EXTRACTED ELECTRON CURRENT

Flowing afterglows have been widely used to isolate reactions of metastable species since all other excited states decay in the first few centimeters from the excitation source, leaving only thermal electrons, ions, metastables and ground state atoms. Molecular ions and metastables which are formed primarily by the three-body reactions $(\text{He}^+ + 2\text{He} \rightarrow \text{He}_2^+ + \text{He})^{54}$ and $(\text{He}^* + 2\text{He} \rightarrow \text{He}_2^* + \text{He})^{55}$ are not significant at the low pressures used in this experiment. In this section, four experimental conditions are established that form the basis for the interpretation of our electron spin polarization measurements:

- 1) The density of source-produced electrons at the extractor is negligible.
- 2) In the absence of reactant gases, the current, I_s , extracted from the afterglow tube is due to electron ejection from the surface of the extraction aperture by 2^3S and 2^1S metastables.
- 3) When reactant gases are injected in quantities sufficient to de-excite all metastables, the extracted current, I_c , consists of electrons produced in the chemiionization reactions.
- 4) All other sources of extracted current can be neglected.

A. Electron Density in the Afterglow

In the afterglow, the rate of electron loss is proportional to the ambipolar diffusion coefficient, D_a , which is related to the free-ion diffusion coefficient, D_+ , by the relation $D_a = D_+(1 + T_e/T_+)$, where T_e and T_+ are the electron and ion "temperatures." For $T_e = T_+ = 300^\circ \text{ K}$, the value of D_a for He^+ ions in He measured by Oskam and Mittelstadt⁵⁶ is nearly equal to the diffusion coefficient for triplet metastables measured by Phelps⁵⁵. However the electron temperatures in the first few centimeters from the source are considerably above 300° K . Therefore it is not unreasonable that, at the low pressures where the diffusion time is of the same order or less than the thermalization time⁵⁷, the ratio of electrons to metastables will be small at positions of 30 to 50 cm from the source.

1. Electron Removal by RF Heating

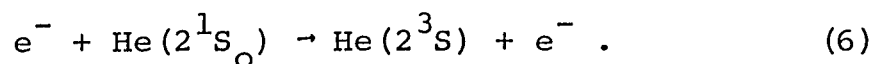
In order to demonstrate that source-produced electrons do not contribute significantly to the extracted current, the electrons in the afterglow can be heated externally by rf power applied to either of two coils shown in Fig. 1. When no reactant gas is injected, the current, I_s , is unchanged by rf heating for pressures between 0.08 and 0.15 torr⁵⁸. At .15 torr, I_s decreases by less than 10%. On the other hand, the current from

chemiionization can be reduced by 2 orders of magnitude when rf power ~~is~~ applied at the gas injection region. (This assumes the gas is injected close enough to the extractor so that the majority of these electrons are not already lost by ambipolar diffusion with their parent ions which is roughly twice as fast as for He^+ ions.)

These results are independent of the type of excitation source used. Also similar results are obtained by collecting electrons and ions with a set of biased grid wires placed across the flow tube. The above facts show that the electron removal processes are effective and that electrons from the body of the afterglow do not contribute to the current I_s over a limited pressure range.

2. Decay Rates for 2^3S and 2^1S Metastables

An independent measurement of the density of source-produced electrons can be determined from the measured decay of the 2^3S and 2^1S densities vs position in the afterglow tube as shown in Figs. 3 and 4. These curves are obtained by monitoring the $1.08\ \mu$ and $2.05\ \mu$ light absorption at a fixed point while moving the electron gun source away from the extractor. If the density of electrons was large, the 2^1S state would be rapidly converted to the 2^3S state by the exchange reaction



Absence of any conversion is evident in Figs. 3 and 4 in

Figures 3 and 4: The average $\text{He}(2^3\text{S})$ and (2^1S) density and the extracted current vs distance, z , from the electron gun source. I_s is the current from surface ejection by $\text{He}(2^{1,3}\text{S})$. I_c is the current of Penning electrons from Argon injected at 4 cm upstream of the extractor at a rate of 1.5 torr liters/sec. Extraction aperture is 1.5 mm diam. by 1.5 mm long.

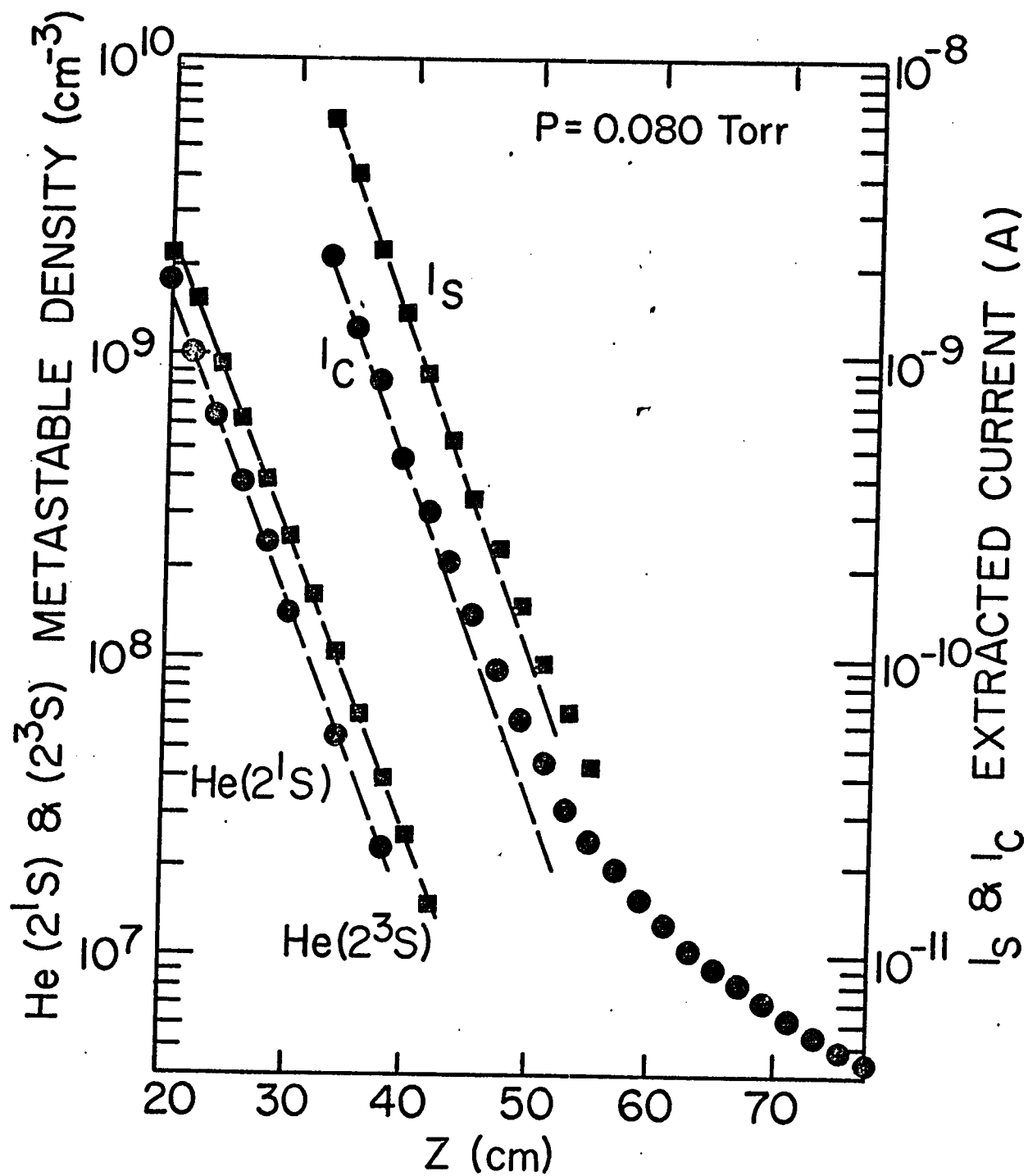


Figure 3

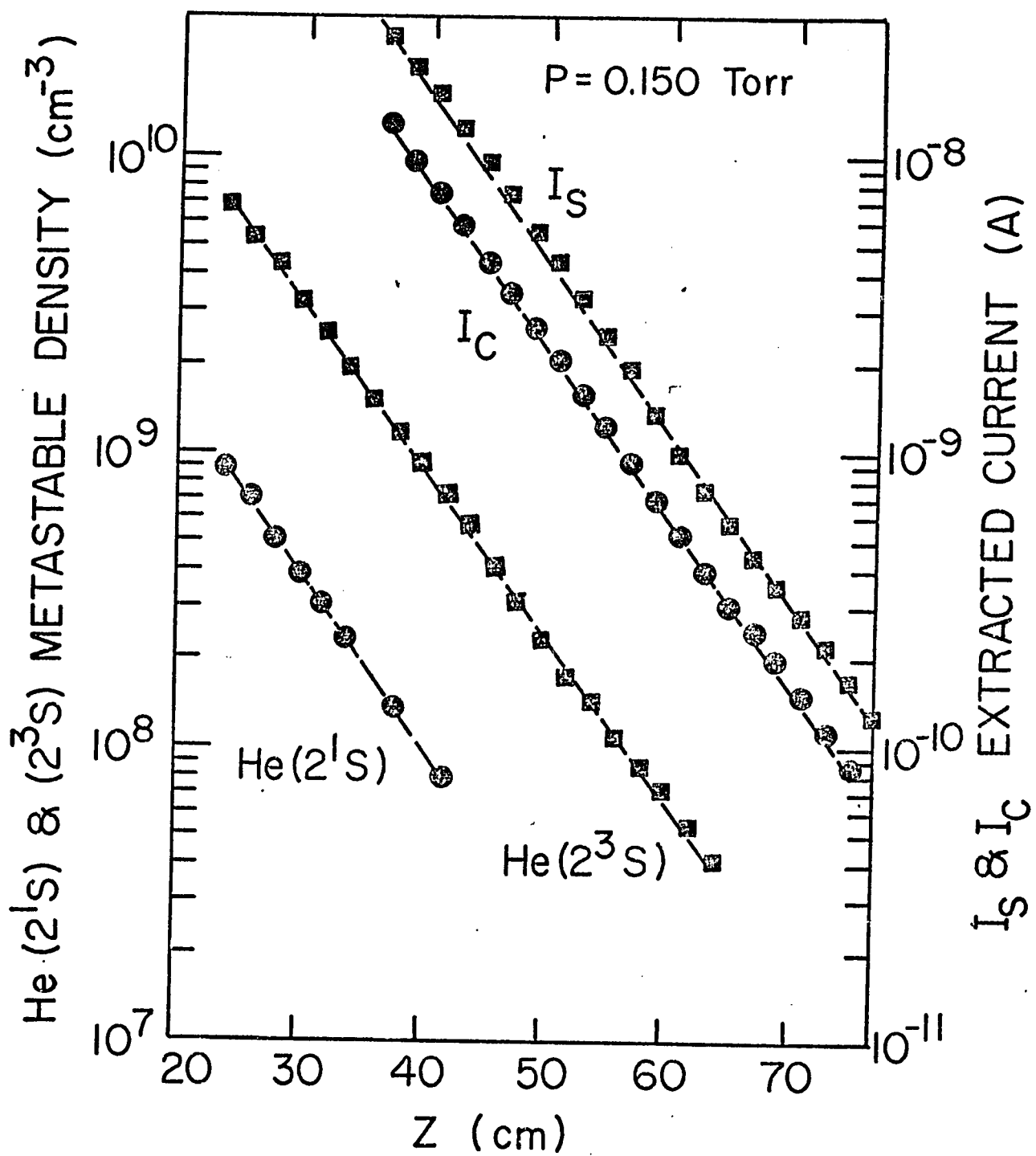


Figure 4

the exponential character of the decay with approximately equal rates for the 2^1S and 2^3S metastables. This is expected from their respective diffusion coefficients of 440 ± 50 and $4700 \pm 25 \text{ cm}^2 \text{ sec}^{-1}$ at 1 torr⁵⁵. The measured decay lengths agree with those calculated from the diffusion coefficients to within 15% (see Appendix A).

An upper limit on the electron density in the after-glow can be calculated from these decay curves. The rate of loss for 2^1S states including diffusion and conversion is

$$\frac{dN_s}{dz} = -\frac{N_s}{d_s} - \frac{Q\bar{v} N_s n_e}{\alpha V_o} \quad (7)$$

where N_s and N_e are the densities of 2^1S atoms and electrons, d_s is the diffusion decay length, Q is the cross section for conversion⁵⁵, \bar{v} is relative velocity of electrons and 2^1S atoms, V_o is the average flow velocity and α is a geometrical factor equal to 1.6 to correct for the higher flow velocity near the tube center. Assuming that the diffusion length for 2^1S atoms is equal to the observed diffusion length for the 2^3S atoms, d_t , and that the total difference in slope between the 2^1S and 2^3S decay curves is due to conversion, then an upper limit on the electron density is

$$\begin{aligned} N_e(z) &\leq \frac{\alpha V_o}{Q\bar{v}} \left(-\frac{d(\ln N_s(z))}{dz} - \frac{1}{d_t} \right) \\ &\leq 2.2 \times 10^{10} \left(-\frac{d(\ln N_s(z))}{dz} - \frac{1}{d_t} \right). \quad (8) \end{aligned}$$

From the data of Figs. 3 and 4, the electron densities at 20 to 25 cm from the source are 2% of the total metastable density. Results of similar measurements in the pressure range of .08 to .15 torr consistently indicated electron densities less than 10% of the metastable density. These are actually over estimates since no curvature is observed in the semi-log plot of N_s that is expected from Eq. (7). Only at pressure of .17 torr and above is conversion clearly evident. The estimates of N_e for these pressures vary from 15 to 60% of the metastable density. This is consistent with the observed changes in extracted current when rf power is applied at these higher pressures.

We conclude from both types of measurements that source produced electrons are not a significant component of the extracted currents for pressures below .15 torr at distances from the source greater than 40 cm. It is also apparent that the current I_s is not due to free electrons in the bulk of the afterglow. The following paragraphs confirm the hypothesis that this current is in fact due to surface ejection from the extraction aperture.

B. Electron Currents From Surface Ejection

1. Residual Background Current

In Figs. 3 and 4, the extracted currents I_s and I_c are also presented. The current I_c was obtained by injecting argon into the afterglow at a fixed point, 4 cm upstream from the extractor. Both curves are displaced laterally from the 2^3S and 2^1S curves since the metastable densities were measured in this case 13 cm upstream from the extractor. It can be seen that both currents I_s and I_c are proportional to the metastable density except for currents below 10^{-10} A in Fig. 4. This "residual background current" is not well understood. However it is small enough to be neglected in the polarization data taken at pressures of .1 torr and above. A reduction in polarizations measured at .08 torr confirms that the residual current is not due to He 2^3S metastables. The slow decay rate has an approximate z^{-2} dependence, perhaps due to non-resonant u.v. photons from the excitation source.

2. Calculation of the Surface Ejection Rate

For extracted currents greater than 10^{-10} A, the linearity of the current I_s with respect to the metastable density is to be expected for electron production by surface ejection. At the same time, the linear dependence precludes the possibility that the current is produced by ionizing collisions between two metastables⁷⁰ in a region

near the extractor. (The rate for the metastable-metastable collision process is also too low to explain the observed currents.) To show that electron ejection from the surface of the extraction aperture is a plausible current source, the expected current can be estimated from the rate of metastables diffusing to the aperture.

We assume that every metastable incident on the area, A , of the extraction opening will strike a wall and the emitted electrons will be efficiently collected into an extracted beam. These assumptions are not unreasonable for the "thick" aperture shown in Fig. 2 for which the length is equal to the diameter. The current I_s is then given in amps by

$$I_s \approx 1.6 \times 10^{-19} A \gamma D (\nabla N) , \quad (9)$$

where γ is the yield of electrons per metastable striking a metal surface, D is the diffusion coefficient, and ∇N is the gradient of the metastable density near the extractor. Next, we assume that the metastable density decays from its average value to near zero at the extractor surface in a distance of 1 cm so that $\nabla N \approx |N|$. Given values of $A = .03 \text{ cm}^2$, $\gamma = .729, 38, 39$, $DP = 470 \text{ cm}^2 \text{ torr/sec}$ and $N = 1.4 \times 10^9 \text{ cm}^{-3}$ (from Fig. 3 at $z = 37 \text{ cm}$), then I_s is estimated from Eq. (9) to be $1.4 \times 10^{-8} \text{ A}$. The measured value from Fig. 3 is $2.6 \times 10^{-8} \text{ A}$ obtained with an aperture 1.5 mm in diameter by 1.5 mm long. The extracted current

is observed to increase with increasing aperture diameter and with decreasing aperture length, indicating that the electrons may originate on the front surface as well as the inside walls of the aperture.

C. Electron Current from Chemiionization

The extracted current I_c of electrons from chemiionization is also linear with respect to metastable density as shown in Figs. 3 and 4. If sufficient gas is injected to de-excite all metastables in a short distance, the initial density of electrons is nearly equal to the density of metastables that reach the position of the gas injector. For a fixed injector position, some constant fraction of these electrons should diffuse through the extraction aperture, resulting in the linear dependence on metastable density that is observed. This also implies that at least for these specific conditions, the electron extractor itself is a linear probe of electron density in a decaying plasma.

1. Ambipolar Diffusion Rates

The exponential decay length of electron density due to ambipolar diffusion with their parent ions can also be obtained in principle by measuring the current I_c while moving both the source and the gas injector together relative to the position of the extractor so that the initial density of electrons is a constant. Alternatively, the injector alone can be moved if the change in initial electron

density is accounted for. However, these types of measurements were only partially successful. The best exponential decay measurements extended only over one order of magnitude but did show as expected that the diffusion rate is roughly twice as fast as that for electrons and He^+ ions in helium⁵⁹. The deviations from a simple exponential decay, which in some cases are quite drastic, are not understood. While this behavior does not have a direct bearing on the interpretation of the polarization results to be reported, it does show that the electron density and extraction system is not as simple as might be presumed from the previous data. We can only conjecture that the space charge potential of the plasma is sensitive to the relative position of the extractor and the gas injector which is a perforated stainless steel ring. It will be shown in Part II that externally applied potentials between the extraction aperture and the rest of the afterglow can increase the extraction efficiency by as much as two orders of magnitude.

2. Surface Emission by Ions

It has been shown that source-produced electrons are not present in the afterglow over a limited pressure range. A second possible extraneous contribution to the current I_c is the ejection of electrons from the extraction aperture surface by the ions produced in the chemiioniza-

ion reactions. As seen in Figs. 3 and 4, the surface-ejected electrons that comprise I_s are extracted with approximately the same efficiency as electrons from the bulk of the afterglow. Therefore the fraction of electrons in the extracted current I_c that are produced by ion-ejection is roughly equal to the yield, γ_i , for those ions.

Yields have been measured for many ion-surface combinations in the energy range of 10 to 1000 eV⁶⁰. There is considerable variation in the surface conditions and the quality of this data. However, several general conclusions are valid for all data at low energy ($E \leq 10$ eV).

1) Values of γ_i for atomically clean surfaces are well known and depend strongly on the ionization potential for the ion and the work function of the surface. The results for several ions incident on atomically clean tungsten and molybdenum are given in Table I.

2) γ_i for molecular ions are substantially lower than for atomic ions with nearly the same ionization energy.

3) In all cases, γ_i decreases for contaminated surfaces.

4) γ_i is relatively insensitive to the substrate material for heavily contaminated surfaces.

Therefore, even though γ_i has not been measured for all the ions present in this experiment nor for our particular heavily contaminated brass surface, it is reasonable to assume from the values in Table I that for Ar^+ ions

Table I

Yield of Secondary Electrons Per Incident Ion on Atomically Clean Surfaces

Ion	He ⁺	Ne ⁺	Ar ⁺	Kr ⁺	Xe ⁺	N ₂ ⁺	H ₂ ⁺	O ₂ ⁺
Ionization Potential	24.58	21.56	15.76	14.0	12.13	15.57	15.4	12.06
Surface (work function)								
W (4.5 eV)	.29 ^a	.21 ^a	.095 ^a	.050 ^a	.013 ^a	.027 ^c	.025 ^c	.01 ^c
Mo (4.3 eV)	.30 ^b	.25 ^b	.122 ^b	.069 ^b	.022 ^b			.008 ^d

^a Ion energy = 10 eV, reference 61.

^b Ion energy = 10 eV, reference 62.

^c Ion energy = 50 eV, reference 33.

^d Ion energy = 50 eV, reference 63.

$\gamma_i \leq .1$ and that for all molecular ions $\gamma_i \leq .05$. These contributions to the extracted current of 5 to 10% are of the same order as the random errors in determining electron polarization and do not affect the conclusions.

D. Post Extraction Excitation

There remains the possibility that the extracted electron beam will produce ionization or excitation of the background gas in the post extraction region. Due to the particular construction of the extractor assembly, the pressure in the volume between the extraction aperture and extraction anode is substantially higher than the value of 10^{-4} torr measured for the rest of the electron beam tube. As long as the level of excitation is below the threshold for a discharge in this region, the measured current may still be proportional to the metastable density in the afterglow. The evidence for this process will be described in detail in Section V as a plausible explanation for the observed reduction in the electron spin polarization for pressures of .15 torr and above.

E. Summary

Given the evidence presented here, the four conditions concerning the sources of the extracted currents, that were stated at the beginning of this section, have been demonstrated. However this conclusion is only valid over a

limited range of parameters: for pressures above .08 torr and below .15 torr, for extracted currents greater than 10^{-10} A, for separations of the excitation sources from the extractor greater than 30 to 40 cm, for an extraction aperture of 1.5 mm diameter by 1.5 mm long, and for an extraction potential of 500 volts.

IV. OPTICAL PUMPING

A. Properties of the Optical Signal

In order to uniquely determine the degree of spin polarization transfer in various reactions, we must be able to measure independently the polarization of the He 2^3S atoms in addition to measuring the polarization of the product electrons. It is in principle possible to determine the relative populations of the 2^3S sublevels by observation of the transmitted or scattered pumping light. The most accessible experimental quantity is the difference ΔI between the amount of light absorbed by the pumped metastables, I , and the amount of light absorbed when the metastables are unpumped, I_0 . The ratio $\Delta I/I_0$ is called the optical signal. However we found that the common phenomenological model^{2,9} used to derive the 2^3S sublevel populations from the optical signal is very sensitive to the assumed spectral profile and to percent absorption of the 1.08μ pumping light (see Fig. 5). As a result, the 2^3S polarizations determined from the optical signal are at best semi-quantitative. (We therefore must infer the He 2^3S polarizations from measurements of electron polarization for many different reacting species.) Since the above effects were not fully appreciated heretofore, we have included in Appendix D a brief explanation of how they occur and compare the predicted and measured polarization.

Figure 5a: The measured optical signal $\Delta I/I_0$ vs percent absorption of the 1.08 pumping light. The flow tube pressure is given in parentheses (in torr).

Figure 5b: Polarization of the He(2^3S) sub-levels, P_3 , vs the optical signal. Solid curves calculated from the thin absorber model² for several values of K and L. Data points are the measured polarizations of electrons produced by chemiionization of N₂.

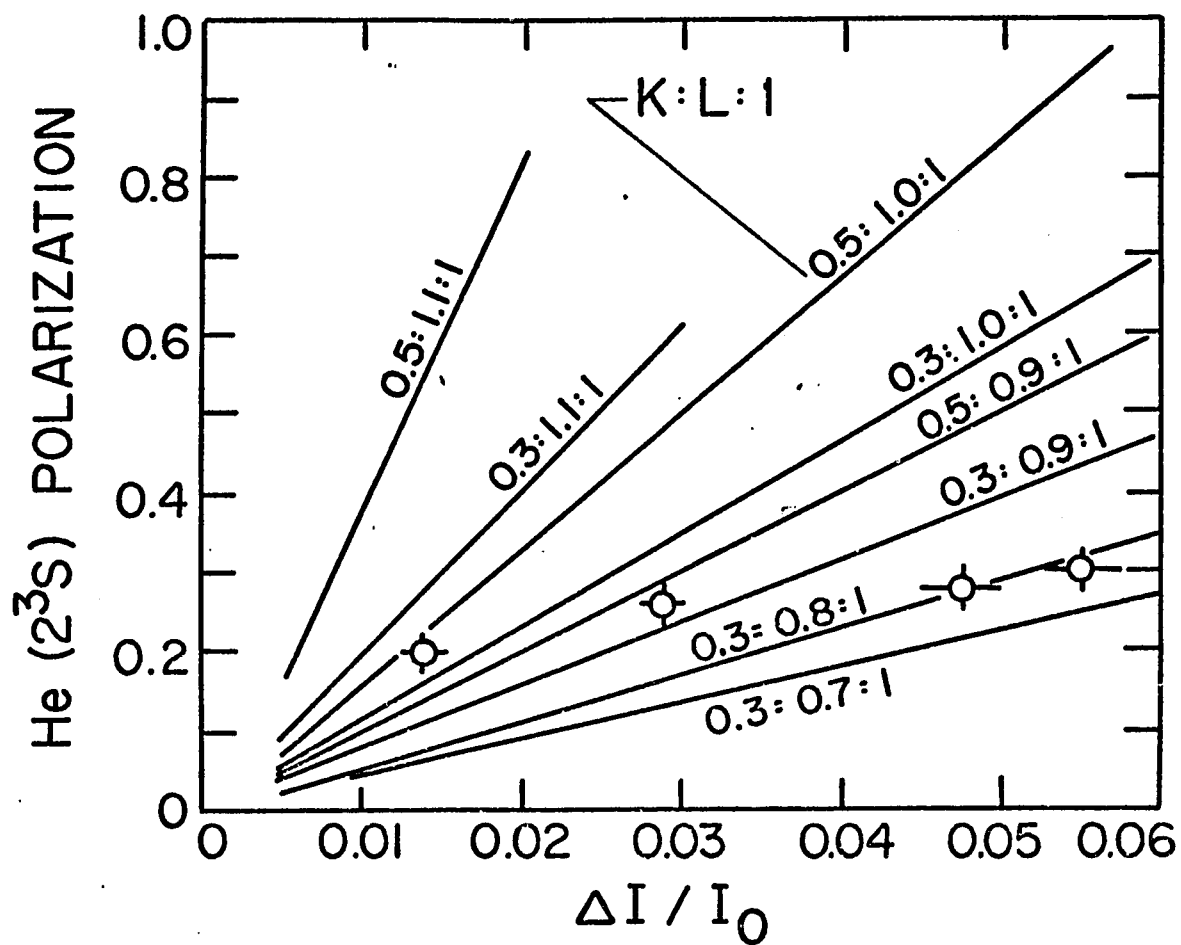


Figure 5b

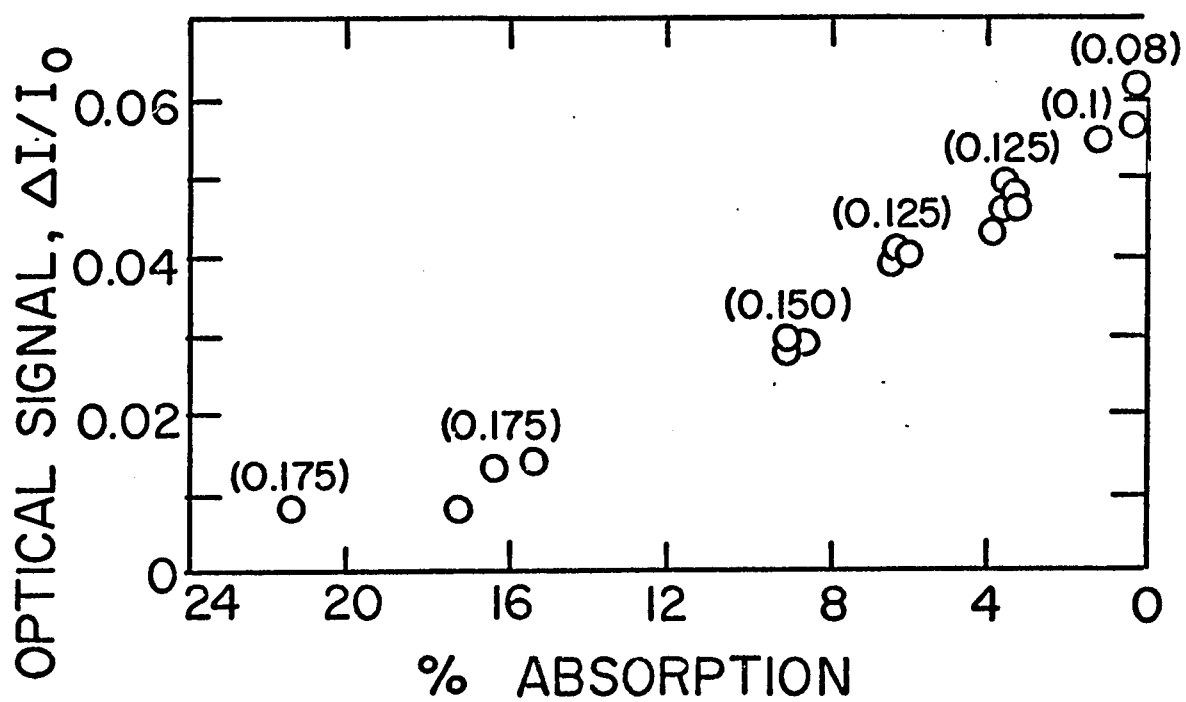


Figure 5a

A derivation of the 2^3S polarization from the optical signal assuming an optically thin sample is given by McCusker et al.² It was decided that it was not worthwhile to improve the model for the optical signal described by McCusker et al. since a direct measurement of the 2^3S sublevel populations is possible but is experimentally difficult. This method was not attempted but is noted in Appendix D for completeness.

B. Limitations to the $\text{He}(2^3\text{S})$ Polarization

In this section, we describe several mechanisms involved in the optical pumping process that limit the ultimate polarizations attainable. In an optically pumped active discharge, there are many relaxation processes which tend to restore the normal Boltzman distribution of the 2^3S sublevels. Most of these processes involve energetic electrons. Since these are not present in the afterglow it is not at all clear what processes limit the observed polarizations to about 35%. Three possible mechanisms are:

- 1) Failure to attain a steady state population of N_+ , N_0 , and N_- ,
- 2) Collision induced mixing of the 2^3P sublevels prior to their spontaneous decay back to the 2^3S state,
- 3) Transitions from the 2^3S to 2^3P states that do not obey the selection rule $\Delta m = +1$ assumed for pumping with right circularly polarized light.

We expect that the 2^3S sublevels have reached steady state since the time for gas to flow past the 10 cm optical pumping path is ~ 2 msec whereas the time constant for obtaining equilibrium measured with similar pumping lamps was $\sim .2$ msec⁶⁴. Also, the optical pumping signal measured as a function of position did saturate after 8 cm. Collisional mixing of the P states should also not be too significant. At a pressure of 0.1 torr the characteristic time between collision that change the J level of the P state is 5×10^{-7} sec^{8,65} whereas the radiative lifetime of the 2^3P state is 1×10^{-7} sec⁶⁵.

The third process listed is not insignificant. Transition in absorption other than $m = +1$ occur in the afterglow due to four processes:

- a) The circular polarizer transmits a small amount of light (1 to 2%) of the opposite polarization ($\Delta m = -1$).
- b) Light rays that are not parallel to the magnetic field induce π transitions ($\Delta m = 0$).

- c) The excitation source produces 1.08μ radiation ($\Delta m = \pm 1$ or 0).
- d) The spontaneous emission from the 2^3P states is partially reabsorbed exciting transitions $\Delta m = \pm 1$ or 0 . This latter process is probably responsible for the 20% reduction of measured electron polarizations observed at metastable densities corresponding to 10% absorption of the pumping light (see Section V).

Processes a, b and d have been included in detailed studies⁶⁶ of optical pumping of He^3 which show that the magnitude of the effects increase with increasing 2^3S polarization. The importance of processes a, b, and c in the present experiment is difficult to estimate but they should be investigated in order to understand the ultimate limitation on the $\text{He } 2^3S$ polarization in the afterglow.

In summary, one result of this experiment is a realization of the importance of light absorption effects in the optical pumping process. An absolute method for monitoring the 2^3S sublevel populations has been suggested which should aid investigations to improve the maximum polarizations attainable in a flowing afterglow.

V. RESULTS

A. Experimental Conditions

Electron polarizations were measured for the chemi-ionization of Ar, H₂, N₂, N₂O, CO, CO₂, CH₄, and NH₃ by spin polarized He(2³S) metastables. The results are shown in Fig. 6 for several different values of afterglow pressure. Each point represents the mean and standard deviation of eight separate polarization measurements. A manifold on the gas injection system allowed two or three gases to be tested sequentially in a single data run or "set" under identical conditions of afterglow parameters. Data points for each set are grouped together horizontally as illustrated by the box in Fig. 6b. The polarization of electrons ejected from the extraction aperture surface by metastables was also measured for each set, and serves as a reference point when comparing results for gases tested under similar, but not identical conditions.

The flow rate of each gas was chosen as the rate necessary to reduce the 2³S₁ density by a factor of 100 within a distance of 4 cm from the injector. These flow rates in torr liter/sec are: Ar, 1.5; N₂, 1.15; N₂O, 0.15; CO, 0.90; CO₂, 0.22, CH₄, 0.80; and NH₃, 0.13. For H₂ the minimum reaction length was 10 cm with a flow rate of 1.25 torr liter/sec (Estimates of the 2³S₁ destruction cross sections obtained from these data are compared with previous

results in Appendix B.) Unless otherwise noted, the data presented here were taken with a microwave excitation source, an extraction aperture of 1.5 mm diam. by 1.5 mm long, an extraction potential of 500 volts, and a reaction length of 4 cm.

B. Correction for He(2^1S) Density

The measured polarizations, P_m , in Fig. 6 are not corrected for a small, unpolarized contribution from the electrons produced by the 2^1S_0 metastables present. For chemiionization reactions we will assume that all metastables produce one electron⁶⁷. Therefore P_m will be

$$P_m = \frac{P_c N_T}{N_T + N_S} \quad , \quad (11)$$

where P_c is the polarization of electrons produced by 2^3S metastables, and N_T and N_S are the densities of the 2^3S and 2^1S states respectively. In the case of surface ejected electrons, the rate of production by the 2^3S and 2^1S metastables, as described by Eq. (9), is limited by their respective electron yields, γ_T and γ_S , and by their diffusion coefficients, D_T and D_S . Therefore P_m is given by

$$P_m = \frac{P_s \gamma_T N_T D_T^{-1}}{\gamma_T N_T D_T^{-1} + \gamma_S N_S D_S^{-1}} \quad , \quad (12)$$

where P_s is the polarization of secondary electrons produced by the 2^3S atoms alone. The ratio γ_S/γ_T appears to

depend somewhat on the particular surface in question but is probably between 0.7 and 1.0^{29,38,39}. We have assumed $\gamma_S/\gamma_T = .85 \pm .15$ in preparing Fig. 7. The ratio of D_T/D_S is unity within experimental error⁵⁵.

Values of P_C and P_S derived from Fig. 6 are given in Fig. 7. The error in the ratio N_S/N_T depends on the random error in the optical absorption measurements (5 to 10%) and on the values chosen for several experimental parameters included in the calculation of the absorption probability (see Appendix C). While an error in this latter quantity could alter the pressure dependence in Fig. 7, it will not change the relative polarizations from the gases at a given pressure since the ratio N_S/N_T is nearly constant for all data points at a given pressure. Ideally, the measured electron polarizations when corrected for the presence of 2^1S state, would be independent of experimental parameters such as the flow tube pressure, the type of excitation source, the 2^3S density, the neutral and ion reactant densities and the reaction length. In the remainder of this section, the observed dependences of the measured polarizations on the above parameters are presented and several explanations suggested. In considering possible secondary reactions in the afterglow tube prior to extraction, it should be noted that for most gases the electrons from chemiionization are rapidly thermalized (see Part II, Section II).

Figure 6a,b,c: Measured electron polarizations, P_m , from chemiionization of gases and surface ejection by spin polarized $\text{He}(2^3\text{S})$ and $\text{He}(2^1\text{S})$ metastables at several values of afterglow pressure; ● surface-ejected electrons; ○ Ar; □ CO_2 ; △ N_2 ; ▲ N_2O ; ■ CO; ▼ NH_3 ; ▽ CH_4 ; ◇ H_2 . Data are uncorrected for 2^1S -produced electrons. Typical values of the 2^3S density measured at 21 cm upstream from the extractor are given at the top of the figure. $\text{He}(2^3\text{S})$ produced with a microwave cavity discharge. Reaction length is 4 cm, the extraction aperture is 1.5 mm diam. by 1.5 mm long, and the extraction potential is 500 volts except for points indicated.

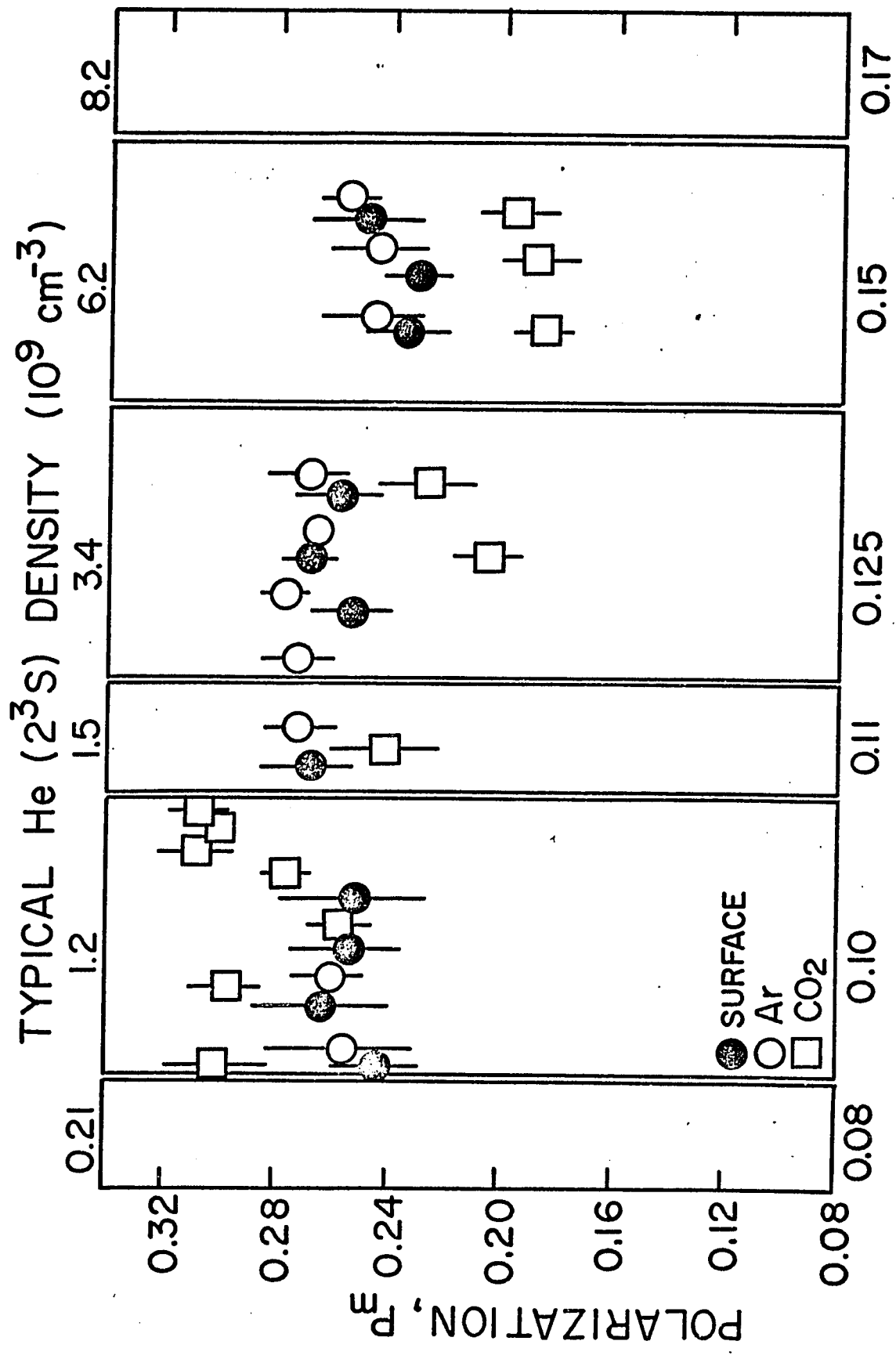


Figure 6a

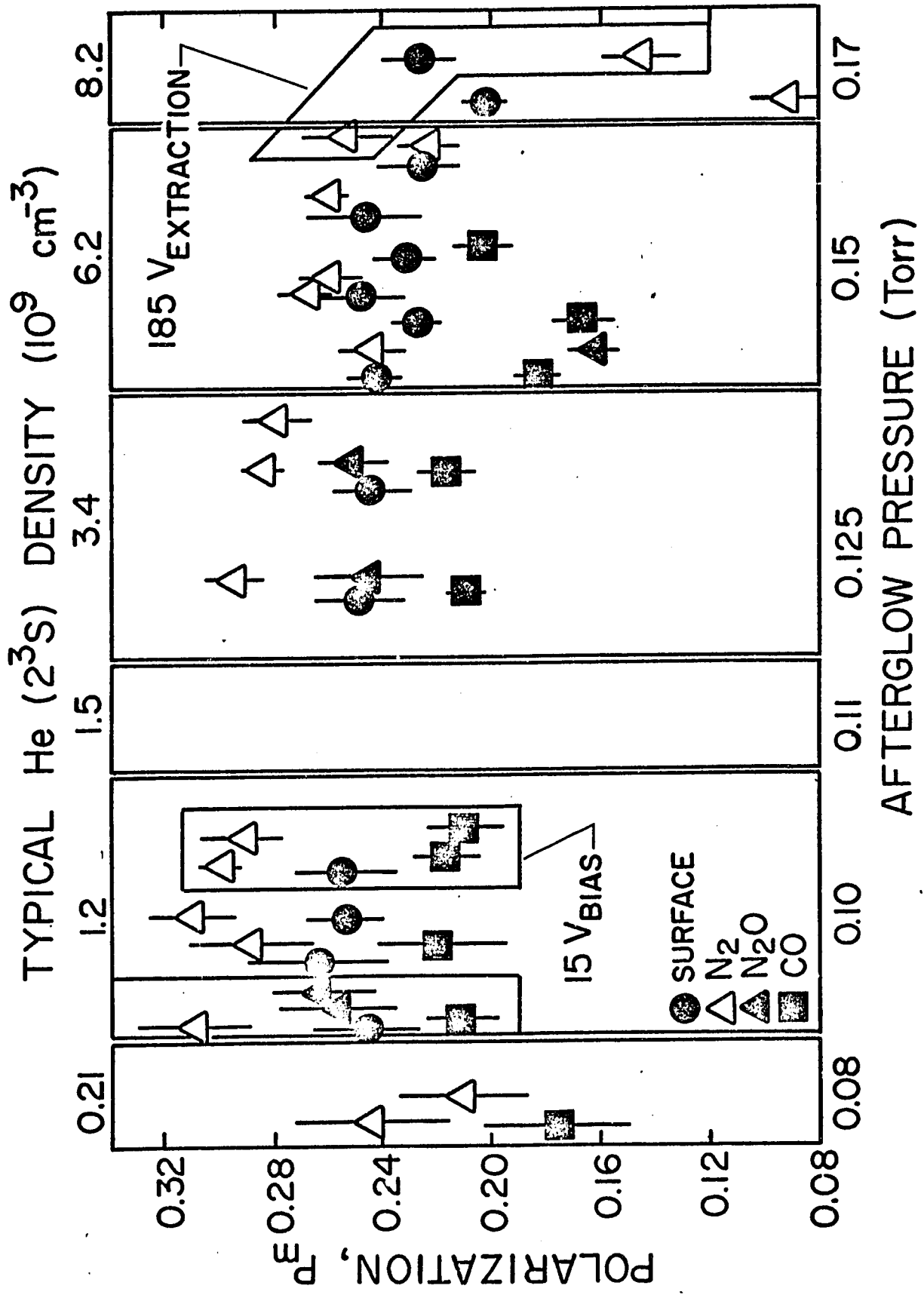


Figure 6b

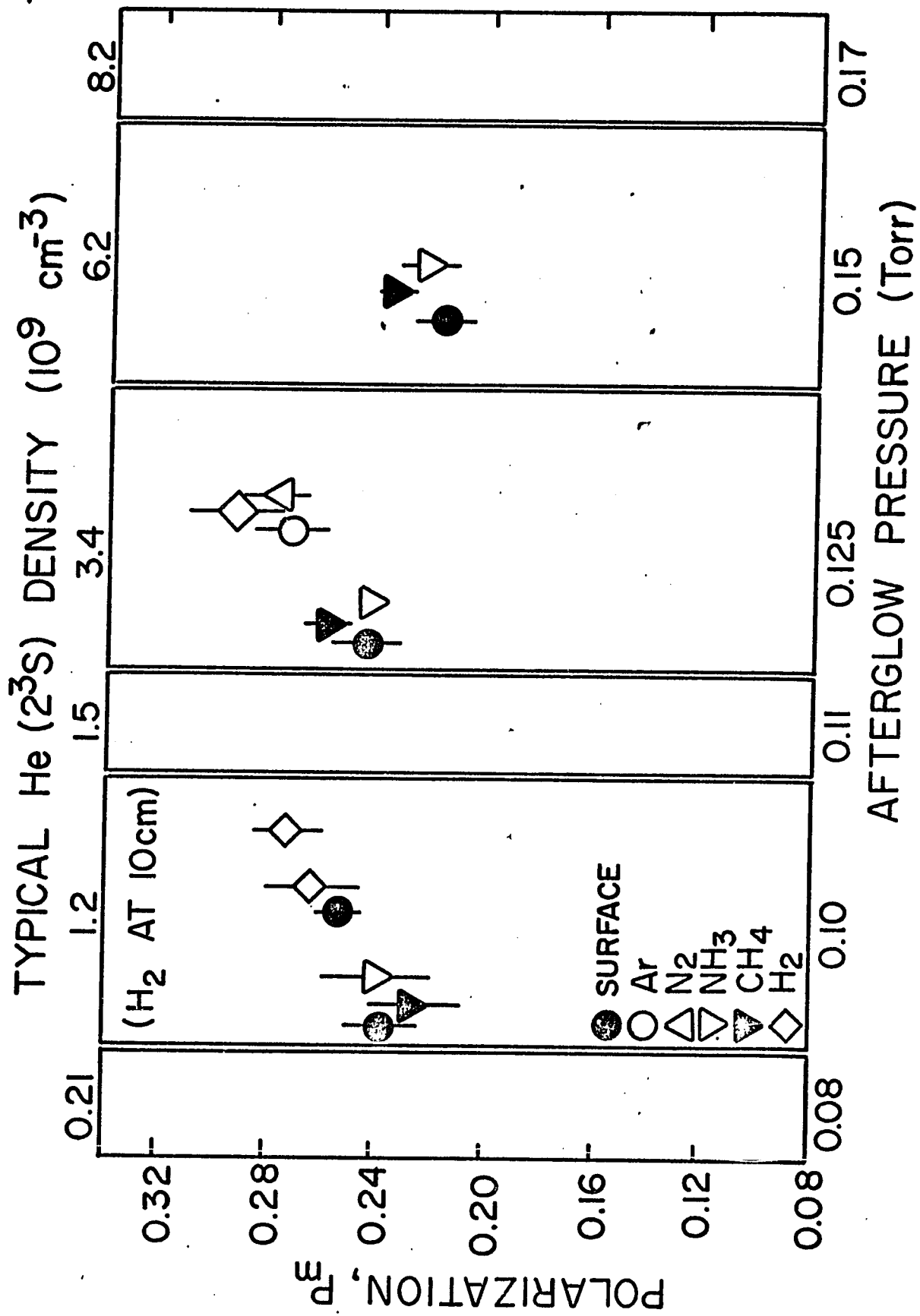


Figure 6c

Figure 7a,b,c: Corrected values of polarizations P_C and P_S derived from the data of Fig. 6 using Eqs. (11) and (12), for several values of afterglow pressure. All afterglow conditions are the same as in Fig. 6.

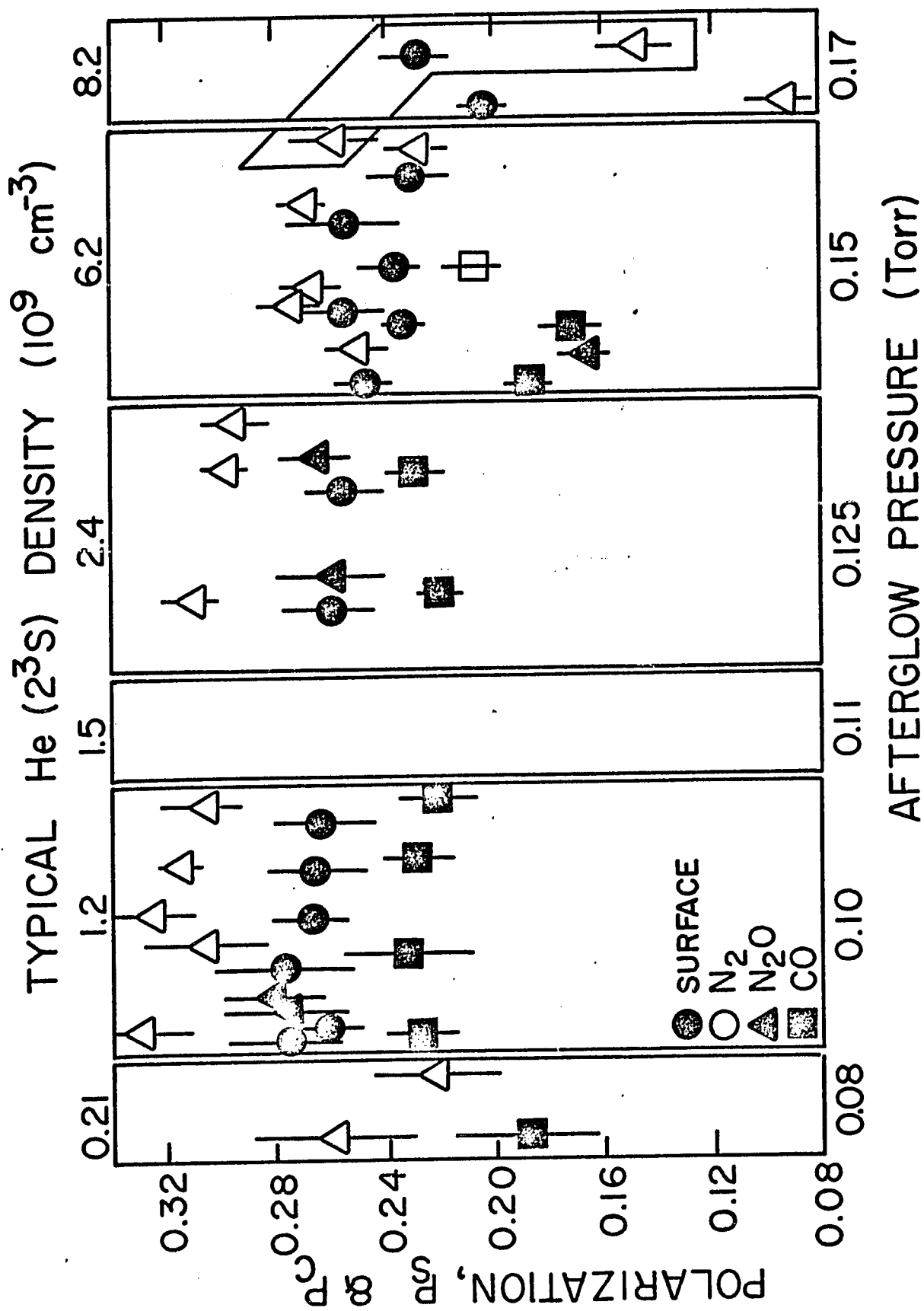


Figure 7a

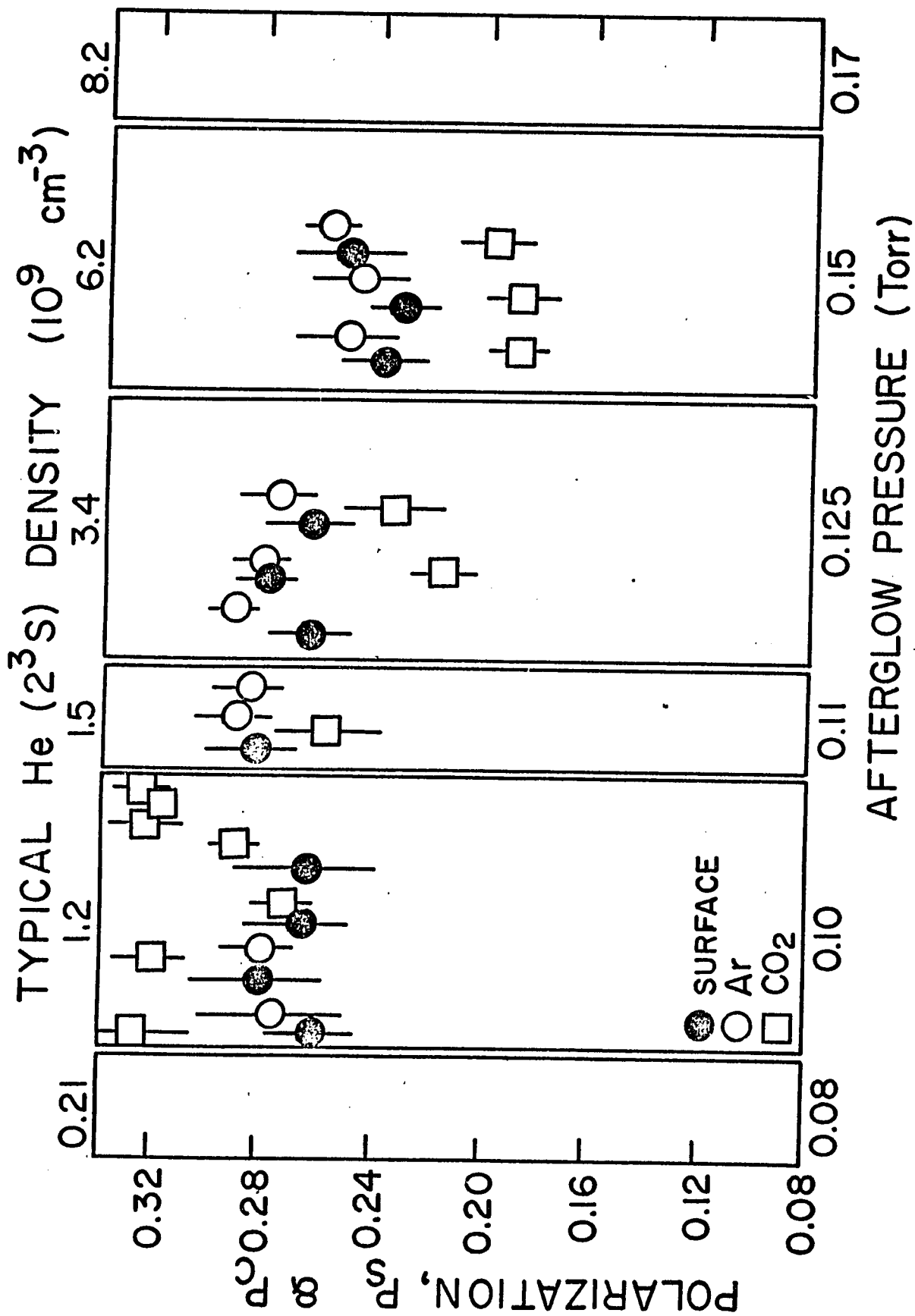


Figure 7b

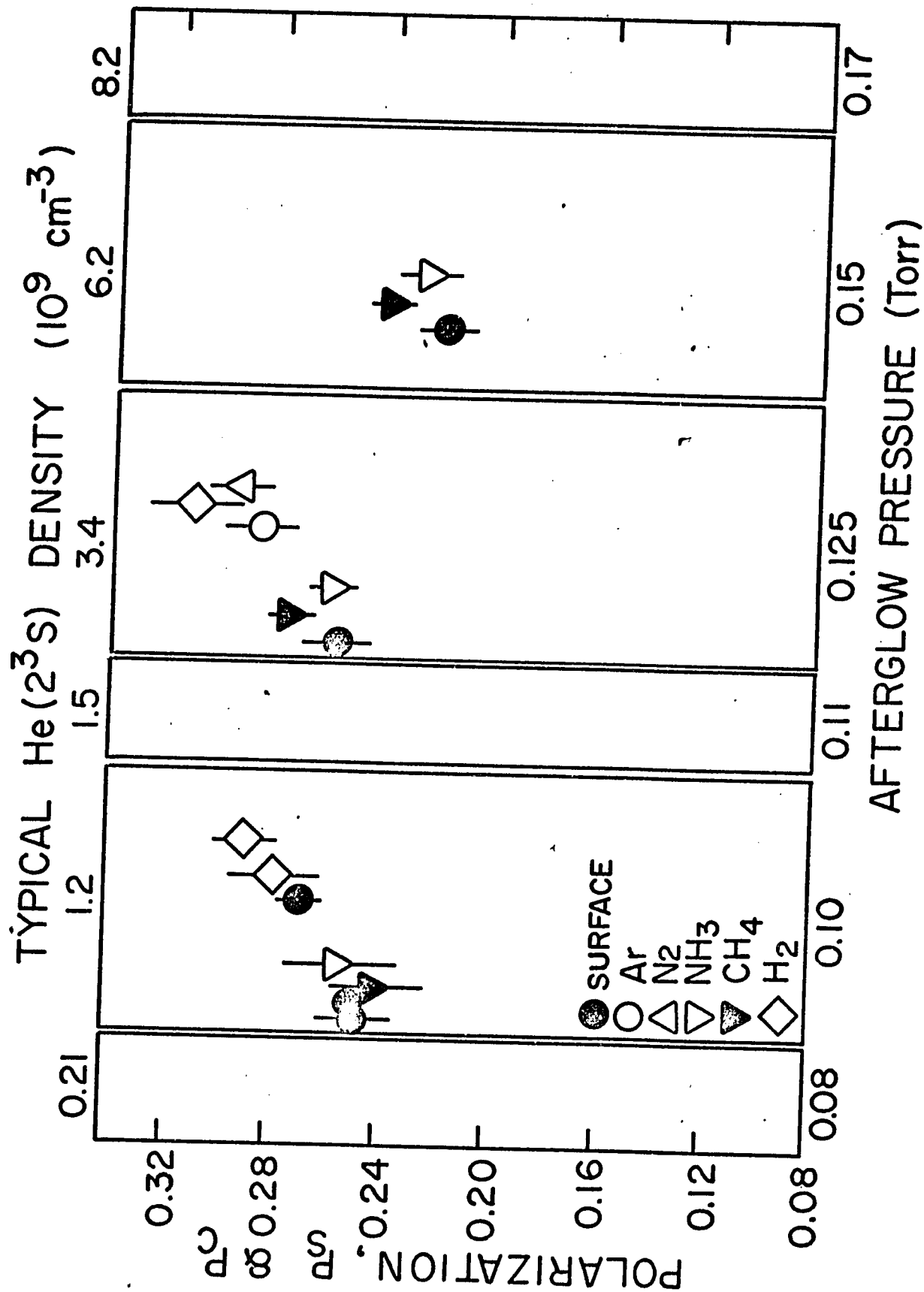


Figure 7c

C. Pressure Effects

Three pressure regions can be distinguished in Fig. 7. First, for pressure of .08 torr or less where the extracted electron current is small the "residual background current" discussed in Section III lowers the measured polarization. A bias of -15 volts between the body of the afterglow and the extraction aperture was used for two data points to improve the extraction efficiency, but with only partial success.

In the second region between .10 and .125 torr, polarizations of both chemiionization and surface-ejected electrons show a slight decrease with increasing pressure which may be due to the 2^3S density dependence of the optical pumping efficiency (see Fig. 11, 12 and discussion below). However, except for CO_2 , the polarizations from all the gases maintain the same relative positions. The difference in the results for N_2 and CO does appear to be significant and outside the statistical error or any fluctuation between different "sets" of data.

In the third region at pressures of .15 torr and above, the polarizations for all gases drop rapidly with increasing pressure. The behavior of CO_2 at lower pressures may be an early onset of this high pressure effect. The most plausible explanation for the loss of polarization at high pressure is ionization or excitation of the back-

ground gas by extracted electrons in the region between the extraction aperture and the extraction anode. The effective pumping speed at this point is limited by the conductance in the annular region in Fig. 2, and estimated to be 10 to 20 liters/sec. The conductance of the 1.5 mm diam. by 1.5 mm long extraction aperture is .29 liters/sec. Therefore the pressure in this region is 1.5% to 3% of the flow tube pressure compared to 0.1% for the rest of the electron beam tube.

This explanation is consistent with the following additional observations.

- 1) Polarizations are independent of the beam tube pressure, which was increased by a factor of 3 by reducing the pumping speed.

- 2) Polarizations from N_2 and surface electrons decreased less rapidly with pressure when the extraction voltage was reduced to 185 V as shown in Fig. 6 .

- 3) Polarizations measured with a higher conductance orifice (.58 liters/sec) begin to drop at a lower flow tube pressure of .125 torr as shown in Fig. 8 .

- 4) The reduction in polarization is less for surface-ejected electrons, produced when only helium is present, than for electrons from chemiionization. This would be expected due to the lower excitation and ionization cross sections of helium.

Figure 8: Measured polarizations at several values of afterglow pressure. The extraction aperture was 1.5 mm diam. by 0.2 mm long. All other afterglow conditions are the same as in Fig. 6.

Figure 9: Measured polarizations at several values of afterglow pressure taken with an electron gun source. All other afterglow conditions are the same as in Fig. 6, except that the metastable density was reduced at high pressures.

Figure 10: Corrected values of polarization P_c and P_s for the electron gun source derived from data of Fig. 9 using Eqs. (11) and (12) for several values of afterglow pressure. All afterglow conditions are the same as in Fig. 9.

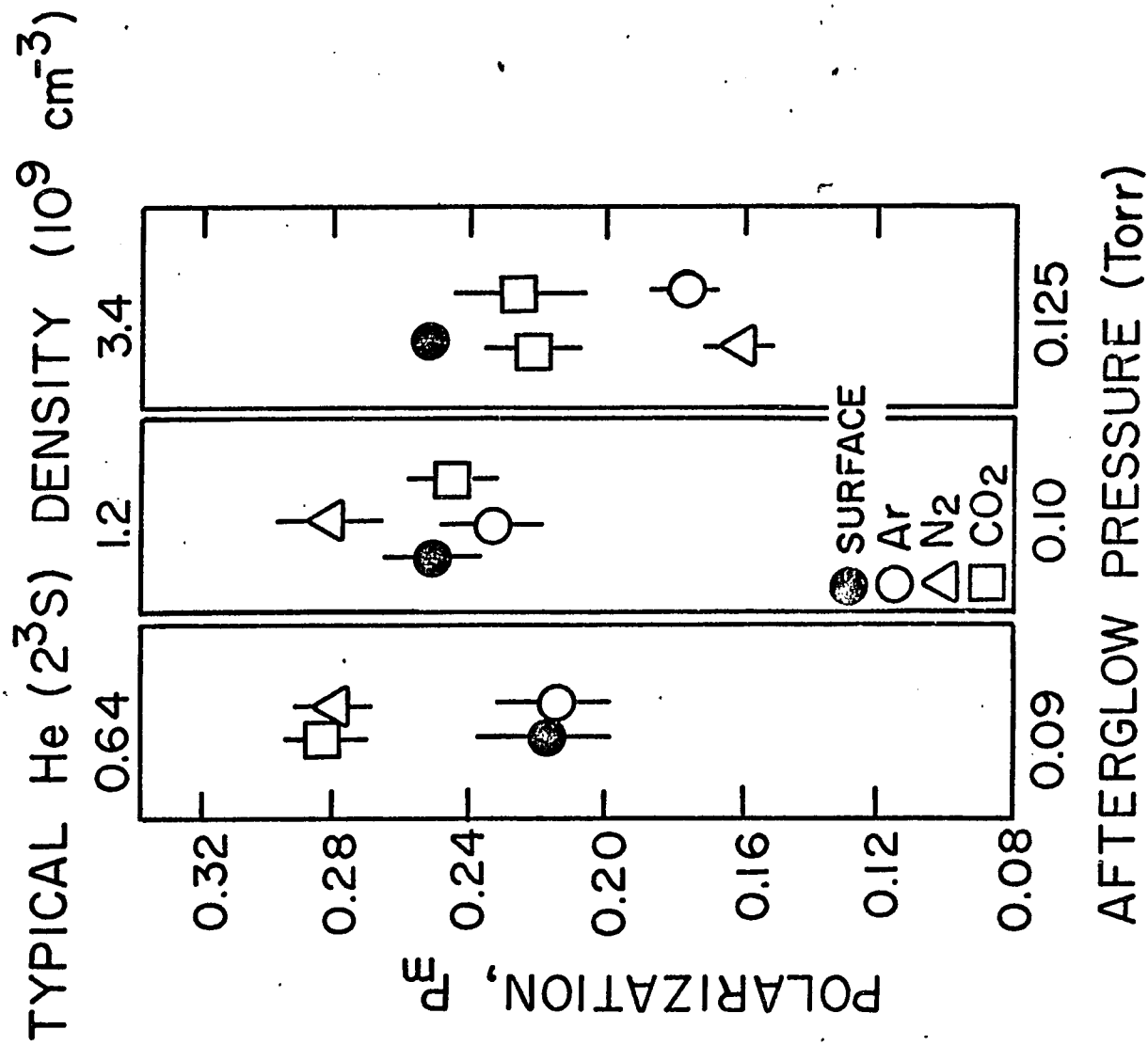
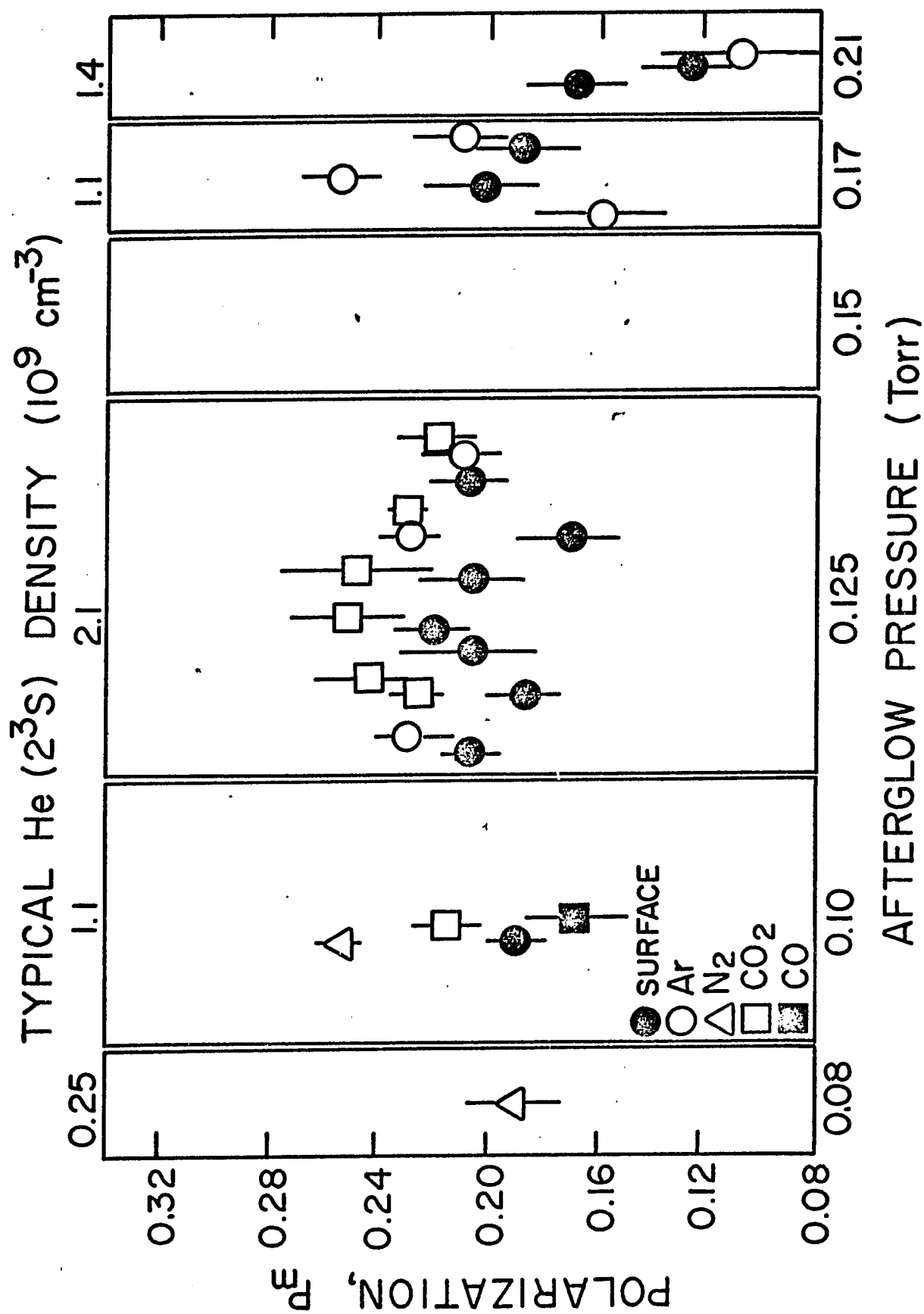


Figure 8



TYPICAL He (2^3S) DENSITY (10^9 cm^{-3})

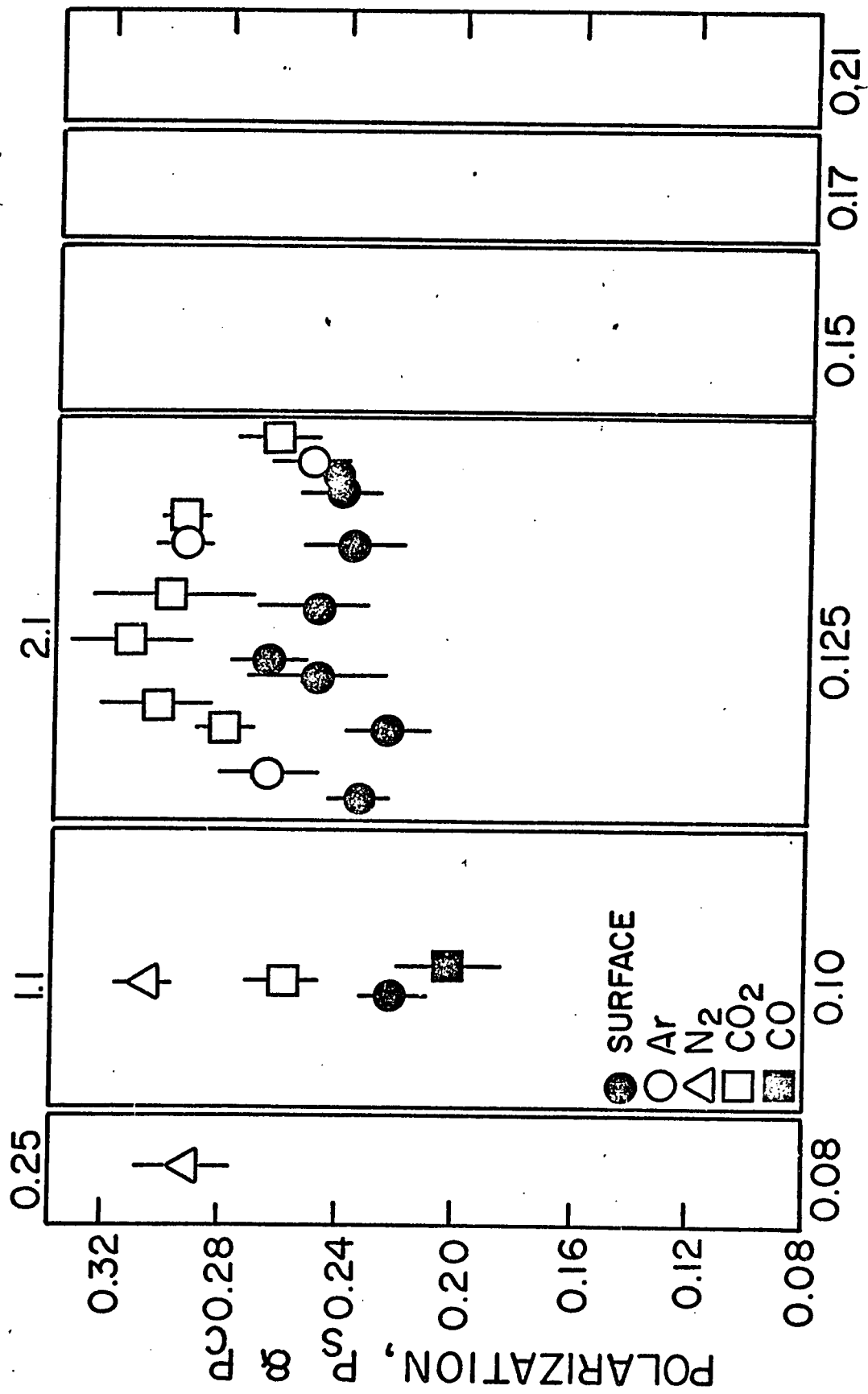


Figure 10

D. Comparison of Two Excitation Sources

Figure 9 shows the measured polarization for electrons from several reactant gases and from the extraction surface obtained with an electron gun excitation source. The pressure dependence of polarization is in general the same as in Fig. 6. However, at .125 torr the polarization for CO_2 does not exhibit the rapid decrease observed when microwave excitation is used.

There is also an overall decrease in the measured polarizations because the N_S/N_T ratio for the electron gun source is 3 to 6 times larger than for the microwave source. Figure 10 shows the values of P_S and P_C calculated from Eqs. (11) and (12) for those data points at which N_S/N_T was measured. These points can be compared with those for the microwave source shown in Fig. 7. At intermediate pressures, where, as discussed above, the quality of the data is expected to be best, the agreement is good, suggesting that the only significant difference between the two sources is the N_S/N_T ratio.

E. Depolarization Processes

The question of whether or not polarization loss mechanisms involving electron collisions in the afterglow tube are important was investigated by observing the dependence of polarization on ion density and reaction length. It should be pointed out that the data presented below are not intended as a thorough study of any particular process but only as a test for major effects.

1. Polarization Dependence on $\text{He}(2^3\text{S})$ Density

Since the ion density in the reaction region is proportional to the upstream metastable density, it can be varied by adjusting the level of excitation at the source. In Fig. 11, 12 the calculated polarizations P_s and P_c are given as a function of metastable density monitored at the position of the pumping lamp. The overall reduction in polarization for data taken with a reaction length of 12 cm is discussed below, and the two anomalously low values for N_2 and CO are assumed to be due to this effect. The roughly 20% decrease in electron polarization at higher metastable densities is quite consistent with that expected as a result of trapping of the $2^3\text{S}-2^3\text{P}$ pumping radiation discussed in Section IV. Further, the fact that the same polarization decrease is observed for electrons produced by surface-ejection and by chemiionization tends to rule out mechanisms involving collisions in the

Figures 11 and 12: Corrected values of polarization P_c and P_s vs the 2^3S density at the optical pumping region.

Fig. 11: Reaction length = 4 cm

Fig. 12: Reaction length = 12 cm

The flow tube pressure = .15 torr.

All other conditions are the same as in Fig. 6. ● surface - ejected

electrons; ○ Ar; ▲ N_2 ; ▲ N_2O ;

▣ CO_2 ; and ■ CO.

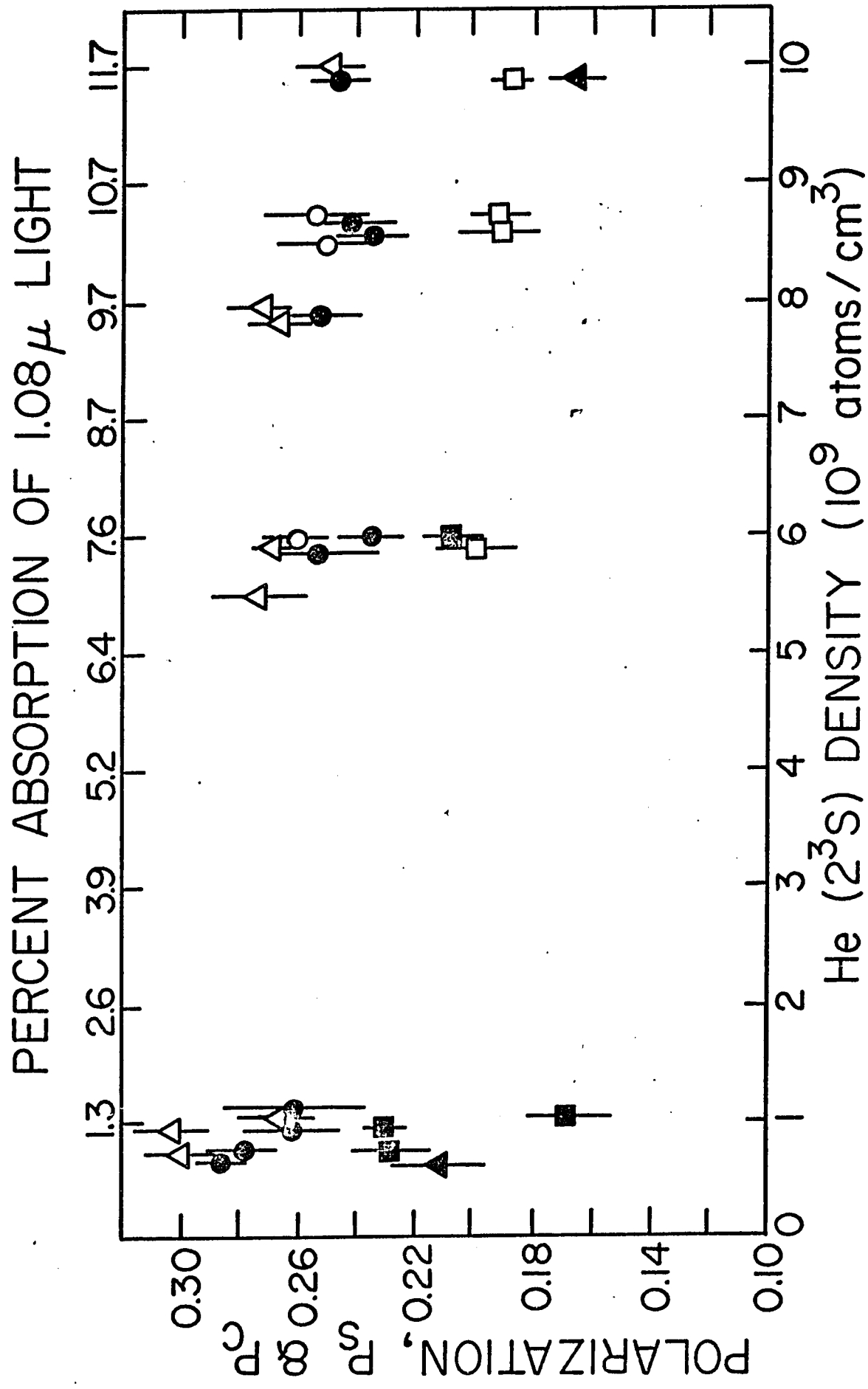


Figure 11

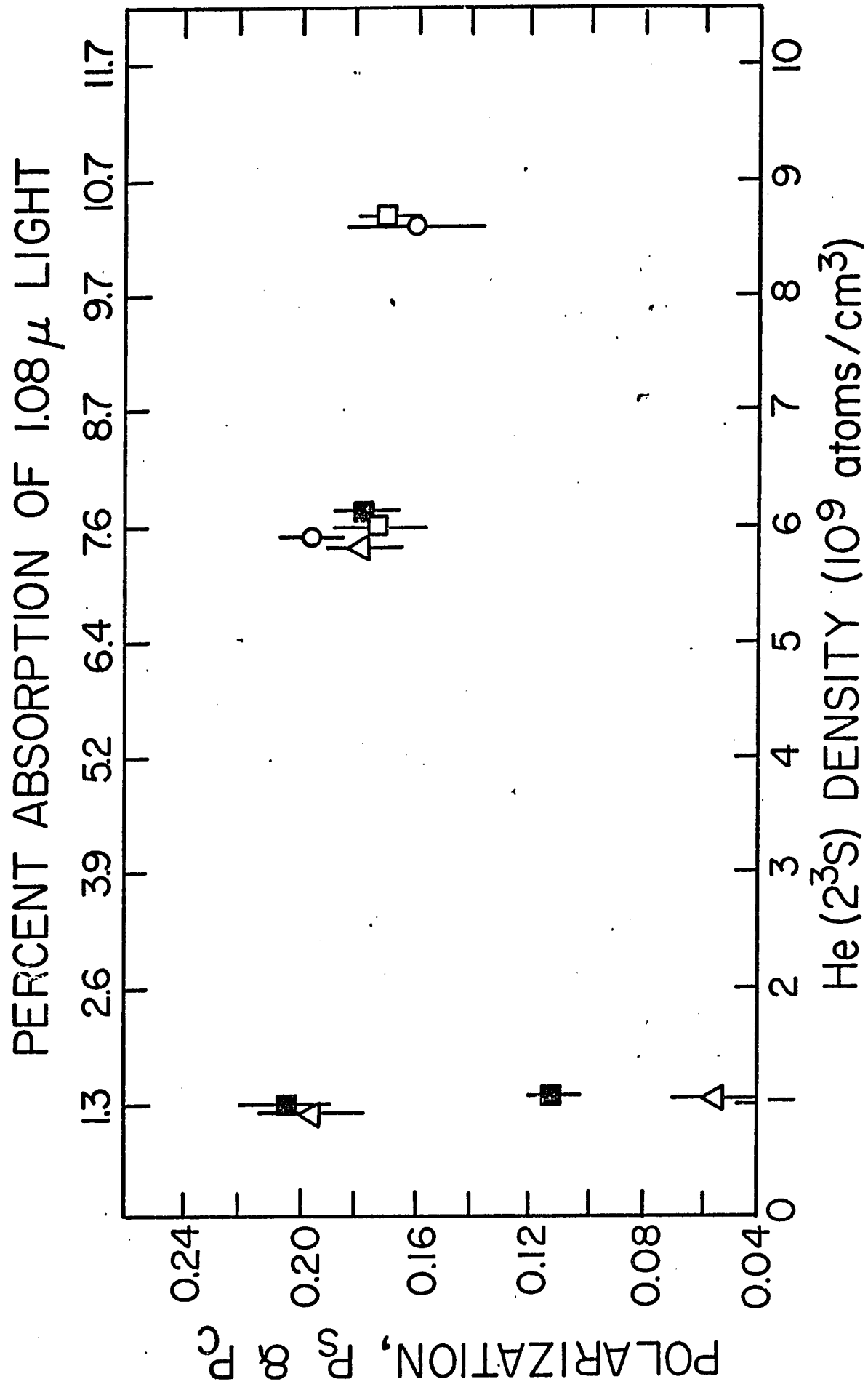


Figure 12

reaction region. One can however use the data in Fig. 11, 12 to extract upper limits for spin exchange rates between electrons and ions produced by chemiionization in the reaction region. This is discussed in Section VI. The observed polarization decrease as a function of 2^3S density accounts for most of the pressure dependence in Fig. 7 between .1 and .15 torr, but does not explain the observed difference in polarization for N_2 and CO nor the rapid decrease in polarization vs pressure for CO_2 .

2. Polarization Dependence on Reaction Length

Dependence of the measured polarizations on the reaction length, L , is given in Figs. 13 and 14 at afterglow pressures of .125 and .15 torr respectively. For Ar , N_2 , CO_2 and CO , data points taken on different runs are distinguished by different symbols. The flow rates of reactant gases remain constant so that the chemiionization reactions are essentially limited to the first 4 cm of the total length L (except in the case of H_2). As L is increased by moving the gas injector upstream, the metastable density, and therefore the subsequent ion density, at the position of the injector is increasing exponentially. The metastable density at the fixed position of the pumping lamp, however, is constant. Therefore electron collisions with the ions or neutrals, but not trapping of pumping light, could contribute to the observed variation in polarization. For $L \geq 16$ cm, backstreaming

Figures 13 and 14: Measured electron polarization, P_m , vs reaction length. Percent absorption is given in parentheses.

Fig. 13: Flow tube pressure = .125 torr

Fig. 14: Flow tube pressure = .15 torr.

All other conditions are the same as in Fig. 6.

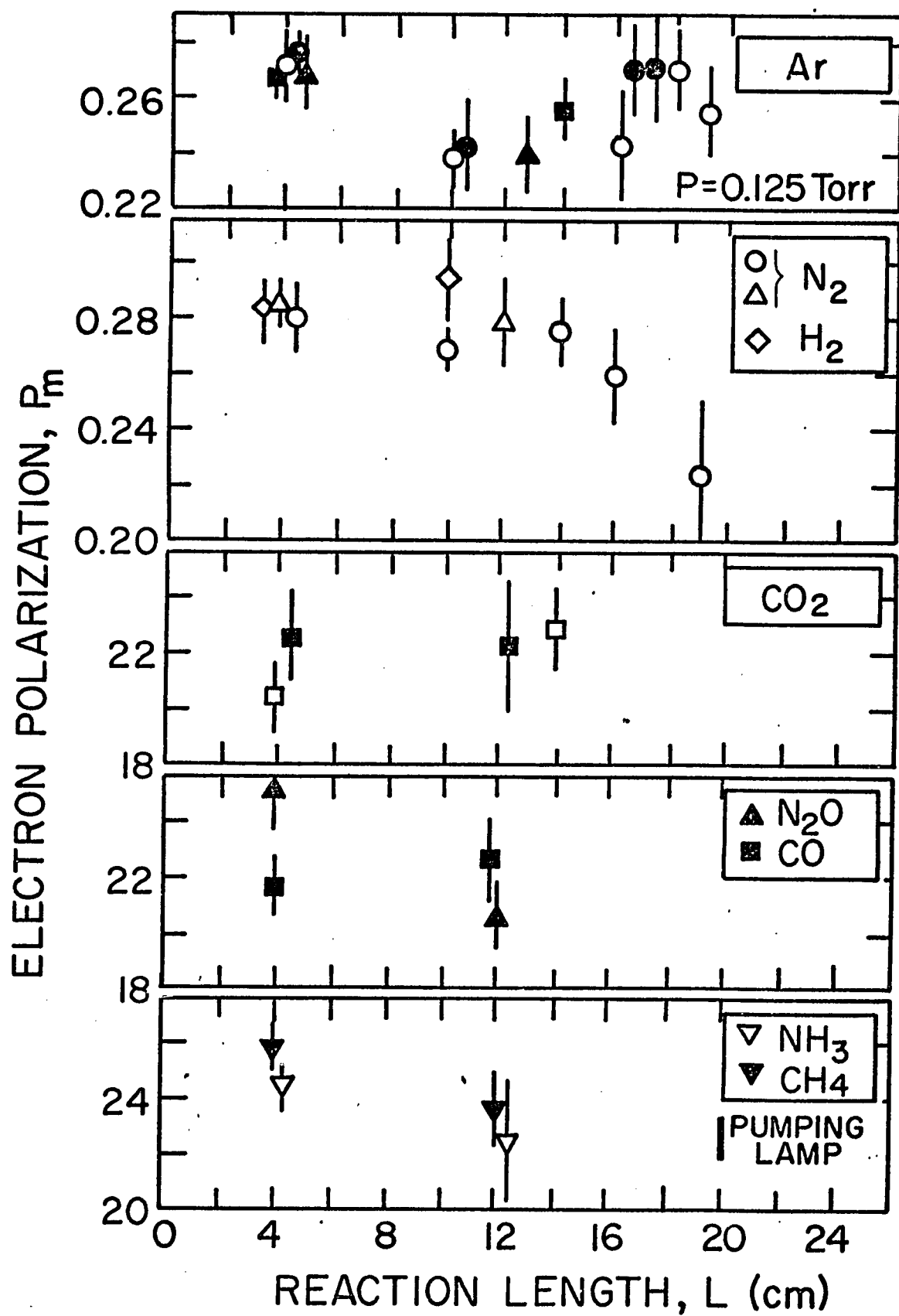


Figure 13

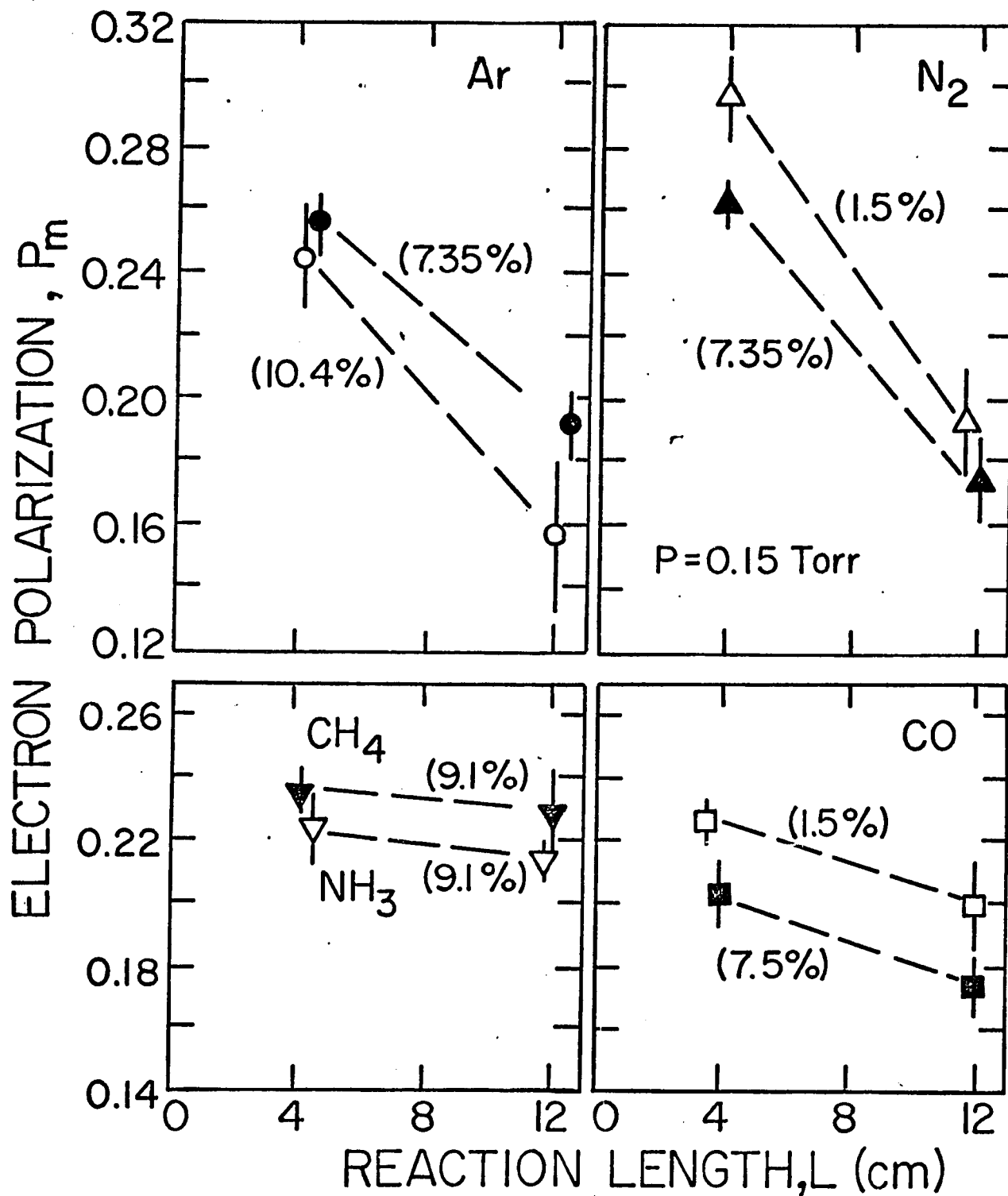


Figure 14

of the reactant gas into the optical pumping region is observed. This degrades the attainable 2^3S polarization by premature chemiionization and is responsible for the reduction in electron polarization for the largest values of L shown in Fig. 13 .

For values of $L < 16$ cm, the data in Fig. 13 taken at .125 torr do not indicate any significant depolarization effects for most reactant gases considering the size of the error bars. In particular, no dependence on L is observed for N_2 , CO, and CO_2 . The apparent minimum in the polarization for Ar is not understood if it is real. N_2O exhibits the largest decrease in polarization in Fig. 13 as it did in Fig. 11 as a function of metastable (and ion) density. It is likely that both of these effects are real and due to the same scattering process between the electrons and the ion or neutral products of the chemiionization reaction. Recent data of West⁶⁸ given in Appendix B shows that $NO^+ + N$ is produced in 50% of the chemiionization reactions of N_2O with $He(2^3S)$. Therefore spin exchange between electrons and N atoms is a possible cause of the polarization loss in addition to spin exchange with the N_2O^+ ions.

The large decrease in polarization with increasing L at .15 torr is not well understood and it may be related to the pressure dependence at constant L for pressures \geq .15 torr (see Fig. 7). However, the decrease is not due simply to electron exchange with ions because there is

little difference in the decay for N_2 and CO taken at two values of metastable density. It is also not due to any simple scattering processes⁶⁹ between electrons and the neutral reactant gas because the same reactant gas density was used at the afterglow pressures of .125 and .15 torr. One possible mechanism that would be pressure dependent is the formation of short lived negative ions of the reactant gas molecules formed by sequential electron attachment and detachment collisions. The importance of scattering processes involving the neutral reactant should be tested further by measuring the polarization dependence on neutral reactant density. This is best done by injecting the gas after the helium metastables are destroyed by prior reaction with another gas in order to eliminate any possible contribution from ions of the gas being studied.

In the next section, upper limits on the cross sections for several collisional depolarization processes are calculated from the result presented here and compared with other available data.

VI. DISCUSSION

A. Spin Polarization Transfer in Chemiionization Reactions

The evidence for spin conservation in the chemiionization of all gases tested, with the exception of CO, is first summarized from the preceding sections. The results are consistent with other measurements that indicate the lifetimes of the collisions prior to the electron ejection are short. The special cases of N_2O and CO_2 are then discussed as an interesting test of the Auger or exchange model for $\text{He } 2^3\text{S}$ de-excitation. Finally, the results for CO are discussed in terms of the possible formation of a Rydberg state of the neutral molecule.

1. $\text{He}(2^3\text{S})$ with Ar, H_2 , N_2 , N_2O , CO_2 , CH_4 , and NH_3
Present Experiment. From results presented in Sections III, IV and V, we conclude that electron spin polarization is transferred to a very high degree and probably completely in the chemiionization of Ar, H_2 , N_2 , N_2O , CO_2 , CH_4 , and NH_3 by optically polarized $\text{He}(2^3\text{S})$ atoms. The experimental basis for this conclusion may be summarized as follows:

- a) In Section III, it was demonstrated that electrons from chemiionization can be isolated from surface-

ejected and source produced electrons.

- b) From the optical resonance signal described in Section IV, the polarization of the $\text{He}(2^3\text{S})$ state is estimated to be on the same order as the maximum electron polarizations observed.
- c) At pressures between .1 and .125 torr, for all gases except CO_2 , the polarizations are nearly identical and independent of pressure, ion density, reaction length, and type of excitation source (the difference in behavior of CO_2 between the two excitation sources is not explained). This suggests that the measured polarizations, when corrected for the $\text{He}(2^1\text{S})$ density, represent the true initial polarization of electrons produced in the chemiionization reactions.
- d) In this pressure range, the polarizations, P_c , for all of these gases lie in a band between 27 and 33 percent. While this is somewhat larger than the quoted statistical error, the spread in results from run to run for Ar and CO_2 indicates that this band more accurately repre-

sents the limits of experimental confidence. Part of the variation may be due to the contribution from surface emission by ions that was estimated to be 10% for Ar and 5% for molecular ions.

- e) It is highly unlikely that all gases would exhibit the same polarization transfer unless that probability is unity.

Within the limits of experimental error, it is concluded that spin angular momentum is totally conserved for these gases. A simple classical estimate¹⁸, would indicate that "collision times" $> 10^{-12}$ sec are necessary for an appreciable "spin flip" to occur during a collision whereas an elastic "collision time" is on the order of 10^{-13} sec. There is no evidence, therefore, that the electrons produced by these chemiionization reactions participate in any collision complexes that have a lifetime more than an order of magnitude longer than an elastic collision.

Other Experiments. In several specific cases, these results have been confirmed by other experiments. For molecular species, some inference concerning long lived collisions can be made from the populations of the

vibrational levels of the product ion. This is best understood in terms of the two state potential model for chemi-ionization that is often discussed^{10,13,71,75b}. According to this picture, the entrance channel is described by a potential $V(R; \text{He}^*, \text{AB})$ that is a function of the separation, R , of the metastable helium atom from a molecule AB . This potential curve is embedded in the continuum of several possible exit channels described by potentials such as $V(R; \text{He}, \text{AB}^+)$ in the case of Penning ionization. The chemi-ionization event is then described as an autoionization of the entrance channel to the exit channel that conserves nuclear position and velocity. The energy of the emitted electron is then given by the difference between the two potential curves for the value of R at which the transition occurred.

If the entrance channel is neither strongly attractive nor near resonant with an exit channel, then no collision complex will be formed in the entrance channel and the neutral molecule, AB , will not be greatly perturbed when the ionization occurs. It is therefore expected that the relative populations of the vibrational levels for a given state of the Penning ion will be the same as those for photoionization of the neutral molecule which is also a

vertical process. These are given by the Franck-Condon factors between the ion and the $v = 0$ level of the neutral molecule. Any strong deviation from these expected populations would then imply that the above assumptions are not valid and that a long lived collision complex may exist.

Vibrational populations for several product ions have been determined by measurements of the energy distribution of the emitted electron^{72,73} and the fluorescence from excited states of the ions^{74,75}. Of interest for the present experiment are the results for H_2 , N_2 , and CO that show good agreement with the expected vibrational populations. (The special case for the $B(^2\Sigma^+)$ state of CO^+ is discussed below.) However this is not true in all cases. Strong deviations from the calculated Franck-Condon factors have been found^{74,75} for $O_2^+(A^2\Pi_u)$, $HCl^+(A^2\Sigma^+)$ and $HBr(A^2\Sigma^+)$ excited by $He(2^3S)$ metastables. It would be quite interesting to study the degree of spin polarization transfer for these reactions to determine if they are associated with long lived complexes. A combination of the techniques of electron spin analysis and optical polarization analysis^{5,6} is particularly suited here since the former is not possible with O_2 (due to spin exchange in the flow tube) and since the non-Franck-Condon behavior may be associated with only one of several final states. To our knowledge, vibrational populations have not been measured for the products of $He\ 2^3S$ with

CO_2 , N_2O , NH_3 , or CH_4 that were tested in the present experiment. In light of the foregoing discussion, the determination of complete spin conservation for the above species is not a trivial result.

Another type of measurement that is sensitive to the collision time is angular distribution of emitted electrons. For long collisions, it is expected that the electrons would be emitted isotropically in the lab frame. Hotop and Niehaus^{13,76} have found that the electrons from the Penning ionization of Ar by $\text{He}(2^1\text{S}, 2^3\text{S})$ are emitted preferentially in the direction of the He atom. They interpret this as a confirmation of their electron exchange model for the ionization process in which an electron in the target atom tunnels to the unfilled 1s orbital of the $\text{He}(1\text{s}, 2\text{s})$ state, simultaneously ejecting the 2s electron into the continuum. This model is more specific than the potential curve description in that it implies that the polarization of the emitted electron will be equal to that of the incident metastable regardless of the final state of the $(\text{He-AB})^+$ system where AB is any atom or molecule.

2. $\text{He}(2^3\text{S})$ with N_2O and CO_2

The chemiionization of N_2O and CO_2 by $\text{He}(2^3\text{S})$ are interesting to examine in terms of this electron exchange model. West⁶⁸ has recently measured the relative distribution of product ions and found for N_2O : 50.5% ($\text{NO}^+ + \text{N}$), 47.1% (N_2O^+), and 2.4% ($\text{O}^+ + \text{N}_2$) and for CO_2 :

68.5% (CO_2^+), 26.7% ($\text{O}^+ + \text{CO}$), and 4.8% ($\text{CO}^+ + \text{O}$). These results for CO_2 agree reasonably well with Hotop and Niehaus⁷⁷. In the case of CO_2 , the available energy requires the dissociated products to be produced in their ground states, in particular $\text{O}(^3\text{P})$ and $\text{O}^+(^4\text{S})$. This is not necessary in the case of N_2O . It is also not certain in either case to what extent the dissociated products are produced directly or in subsequent predissociation of the parent ions CO_2^+ and N_2O^+ ^{78,79}. However if we assume that the products are produced directly in their ground electronic state, then in 53% of the reactions of N_2O and 30% of the reactions of CO_2 , spin angular momentum conservation alone does not require that the product electron preserve the spin orientation of the $\text{He}(2^3\text{S})$ metastable. The fact that measured electron polarizations from these reactions are no less than 85% (if not 100%) of the $\text{He}(2^3\text{S})$ polarization supports the electron exchange model.

3. $\text{He}(2^3\text{S})$ with CO

CO is the only reactant gas for which the electron polarization is significantly lower than that from the other gases tested, in particular N_2 . The data of Fig. 6 to 14 demonstrates that this difference is independent of pressure, type of excitation source, 2^3S density, ion density, and reaction length. Therefore, it cannot be explained by depolarizing collisions in the afterglow tube prior to extraction. Comparison of the results in

Fig. 7 for N_2 and CO shows that the degree of spin polarization transfer for CO may be as low as 70%, assuming 100% for N_2 .

A possible explanation of the observed results is the near resonance of the $He(2^3S)$ and the $CO^+(B^2\Sigma^+)$ state ($B, v' = 0$ at 19.67 eV; $v' = 1$ at 19.88 eV) as pointed out by Richardson and Setser^{75b}. Therefore excitation transfer is likely to occur, forming a Rydberg level of CO which may subsequently autoionize or dissociate into $C^* + O$. Excited carbon atoms are observed in 4% of the $He(2^3S) + CO$ reactions⁸⁰. The relative population of the $CO^+(B)$ state which has been estimated at 27%^{75b} and 53%⁸⁰ is sufficient to explain the 30% reduction in spin polarization observed if this level is produced by autoionization of a Rydberg state. It is difficult to say whether or not the measured vibrational populations of the $CO^+(B)$ state^{75b}, ($v_0:v_1 = 100:17$), are in accord with the Franck-Condon factors^{72a}, ($v_0:v_1:v_2 = 100:40:15$), because the populations are limited primarily by the available energy. (The $v = 1$ state is .061 eV above the $He(2^3S)$ state.) Further study of this reaction using polarization analyses of the radiation from the $CO^+(A)$ and $CO^+(B)$ states may clarify the role of excitation transfer.

B. Spin Polarization Transfer in Surface Ejection

From the data of Fig. 7 , the polarization of surface-ejected electrons, P_s , emitted as a result of collisions of the $\text{He}(2^3\text{S})$ atoms with the brass extraction aperture , is seen to lie in the same band of polarizations observed from chemiionization of the atoms and molecules studied. If our earlier interpretation is correct, that spin angular momentum is totally conserved (or very nearly so) in the chemiionization reactions studied, then it follows that it is also conserved to a large degree in electron-ejecting $\text{He}(2^3\text{S})$ -surface reactions. This result is at variance with accepted theoretical models for electron ejection from atomically clean metallic surfaces²⁶, in which the electron is thought to come from the conduction band of the metal with no spin orientation preference. For our dirty surfaces, we are inclined to interpret the observed high degree of spin angular momentum conservation in terms of chemiionization of loosely bound adsorbed species, in partial agreement with the work of Allison et al.⁴⁰

They measured the energy spectrum of electrons ejected from a contaminated stainless steel surface and observed a double-peaked distribution. They attributed the higher energy electrons (4-13 eV) to chemiionization of adsorbed species and the lower energy electrons (0-4 eV)

to Auger neutralization of the product ion from the chemi-ionization reaction, with the simultaneous ejection of an electron from the conduction band. However, in their measurement, the high energy peak accounted for only 1/3 of the total yield of electrons.

Donnally et al.⁴¹ have previously reported a spin polarization transfer of 66% from an oriented $\text{He}(2^3\text{S})$ atomic beam to electrons ejected from contaminated gold and tungsten surfaces. Allowing for the experimental uncertainty in the measurements reported here, we conclude that for our contaminated brass extractor surface, $80 \pm 10\%$ of the surface-ejected electrons preserve the spin orientation of the incident $\text{He}(2^3\text{S})$ and probably come from chemiionization of adsorbed atoms. Thus there seems to be qualitative agreement between all three experiments that many electrons ejected from contaminated surfaces result from chemiionization. However the results of the present experiment and those of Donnally et al. suggest that a much lower fraction of electrons come from the metal itself, than would be expected from the energy distribution measured by Allison et al., perhaps reflecting only that the surfaces employed in the three experiments are different from one another.

It is quite desirable to extend these polarization transfer measurements to include polarized $\text{He}(2^3\text{S})$ and He^+ ions incident on atomically clean surfaces. This would

further test the assumed identity of the ejection process for these two species (see Section I and references 26-29) and test for any spin correlation between the two electrons involved in the Auger neutralization process for an incident ion. If there is indeed little or no correlation, then polarized $\text{He}(2^3\text{S})$ metastables incident on a variety of clean surfaces would be a sensitive test of the degree of resonant ionization of the metastable upon approach to the surface vs the degree of Auger de-excitation of the metastable. The former would yield unpolarized electrons whereas in the latter process the electrons would be polarized.

C. Collisional Depolarization Processes

Several collision processes were suggested in Section V that would contribute to the decrease in observed polarization with increasing ion density and reaction length. It is our purpose here to estimate upper limits on the cross sections for these processes by attributing the entire decrease in polarization to each process separately. The results are briefly compared with the available data.

The polarization $P_{(z)}$ of electrons that have undergone spin exchange with ions for a distance z in the after-glow tube can be shown to be given approximately by

$$\ln(P_0/P_{(z)}) = \frac{Q_{ex}^i v}{\alpha V_0} N_0^+ d_A \left(1 - e^{-\frac{z}{d_A}}\right) \quad (15)$$

where P_0 is the initial polarization of electron, N_0^+ is the initial density of ions, d_A is the decay length (cm) for ambipolar diffusion, v is the relative ion-electron velocity, V_0 is the average or bulk flow velocity in the tube, $\alpha = 1.6$ is a geometric correction factor for the parabolic flow velocity in the tube, and Q_{ex}^i is the cross section for electron ion exchange. These cross sections have been calculated for all the data points from Figs. 11 to 14. The smallest value of the upper limits thus obtained for each ion is 2 to $3 \times 10^{-14} \text{ cm}^2$, with the exception of

N_2O for which it is $8 \times 10^{-14} \text{ cm}^2$.

These values substantially lower than the value of $5 \times 10^{-13} \text{ cm}^2$ calculated by Goldwire⁸¹ for the $^3\text{He}^+$ ion with electrons at 300° , and the recently measured value of $3 \times 10^{-13} \text{ cm}^2$ for Sr^+ ions⁸². The cross sections for He^+ and Sr^+ are expected to be among the largest for ion electron exchange due to their outer ns electron. It is interesting to note that the behavior of the H_2^+ ion apparently does not closely resemble that of the He^+ ion with respect to electron exchange.

If the polarization decrease in the case of N_2O is attributed entirely to spin exchange with the neutral $N(^4S_{3/2})$ produced, the upper limit on the cross section is $Q_{\text{ex}}^n = 4 \times 10^{-14} \text{ cm}^2$. This result is obtained by assuming the initial density of N atoms is one half the metastable density, N_m , and that there is no wall recombination of N atoms. Then the resulting polarization $P_{(z)}$ due to neutral spin exchange is

$$\ln P_o/P_{(z)} = \frac{Q_{\text{ex}}^n v z \frac{1}{2} N_m}{\alpha v_o} . \quad (16)$$

Q_{ex}^n is of the same order as the alkali spin exchange cross sections at thermal energies⁸³.

SPIN POLARIZATION TRANSFER REACTIONS

PART II:

A Polarized Electron Source

I. INTRODUCTION

There has been increasing interest, particularly in the past five years, in spin polarization effects in electron atom scattering. We describe here the flowing helium afterglow as a source of polarized electrons, that has produced beam currents of 1 to 3 μA with electron polarizations of 30 to 20 percent with an energy spread less than 0.5 eV. In this introduction, we will briefly summarize the types of spin dependent processes that can be studied and then several other polarized electron sources that have been developed.

Most investigations thus far have been concerned with one of two spin dependent interactions: electron exchange, as in electron scattering from alkali atoms⁸⁵⁻⁹¹, and the spin-orbit interaction, as in electron scattering from mercury⁹² or from neon near energy resonances⁹³. The spin dependence of these interactions has also been studied in electron scattering from molecules⁹² and surfaces^{92,94}.

For even the simplest case of elastic scattering involving electron exchange or a spin-orbit interaction, three quantities must be determined to completely define the scattering process. These are: a) the amplitude f for "direct" scattering with no spin change of the scattered electron, b) the amplitude g for spin reversal

between the incident and scattered electrons, and c) the relative phase of f and g . Without a source of polarized electrons, specifying all three quantities is difficult in the case of electron alkali scattering, requiring two separate experiments^{86,87}, and impossible in the case of spin-orbit scattering. The need for polarized electron sources is even more important for inelastic exchange scattering^{88,89} or for combinations of exchange and spin-orbit scattering⁹⁰ involving four or six amplitudes respectively.

Many processes have been proposed as bases for polarized electron sources^{47,95}. Several that seem most promising for low energy scattering are 1) photoionization of alkali atoms by circularly polarized light (Fano effect)⁹⁶, 2) field emission⁹⁷ and photoemission⁹⁸ from magnetic materials, 3) Mott scattering from unpolarized atomic beams⁹⁹ and 4) the chemiionization of atoms by optically pumped helium metastables to be described here. Not only does each source have its own strengths and weaknesses, but each type of scattering experiment places particular requirements on the polarized source to be used as well. For example electron injection into high energy accelerators requires pulses of $\sim 10^9$ electrons

for one microsecond at a fairly slow repetition rate¹⁰⁰. Therefore, conventional figures of merit should be viewed with caution when comparing sources without a particular experiment in mind.

The common figures of merit are derived from the electron-optical and signal-to-noise characteristics of the source. The best measure of the usable current from a source is given by the "brightness,"¹⁰¹ defined as the current density per unit solid angle. For a beam of circular cross section, the brightness is given by

$$B = \frac{I}{\pi^2 (r_o \theta_o)^2} \quad (17)$$

where r_o is the minimum beam radius (i.e. at the source) and θ_o is the angular spread at that point. The quantity $\epsilon = r_o \theta_o$ is called the "emittance" of the beam. If the beam is to be used in a scattering experiment at an energy and magnetic field different from that of the source, the effects of these fields on ϵ must be considered. If the electrons emerge from the source with an energy E_o in an axial magnetic field H_o and are to be scattered at an energy E in a region of negligible magnetic field, then the effective emittance¹⁰⁰ at the

position of the scattering experiments is

$$\epsilon_{ff} = r_o \theta_o \left(\frac{E_o}{E} \right)^{1/2} \left(1 + \frac{1}{2} \frac{e}{m} \frac{r_o H_o}{v_o} \right) \quad (18)$$

where $v_o = (2E_o/m)^{1/2}$.

To compare sources of different polarization, the effective intensity is given by $P^2 I$ because the spin dependent signal from a scattering event varies linearly with the polarization whereas the statistical signal-to-noise varies as the square root of the current. Other considerations that can be important are the energy spread of the beam and the ability to reverse the spin polarization direction without influencing the beam trajectory. Several recent articles have attempted to compare various sources based on these figures of merit^{95c,d,e,100}.

In the remainder of Part II, we describe the use of the optically pumped, flowing helium afterglow as a source of polarized electrons. It was shown in Part I that spin polarization as high as 30% has been obtained from the chemiionization of several atomic and molecular gases by optically oriented $\text{He } 2^3S_1$ metastables. By suitable choice of afterglow parameters, a current of several microamps can be extracted with an energy spread of a few tenths of an electron volt or lower. These results are a major

improvement over the initial investigation by McCusker et al.²⁻⁴ in which electrons were extracted from an active helium discharge. Further, since the direction of spin polarization is determined by the direction of circularly polarized light used, the spin polarization can be simply and rapidly reversed in order to eliminate any instrumental asymmetry that may be present in an experiment. Finally the entire apparatus is extremely simple and relatively inexpensive. The only major component is a large mechanical pump. Therefore this source is well suited for low energy electron scattering experiments that require high currents and high energy resolution.

II. EXPERIMENTAL TECHNIQUE

A. Overview

The apparatus used is the same as that described in Part I. We will emphasize here only those details pertinent to optimizing the flowing afterglow as a source of polarized electrons. Many effects that could limit electron polarization are discussed in Part I. The schematic of the afterglow tube shown in Fig. 15 is similar to that of Fig. 1 except that a second pumping lamp has been added and the position of the reactant injector is changed. Helium 2^3S and 2^1S metastables are produced by either a microwave discharge or an electron gun. The 2^3S state is then optically pumped by circularly polarized resonance radiation to preferentially populate either the $m_s = +1$ or $m_s = -1$ state. Electrons are produced by the chemiionization of a reactant gas injected near the extraction aperture. The extracted electrons are focused by two Einzel lenses and accelerated to 120 keV in order to analyze their spin polarization by Mott scattering. The second lens can also be operated as a filter lens to measure the energy spread of the beam.

B. Helium Metastable Source

The microwave cavity was used for most of the data presented here because it produces a low singlet to

triplet metastable ratio of .06 at a flow tube pressure of .10 torr compared to a ratio of .5 for the electron gun source. This limits the electron polarization to roughly 70% of the $\text{He}(2^3\text{S})$ polarization when the electron gun source is used.

This 2^3S density obtained with the microwave cavity is nearly independent of microwave power above 30 watts. The 2^3S density at the extractor is then limited by diffusion losses to the flow tube walls and hence by the distance from the source for a given beam tube pressure. For a source-to-extractor separation of less than 30 to 40 cm, the polarization is degraded by source produced electrons that cannot be removed prior to extraction and by relaxation of the $\text{He}(2^3\text{S})$ polarization due to electron excitation and exchange. Therefore a trade off is reached between polarization and current. The smallest source to extractor separation tested was 30 cm. with a configuration shown in Fig. 16 .

The same general limitations apply to the electron gun source. In this case, the 2^3S density increases linearly with emission current, so that higher densities could be obtained by use of a larger filament or multiple filaments. (The filament used was .005 in. in diameter by 1.5 in. long, operated at an emission current of 0.12 A and accelerating voltage of 75 V.) However, the lateral dimension of the excitation region, which normally extends

Figure 15: Schematic of flow tube used to obtain maximum polarization and current.
Refer to Figs. 1 and 2 for a schematic of the whole apparatus and a detail view of the electron extractor.

Figure 16: Schematic of an early version of the flow tube without a reactant gas injector.

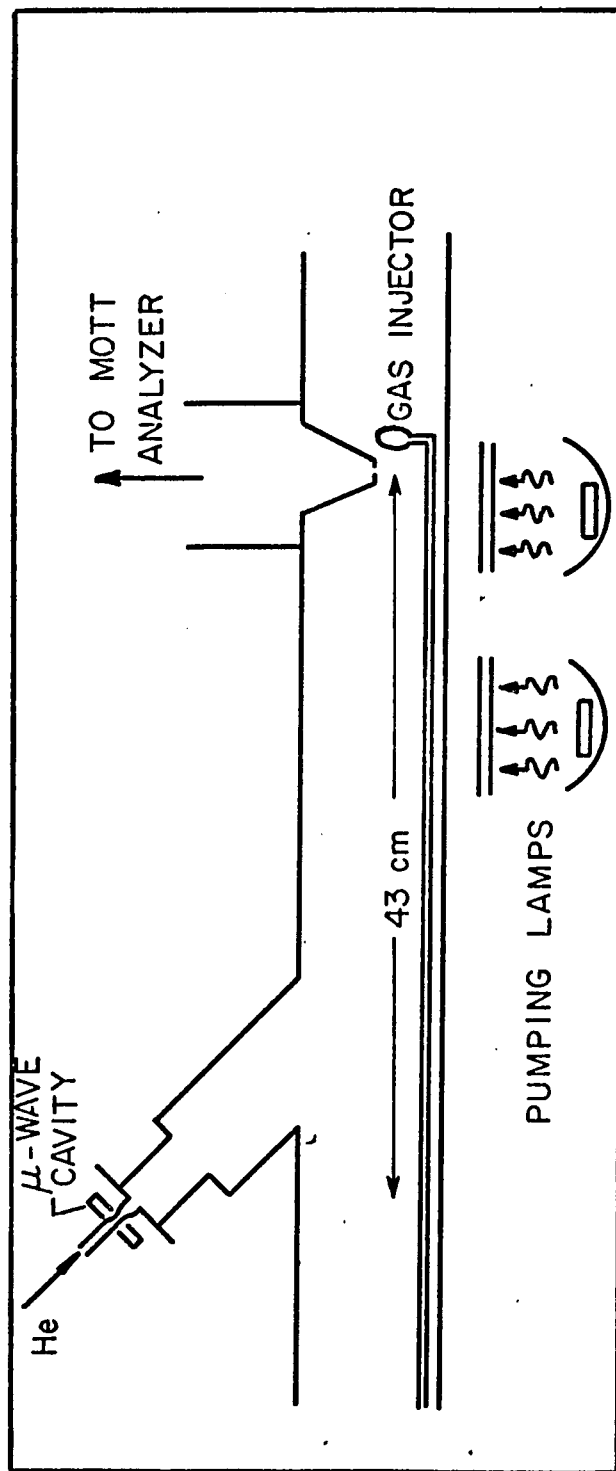


FIGURE 15

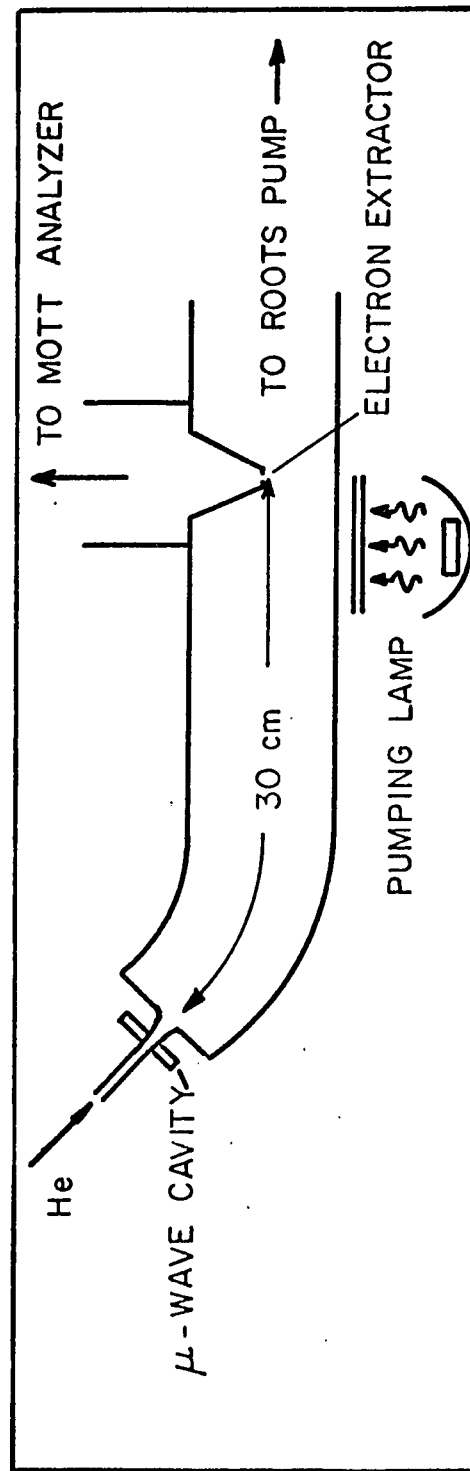


FIGURE 16

some 10 cm from the filament, also tends to increase with emission current.

A similar trade off between polarization and current is made as a function of pressure for a given source position. As discussed in Part I, Section III, the unpolarized, source-produced electrons account for less than 5% of the extracted current for pressures below .15 torr, but they increase rapidly for higher pressures because diffusion to the walls is slower. This can be compensated at least partially by the use of rf heating near the source to enhance the ambipolar diffusion rate. However the rf must be shielded from the chemiionization region to avoid enhanced diffusion losses of the polarized electrons produced there. Other limiting effects on the polarization at higher pressures are discussed in detail in Part I, Section IV and V and mentioned in the following sections on optical pumping and electron extraction.

C. Optical Pumping

The 2^3S state is optically pumped in the usual manner⁹ by the absorption of circularly polarized 2^3S-2^3P resonance radiation with subsequent return to the 2^3S state by spontaneous emission. The use of two pumping lamps instead of one increases the electron polarization by a factor of about 1.2. Each lamp was filled to 10 torr of Helium and excited in the tank circuit of a 100 MHz multi-

vibrator which dissipates 400 watts^{4,102}. Typical photon flux in the 2^3S-2^3P resonance line is 10^{17} photons/sec. The lamps must be well shielded to prevent rf heating of the electrons in the afterglow. This can reduce the extracted current by a factor of 10 or more due to enhanced diffusion to the walls.

A weak magnetic field of 5 gauss in the direction of the pumping light is used to overcome the earth's magnetic field so that there is a unique quantization axis. In the present experiment, electrons are extracted along the field direction so that they are longitudinally polarized. Transverse polarization could be obtained directly by rotating the pumping lamps by 90° about the flow tube axis or by extracting the electrons along the flow tube axis. In either case, a small net magnetic field is desired in the direction of the pumping light (and therefore perpendicular to the extracted beam velocity) to maintain a unique quantization axis. By nulling the earth field, this net applied field can be made arbitrarily small thereby reducing any deflection of the extracted beam.

As discussed in Part I, Section IV any one of several processes could be responsible for limiting the maximum observed polarization to about 30% and for the relatively small effect of a second pumping lamp. Two of these are fundamental processes that limit the optical pumping efficiency at high pressure and high metastable density.

Collisional mixing of the $2^3P_{0,1,2}$ states becomes significant for pressures above 0.5 torr^{8,9}. This is not a problem here however, since our results for extracted current discussed in the next section indicate that as a polarized electron source, the afterglow does not need to be operated at pressures above .2 torr. On the other hand, radiation trapping of the 2^3S-2^3P pumping light is thought to be responsible for the decrease in polarization with increasing metastable density shown in Fig. 11.

D. Extraction of High Currents

1. Gas Injection

The polarization and current that can be realized depend somewhat on the particular gas used. Results for N_2 and CO_2 are presented in the next section. (The polarization obtained for several other common gases was described in Part I.) However, some general comments apply to all gases. First, by placing the injector downstream of the extractor as shown in Fig. 15, the helium metastables can be completely reacted very near the orifice by backstreaming gas. The flow rate of gas injected in this configuration is typically 4 torr liters/sec which is 10% of the He flow. This avoids losses of metastables and electrons by diffusion to the gas injector surface when it is placed upstream of the extractor.

Second, a gas should be chosen that has a large cross section for chemiionization as well as for rotational and vibrational excitation by low energy electrons. In this way electrons are produced in a small region and then rapidly thermalized from their initial energy, which ranges from 1 to 9 volts depending on the particular gas. This also has the desirable effect of reducing the electron loss by ambipolar diffusion. For example, from the measured fractional energy loss per collision^{84,103} a simple calculation shows that the energy of an electron will be reduced from 1.5 eV to .05 eV in an average of 60 collisions with CO₂ compared to 1.2×10^4 collisions for He.

2. Electron Extraction

The electrons extracted from the afterglow tube pass through the small extraction aperture and are accelerated by a voltage, V_a , of typically 500 volts. This beam energy was achieved by floating the entire flow tube and extraction aperture negative with respect to the grounded extraction anode¹⁰⁴. The beam currents that are reported here were measured to the inner cup (12 mm diameter) of a movable collector shown in detail in Fig. 2. The current to the inner cup was typically 5 times the current to the outer one (25 mm diameter). An upper limit on the beam emittance for the current to the inner cup can be estimated by the product of the cup radius and the maximum angular divergence,

which is determined in this case by the diameter of the cylindrical focus electrode. This upper limit is 20 mrad cm. A lower limit of the emittance is the product of the radius of the extraction anode (.16 cm) and the minimum angular divergence given by the ratio of axial and perpendicular velocities, v_a and v_{\perp} , such that $\theta \approx v_{\perp}/v_a = (E_{\perp}/E_a)^{1/2}$. If E_{\perp} is equal to the measured energy spread of the beam ($\leq .5$ ev) and $E_a = 500$ ev then $(r\theta)_{\min} \approx 5$ mrad cm at 500 eV. No attempt was made to improve the electron-optical quality of the beam or increase the extracted current by changes in the geometry of the extraction anode or the first lens element.

According to the extraction scheme just described, the electrons in the afterglow simply diffuse through the extraction aperture before being accelerated by the extraction field. It was observed that a large increase in current can be obtained if the afterglow tube is biased with a potential, V_b , of 10 to 20 volts negative with respect to the extraction aperture. For the largest aperture used (2.0 mm orifice) a maximum in the extracted current as a function of bias voltage indicates some type of focusing effect is present. Since there is very little degradation of polarization for bias potentials up to 20 volts, it is obvious that the bias increases extraction efficiency rather than initiating a discharge.

Since most of the potential drop in a gas diode occurs at the cathode and not the anode, it was not anticipated that electrons could be accelerated out of the afterglow in this manner. However, the energy distribution of the extracted beam shows that the electrons are in fact extracted from a plasma at the potential of the flow tube, independent of the extraction aperture potential. It should be noted that the entire extraction cone that protrudes into the afterglow tube, except for the 0.5" diameter aperture disc, was coated with PVC insulation. It is not known what effect a larger exposed surface area would have on the extraction characteristics.

In Part I, electron polarizations were shown to decrease rapidly at pressures above .125 or .15 torr depending on the extraction aperture size. This effect was described in some detail and attributed to ionization or excitation of the background gas by the electron beam in the region between the extraction orifice and the extraction anode. Elimination of this problem by increasing the effective pumping speed or by lowering the accelerating voltage offers the possibility of improved source performance and should be investigated further.

E. Filter Lens

The filter lens (Fig. 17) used in this experiment to measure the energy distribution of the electron beam was

designed by J. Kessler and is very similar to the lens of Kessler and Lindner⁴⁵ and Simpson and Marton⁴⁴. The principle of operation for this type of lens is discussed in detail by Simpson¹⁰⁵. It is best viewed as two short focus lenses symmetrically placed about a retarding plane. Let E_0 be the beam energy relative to the retarding plane potential, U_r , such that at $U_{r_0} = -E_0$ the electrons have zero energy at the retarding plane. Then, for U_r near $-E_0$, the potential of the bias electrode, U_b , is chosen so that the first lens images the entrance aperture on to the center aperture. Those electrons with sufficient energy to pass through the retarding plane are imaged by the second lens on to the exit aperture. U_b is typically within 2% of U_{r_0} . The "range" of the lens is the maximum beam energy in the retarding plane for which the beam diameter there is smaller than the center aperture. For a monoenergetic beam, the range is observed as the range of retarding voltages near cut-off for which the transmission is a constant (to within 10%). The range and resolution of the lens are determined primarily by the entrance aperture size.

For proper operation of the lens, the 5 gauss field used for optical pumping is turned off. The residual component of the earth field perpendicular to the beam necessitated substantial beam steering to center the beam on the entrance aperture and introduced some dependence of the optimum resolution on beam steering and focus. The bias

potential U_b for the best resolution was $U_b = -490$ for $E_0 = 500$ V. The dimensions of our lens are given in Fig. 17. In units of $1/16''$, the diameter of the entrance and retarding plane apertures was 0.64. The retarding plane aperture was chosen twice as large as Simpson and Marton.⁴⁴ to minimize beam steering effects. From Table I of Simpson and Marton⁴⁴ we expect a range of 1 to 4% of E_0 and a resolution (90% to 10% transmission) of $\sim .05\%$ of E_0 . Figure 18 shows a transmission curve under optimum conditions for electrons produced by chemiionization of N_2 . The range is 13 V or 2.6% of 500 V and an energy spread of .36 V or .07%. As will be shown in the next section, this energy spread probably represents the resolution of the lens as is expected from Simpson and Marton's results. To accurately measure the energy spread of beams from the afterglow will require improved magnetic shielding so that a resolution of 20 mv can be obtained.

Figure 17: Filter lens

Figure 18: Transmitted current through filter ions vs retarding voltage. Curve a: electrons from the chemiionization of N_2 . Curve b: electrons ejected from the surface of the extraction aperture by $He(2^3S)$. Filter lens bias electrode at -490 V, beam energy is 500 V. Extraction aperture is 2.0 mm by 0.2 mm.

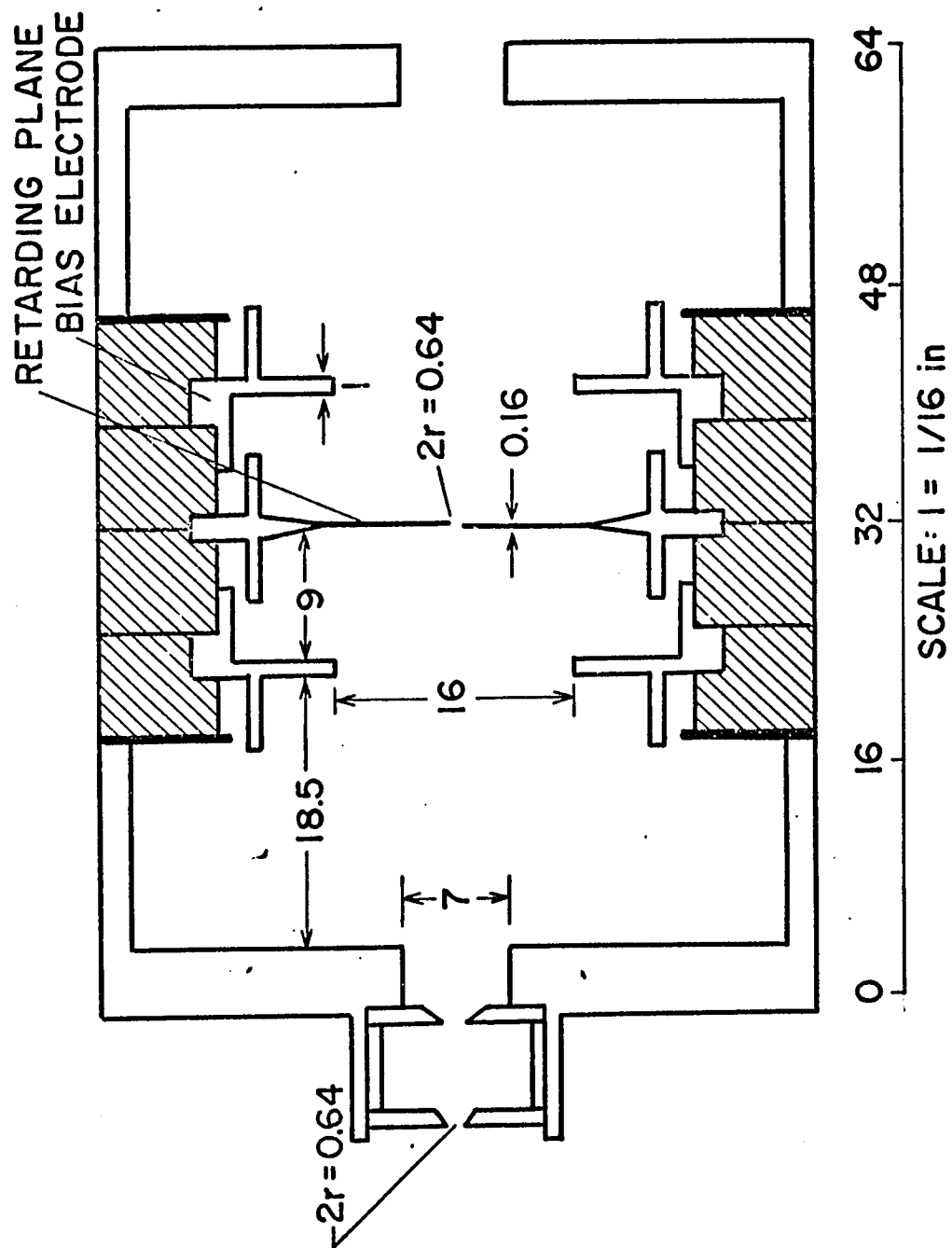


FIGURE 17

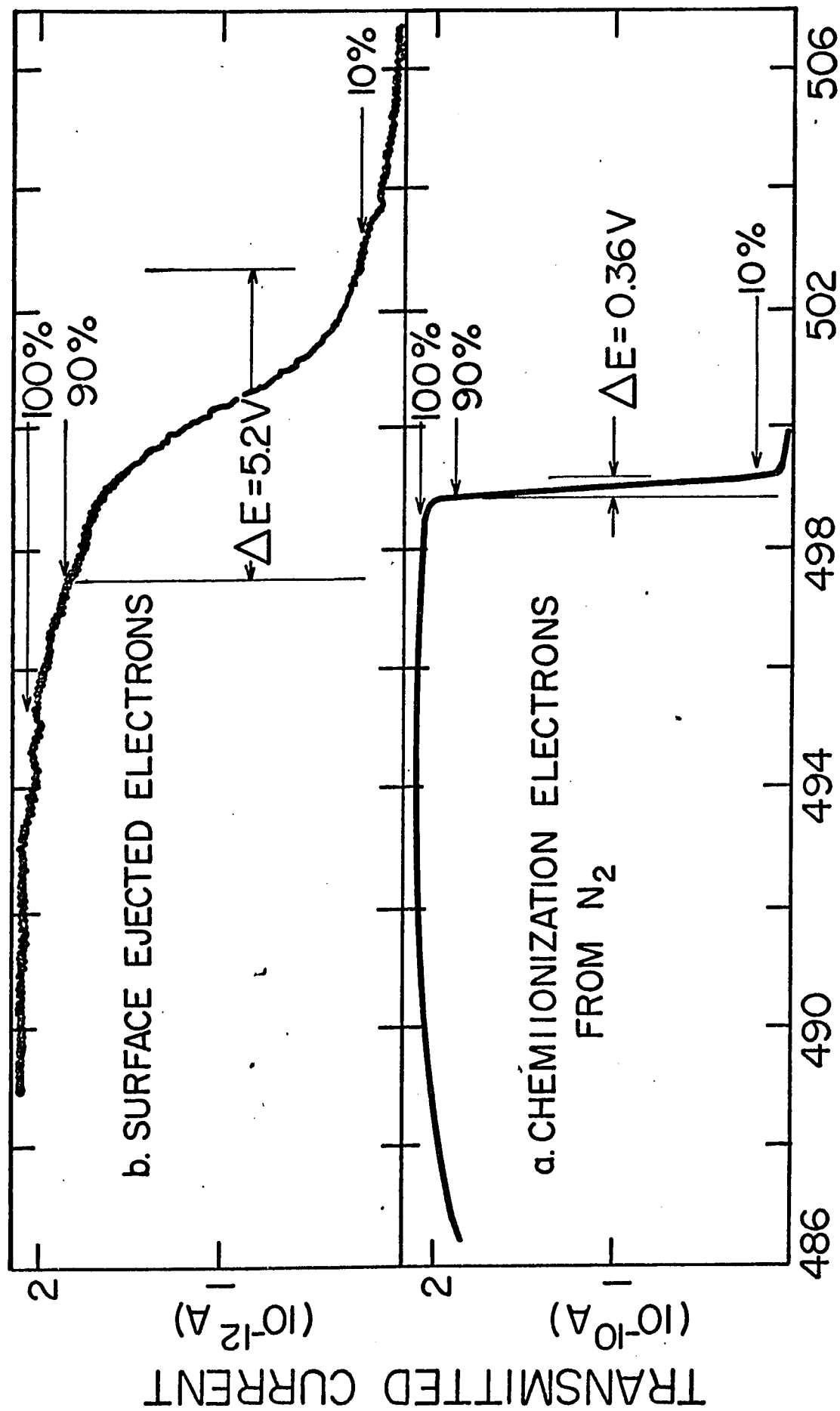


Figure 18

III. RESULTS

A. Efficiency of Electron Extraction

Although the current extracted from the afterglow is reproducible, it is strongly dependent on many parameters therefore graphs of extracted current vs a single parameter can be misleading. One set of typical data is first plotted as a function of the accelerating voltage V_a and the bias voltage V_b to show the qualitative difference in the effect of these two potentials. We then compare the extracted current under several operating conditions to the total current of helium metastables in the flow tube. It will be seen that extraction efficiencies on the order of 50% can be obtained.

In Fig. 19 the extracted current is plotted vs V_a for data taken with $V_b = 0$, an aperture 1.5 mm (diameter) by 1.5 mm (length), and CO_2 injected 3 cm upstream from the extractor. The current is also shown as a function of V_b at $V_a = 0$ and 500 volts. As expected the current is nearly independent of V_a since this field does not penetrate into the body of the afterglow. A value of $V_a = 500$ volts was chosen for normal operation only to minimize deflections of the beam in the earth's field. On the other hand the

Figure 19: Extracted current vs a) accelerating potential V_a and b) bias potential V_b . The current was produced by the chemi-ionization of CO_2 at 3 cm from the extractor, using a 1.5 mm x 1.5 mm extraction aperture.

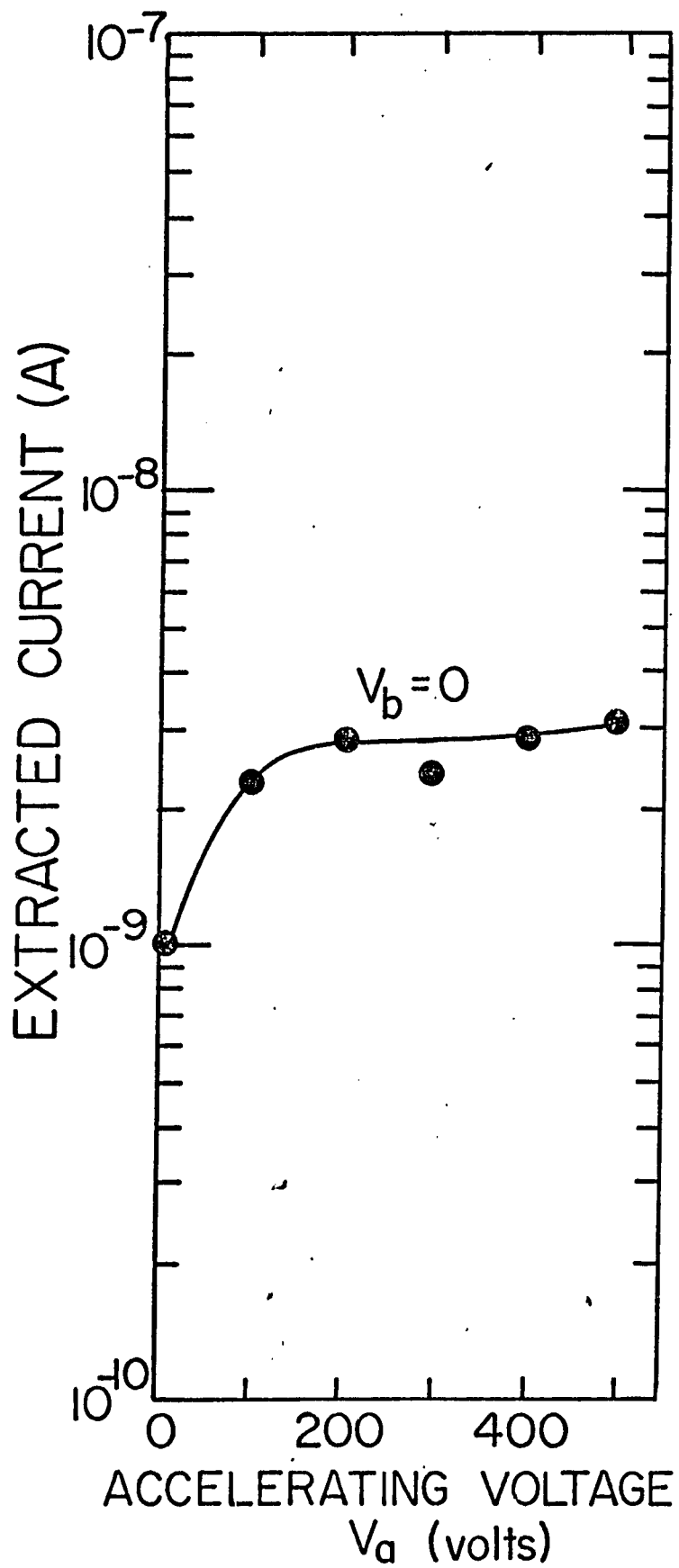
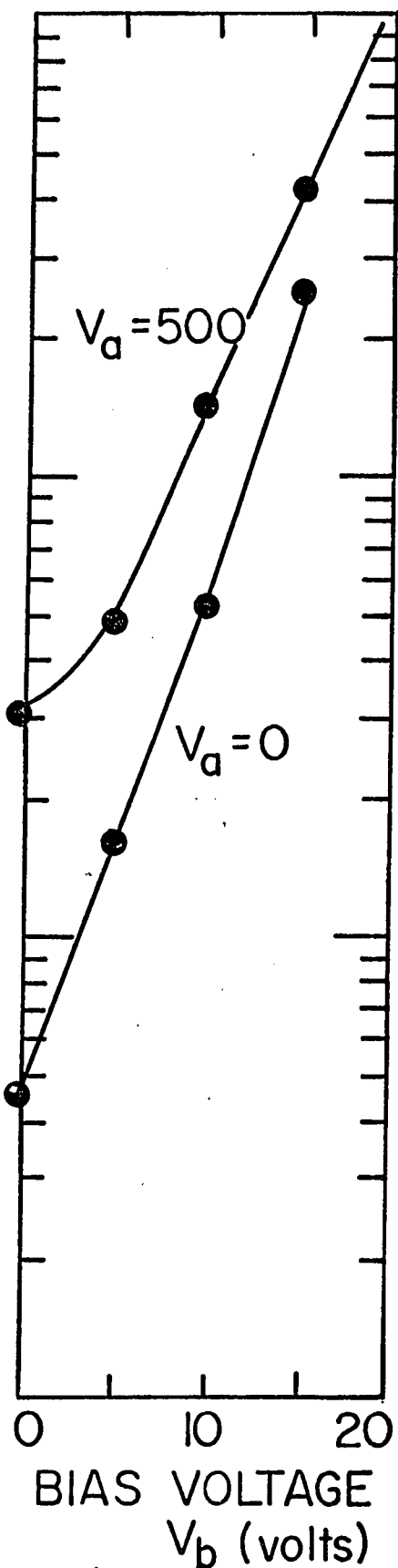


FIGURE 19a.



19b.

bias potential V_b is very effective in extracting electrons.

The maximum possible extracted current, $I_{\max}(z)$, can be calculated by integrating, over the cross section of the tube, the flux of metastables that reach the point z .

Assuming one electron is produced per metastable, then

$I_{\max}(z)$ is

$$I_{\max}(z) \approx \int_0^{2\pi} \int_0^R v(r) N(z, r) r dr d\theta \quad (19)$$

where

$$V(r) = 2v_0 \left(1 + \left(\frac{r}{R}\right)^2\right)$$

$$N(z, r) = N_0(z) \cdot J_0\left(\frac{2.4r}{R}\right)$$

and v_0 is the average flow velocity, $N_0(z)$ is the metastable density at the center of the tube at z , and J_0 is the zeroth order Bessel function. (See Appendix A for a discussion of $V(r)$ and $N(z, r)$.) The measured metastable density, $\bar{N}(z)$, is the average density across the tube and is equal to $0.59 N_0(z)$. Integration of (19) gives

$$\begin{aligned} I_{\max}(z) &= 3.2 \times 10^5 \bar{N}(z) \quad (\text{electron/sec}) \quad (20) \\ &= 5.2 \times 10^{-14} \bar{N}(z) \quad \text{Amp} \end{aligned}$$

assuming the tube radius, R , is 5 cm and $v_0 \approx 4.2 \times 10^3$ cm/sec. The metastable density at the extractor ($z = 0$) is estimated from the measured absorption of the pumping

lamp at $z = 21$ cm and the measure diffusion decay length

d. The uncertainty in the results is roughly a factor of 2.

In Table II , the measured current is given as a percent of I_{\max} at the extractor for several conditions of afterglow pressure, reactant gas, aperture size and bias voltage, all taken with the injector placed 1 cm downstream of the extractor. For the 2 mm orifice and CO_2 as a reactant gas, a small bias voltage--in this case 5 volts--increases the current by a factor of 200 so that roughly 40% of all electrons created in the tube are extracted into a usable beam. We conclude that no major increases in extracted current can be obtained by either larger extraction apertures or redesigned extraction optics although the latter may improve the electron-optical quality of the beam. The order of magnitude difference in the currents obtained with CO_2 and N_2 is probably due to the much slower thermalization of electrons in N_2^{84} resulting in a larger diffusion loss.

B. Energy Spread of the Extracted Beam

Figure 18 shows two examples of the transmitted current through the filter lens as a function of retarding voltage: (a) electrons from the chemiionization of N_2

TABLE II
Electron Extraction Efficiency

		Pressure (torr)			
		.90	.100	.125	.150
He (2 ³ S) Decay Length (cm)		5.0	5.5	6.5	8.2
He (2 ³ S) Density: $\bar{N}(0)$ (cm ⁻³)		1.1 x 10 ⁷	2.7 x 10 ⁷	1.3 x 10 ⁸	5.1 x 10 ⁸
$I_{\max}(0)$ (A)		5.8 x 10 ⁻⁷	1.3 x 10 ⁻⁶	7.0 x 10 ⁻⁶	2.7 x 10 ⁻⁵
Extraction Aperture	Bias	Reactant Gas	Extraction Efficiency % of $I_{\max}(0)$		
2.0 mm x 0.2 mm	Biased	CO ₂	17	37	37
	↓	N ₂	2.6	8.1	
		No Gas	.64	.45	
	No Bias	CO ₂	1.04	.2	
	↓	N ₂	.6	.74	3.7
		No Gas	.19	.12	.11
1.5 mm x 1.5 mm	Biased	CO ₂		2.9	2.7
	"	N ₂	1.4	.71	.45
	No Bias	CO ₂		.11	
	↓	N ₂		.081	.27
		No Gas		.045	.03

injected 1 cm downstream from the extractor and (b) electrons ejected from the extractor orifice surface when no reactant gas is present. All of the measurements were taken with the 2.0 mm orifice at a pressure of .125 torr. The energy spread, ΔE , for surface ejected electrons is typically 3 to 5 eV. On the other hand, for the molecular gases CO_2 , N_2 , and C_2H_2 injected at -1 cm from the extractor, $\Delta E = .35$ to .5 eV. The initial energies of electrons from these gases are primarily 1 to 3 eV for CO_2 1 to 5 eV for N_2 and at 9 eV for C_2H_2 ^{72a,73,106}. Since the measured energy spreads are nearly the same for all three species, this result indicates that the electrons have been thermalized before extraction. This is confirmed by a measurement of ΔE for CO_2 as a function of injector position from $z = -1$ cm to $z = 15$ cm. The energy spread decreased from .5 eV to .35 eV with increasing distance. For a path length of 15 cm, corresponding to a thermalization time in the flow tube of 3.5 msec, the electrons are in thermal equilibrium with the background gas at 300°K. Therefore the measure energy spread is either a property of the extraction geometry or the resolution of the filter lens which is the most likely since the lens resolution is expected to be on this order.

When the afterglow tube was biased negatively relative to the extraction aperture, the energy of the extracted beam increased by the same amount but the energy spread remains unchanged. Therefore, for the same conditions of electron extraction at which the polarization and current measurements were made, we conclude that the energy spread of the beam is less than .5 eV and may be as small as .025 eV.

C. Polarization and Current

In Figs. 20 to 24 the polarizations and extracted currents obtained for several afterglow conditions are presented. For each data point, the afterglow pressure and the bias potential are given in parentheses. For current greater than 10^{-8} amps, the beam must be defocused at the filter lens to maintain a counting rate at the Mott scattering detectors less than $2 \times 10^4 \text{ sec}^{-1}$. No evidence of any polarization dependence on the focusing condition was found. Therefore the measured polarizations at high currents are a true sample of the beam polarization.

The data in Fig. 20 was taken with a 30 cm long afterglow, a microwave source, a 1.5 mm by 1.5 mm extraction aperture, but with no gas injected and no bias potential

applied. Most of the points were taken with the same 45° elbow termination on the flow tube as shown in Fig.16 . Two types of nozzles were used as indicated in the inset. The reduction in polarization at low pressures for the converging-diverging nozzle relative to the horn shaped nozzles depends as much on the method of mounting the nozzle as it does the shape of the nozzle itself. (Compare this mounting to that used in Fig.23 to24.) For this relatively short afterglow, any reduction in the diffusion losses near the source will tend to increase the density of source produced electrons in the afterglow and increase the spin relaxation in the optical pumping region thus lowering the measured electron polarization. Four data points in Fig. 20 were taken with the 45° elbow replaced by a 15 cm straight section but with the horn nozzle. In this case the low polarization at low pressure is probably due to optical pumping relaxation by the 1.08μ (2^3S-2^3P) radiation from the microwave discharge that propagates down the tube axis.

For all of the remaining graphs, the afterglow configuration was similar to that in Fig.15 with CO_2 or N_2 injected 1 cm downstream of the extractor. In Fig.21 to 23 the extraction aperture is 1.5 mm diam. by 15 mm

long. The electron gun source results, shown in Fig. 21, demonstrate that the maximum polarization is limited to $\sim .22$ by the high ratio of 2^1S to 2^3S metastables. The results for the microwave discharge source used with the 1.5 mm by 1.5 mm extraction aperture are shown in Figs. 22 and 23. In Fig. 22 a horn shaped nozzle was mounted directly onto the "Y" section whereas in Fig. 23 a converging-diverging nozzle was used with an additional 10 cm long, 5 cm diameter tube between the nozzle and the "Y" section. The data points for both configurations lie in the same band with slightly higher currents and lower polarizations obtained with the shorter afterglow.

Finally in Fig. 24 the results for a 2.0 mm diam. by 0.2 mm thick orifice are given. The microwave cavity is mounted as in Fig. 15. An order of magnitude improvement in the extracted current was obtained with this extractor. As shown in Table II the extraction efficiency is on the order of 40% so that another order of magnitude improvement in current is not expected. The reduction in polarization at high pressure and high current is due to the ionization in the region between the extraction aperture and the extraction anode as described in Part I, Section V.

Figure 20: Electron polarization vs extracted current. Flow tube length = 30 cm, termination as shown in inset. Microwave source used with 1.5 x 1.5 mm aperture. No gas injected and $V_{\text{bias}} = 0$. Flow tube pressure is given in parentheses in m torr.

Figure 21: Electron polarization vs extracted current. Electron gun source used with 1.5 x 1.5 mm aperture. Pressure (mtorr) and V_{bias} given in parentheses above data points, electron gun-extractor separation (cm) given below data points. Gas injected at -1 cm.

Figure 22 and 23:

Electron polarization vs extracted current. Microwave source with termination as shown in inset. Extraction aperture = 1.5 x 1.5 mm. Pressure (mtorr) and V_{bias} given in parentheses above data points. Gas injected at -1 cm.

Figure 24: Electron polarization vs extracted current. Microwave source with termination as shown in inset. Extraction aperture = 2.0 x 0.2 mm. Pressure (mtorr) and V_{bias} given in parentheses above data points, gas injected at -1 cm.

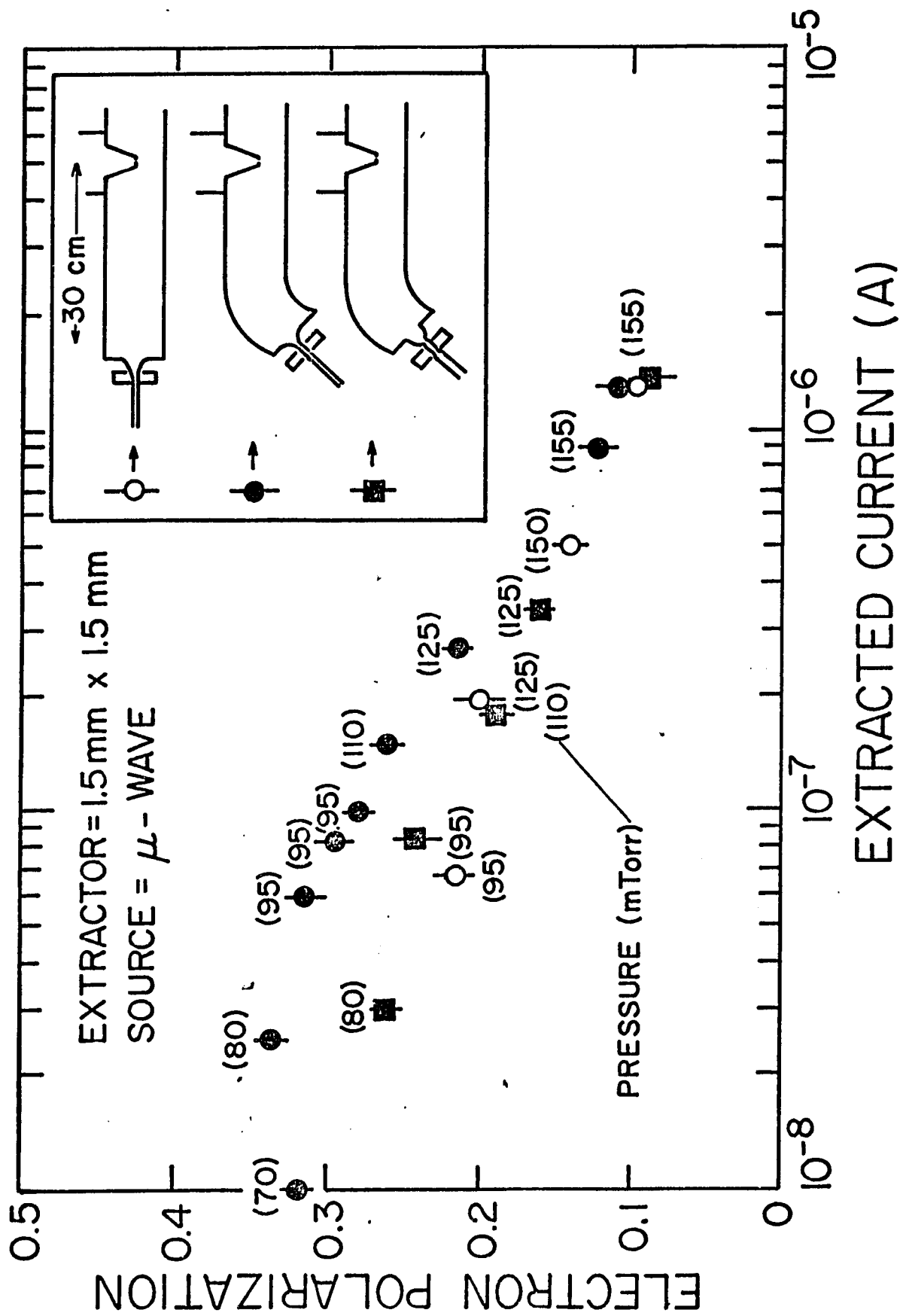


FIGURE 20

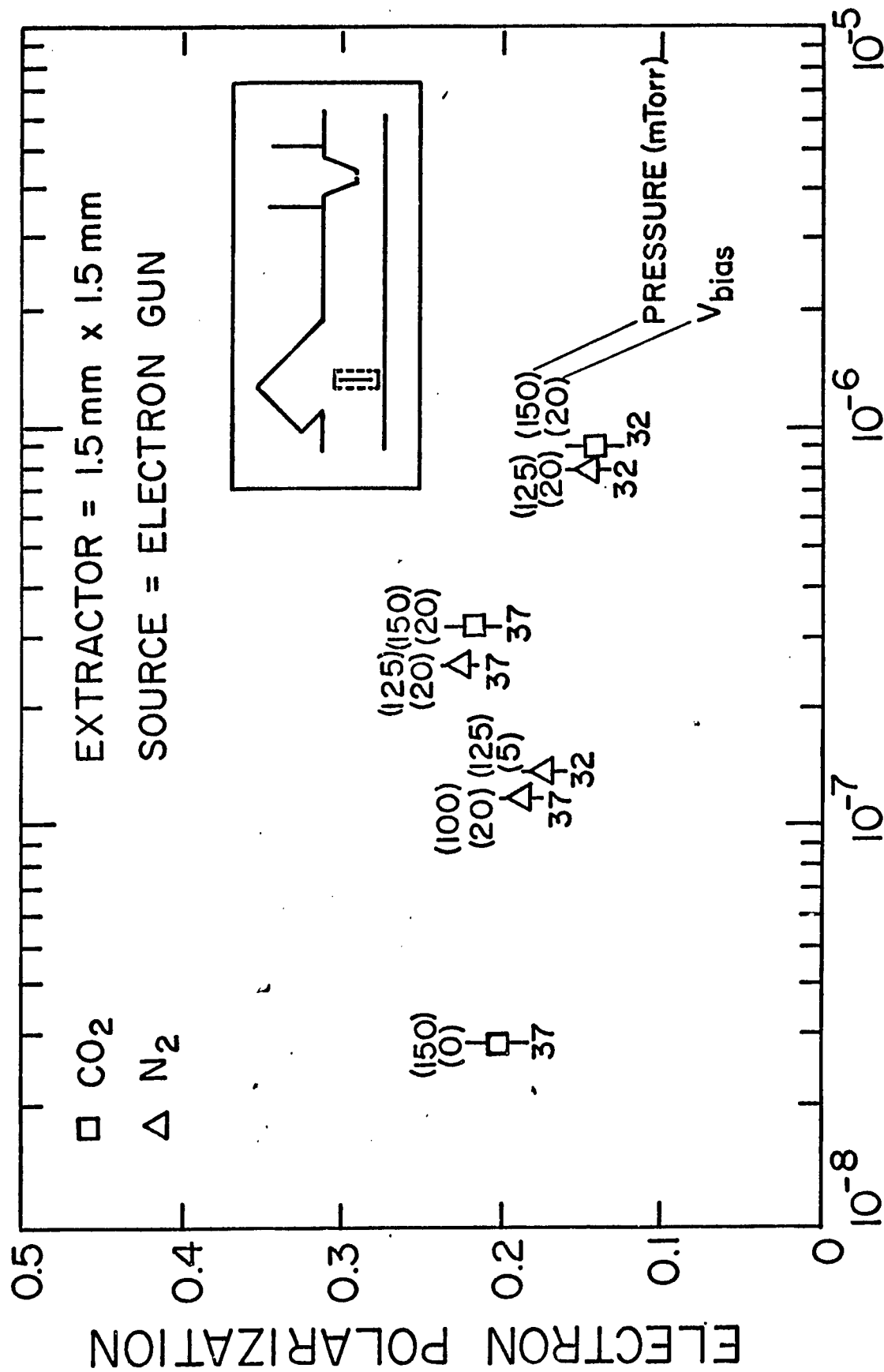


FIGURE 21

EXTRACTED CURRENT (A)

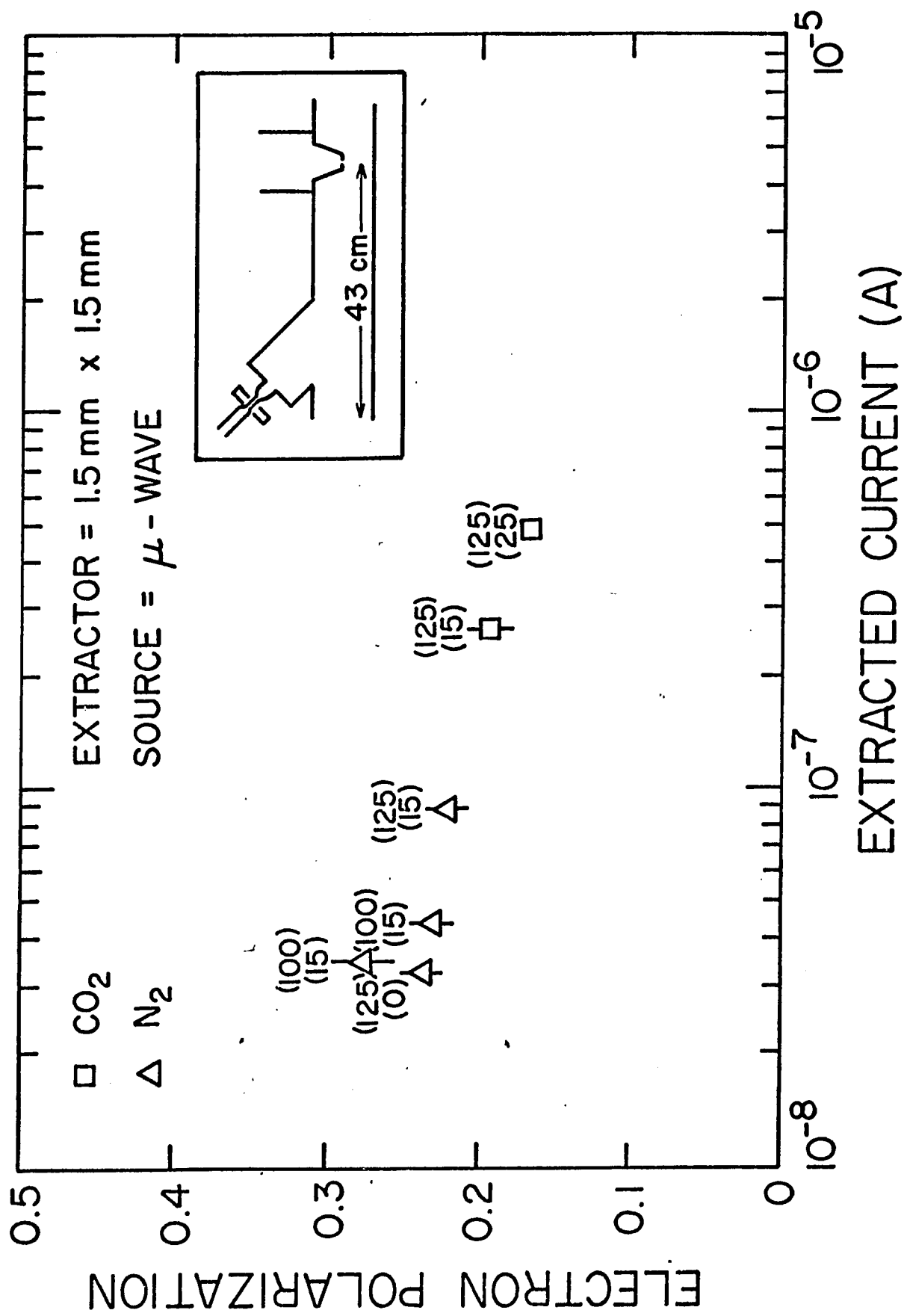


FIGURE 22

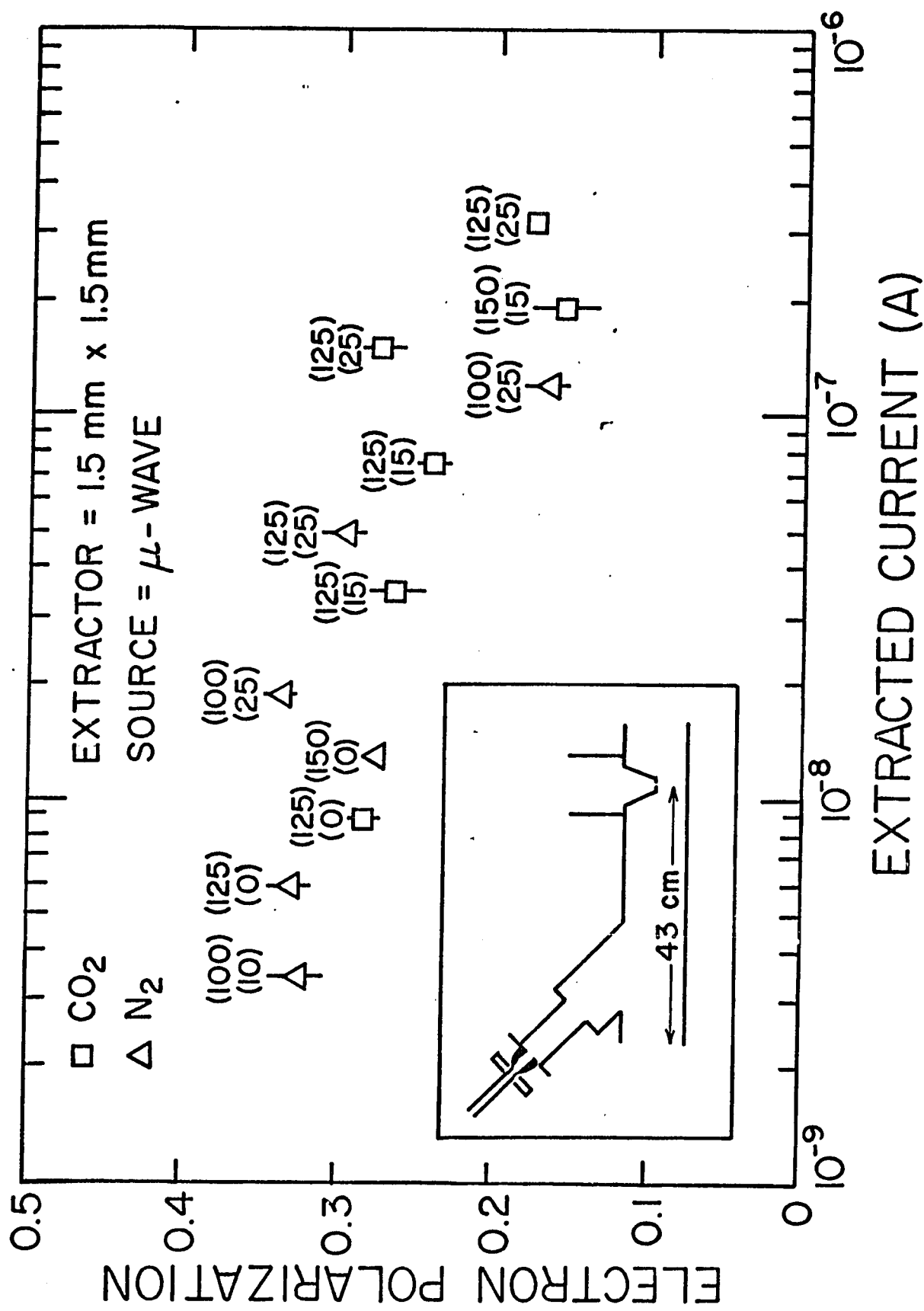


FIGURE 23

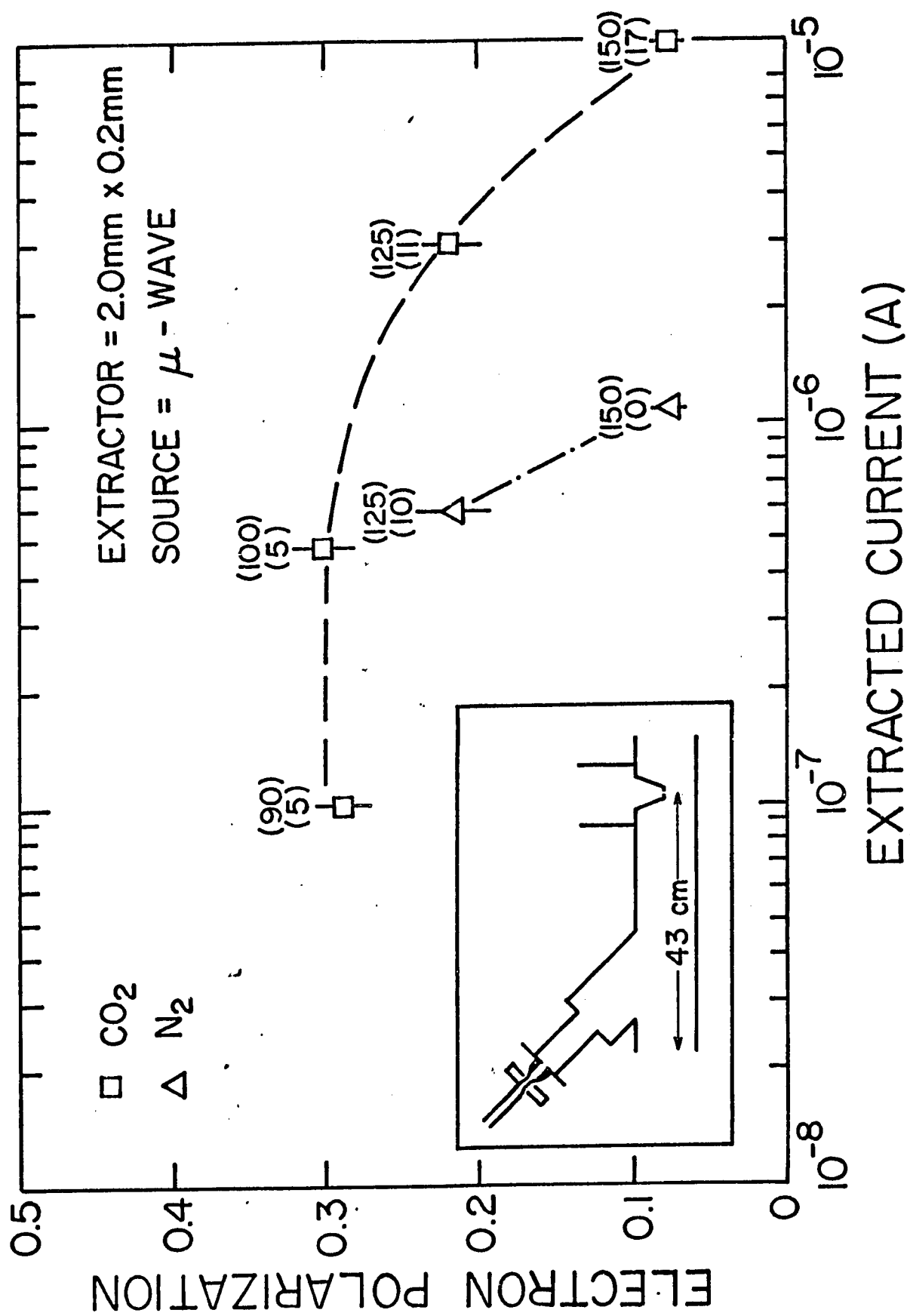


FIGURE 24

IV. CONCLUSIONS

In this section, we summarize the basic achievements of the optically pumped, flowing helium afterglow as a source of polarized electrons and list several possible improvements. The best polarization and current data points that have been obtained are $P = .30$, $I = 5 \times 10^{-7}$ A; $P = .21$, $I = 3 \times 10^{-6}$; and $P = .075$, $I = 1.0 \times 10^{-5}$ A. The beam energy is 500 eV in a magnetic field of 5 gauss with an energy spread of ≤ 0.5 eV and a beam emittance ϵ , $5 \leq \epsilon \leq 20$ mrad cm. A redesign of the electron extraction optics is not expected to greatly increase the total current but may improve or at least measure accurately the beam emittance. The minimum potential necessary to extract electrons with high efficiency is probably on the order of 20 to 30 volts. A higher resolution energy analyzer is needed to determine the actual energy spread which may be as low as .025 eV.

The major cause of reduction in polarization at high pressures is believed to be ionization of background gas between the extraction aperture and the extraction anode. Elimination of this effect should result in polarizations of $\sim .25$ at 10^{-5} A. Further investigation of the optical pumping process is needed to define the mechanisms

that now limit the maximum polarization to .35. Ultimately the upper limit on polarization vs current will be determined by the effects of trapping of the $1.08\ \mu$ pumping radiation at high metastable densities. The electron beam can be extracted with either longitudinal or transverse polarization, and the spin direction can be modulated at frequencies on the order of 50 Hz for synchronous detection of a spin dependent scattering amplitude. We conclude that this source of polarized electrons is well suited for many types of experiments and in particular those requiring high currents, high energy resolution, and ease of polarization reversal without perturbation of beam trajectory.

SPIN POLARIZATION TRANSFER REACTIONS:

PART III

Electron Scattering from O_2 and NO

I. INTRODUCTION

In Part I and II of this thesis we have shown that an optically pumped, flowing helium afterglow is a good source of spin polarized electrons for investigating spin dependent scattering processes. In this part, we describe a general method of measuring the total spin reversal cross section for thermal electrons scattering from atoms or molecules, S , described by the reaction



where the arrows (\uparrow , \downarrow) schematically indicate the spin state of the electron. Preliminary results are presented for electron scattering from O_2 and NO. Since these data were taken primarily to demonstrate feasibility of the method, there remain several possible sources of systematic error which have not been thoroughly studied. However one general result is clear: The probability of spin reversal including electron exchange with the unpaired π orbital electrons of O_2 or NO is small, being less than 1% of their momentum transfer cross sections at thermal energies.

If the species S is a non-singlet atom or molecule, then the above reaction (21) is most often due to the mechanism of electron exchange and is referred to as "spin exchange." However, as will be discussed below, there are special cases such as resonant formation of O_2^{-*} in which spin-orbit effects can contribute significantly to the spin

reversal process so that the mechanism could be a "spin flip" of the incident electron by a magnetic dipole interaction¹²⁵. In the present experiment only the rate of electron spin reversal is measured so that these two processes are indistinguishable. For the sake of simplicity we describe our measurements in terms of the spin exchange process. The resulting reaction rates or cross sections have been computed based on the standard definition of a spin exchange cross section which may differ by a numerical factor from the definition of a spin flip cross section. We also consider the possible contribution of spin exchange collisions between electrons and the O_2^+ ions. For heavy elements such as xenon, depolarization by spin orbit effects in elastic scattering may also be observable⁹².

The basic apparatus and technique are very similar to that described in Parts I and II. A swarm of spin polarized electrons is prepared in a flowing gas reactor by the chemiionization of a reactant gas by spin polarized $He(2^3S)$ metastables. For simplicity, we will refer to this reactant gas as the "Penning" gas, X, although strictly speaking Penning ionization is not always the only reaction channel available (see Eq. 1). In Part I, it was shown that, for the typical densities of the X^+ ions, spin exchange between the free electrons and these ions was small if not negligible. Therefore this swarm of polarized electrons

will flow down the tube without loss of polarization over a path of 20 cm or more in which the only species present are He (ground state) X, X^+ and thermal electrons. At some point the sample gas, S, whose spin exchange rate is to be studied, is injected. After a reaction length L the electrons can be extracted from the swarm and their polarization measured by Mott scattering. The reaction rate or thermally averaged cross section is obtained from the dependence of the electron polarization on L and the density of S. The data analysis will be shown to be identical to the formalism used for ion-molecule reactions studied in similar flowing gas reactors.

The unique features of this method are a) the rate of spin changing collisions is measured directly and b) it is not necessary to produce or monitor any degree of spin polarization of the atomic or molecular system involved. There have been many experiments on the spin exchange of electrons with species that can be polarized directly by optical pumping^{107,108} in swarm experiments or with inhomogeneous magnetic fields¹⁰⁹ in beam experiments or that can be polarized indirectly by the spin exchange process itself. Thus far these have been limited to S states of atomic systems. In the case of the swarm experiments, the spin exchange rate must be inferred from the size, width or shifts in a magnetic resonance transition. The present method avoids these difficulties. It is also noted

that the simplest of all exchange reactions, that of electron scattering from atomic hydrogen, has not been measured (although several theoretical calculations have been made¹¹⁰). Such an experiment can be easily done with the method described here.

II. EXPERIMENTAL TECHNIQUE

A. Flowing Gas Reactor

A schematic diagram of the flowing gas reactor is shown in Fig. 25. It consists of five basic regions:

- 1) helium excitation source to produce the $\text{He}(2^3\text{S})$ state,
- 2) optical pumping region to orient the 2^3S atoms in the $m_s = +1$ (or -1) sublevel,
- 3) chemiionization of the gas X injected into the flow stream to produce spin polarized electrons and remove the 2^3S states,
- 4) a reaction zone of length L defined by the position of the injector for the sample gas S and the electron extractor (5)..

After the electrons are removed from the flow tube (at $\sim .1$ torr) into a differentially pumped beam tube (at $\sim 10^{-4}$ torr), they are accelerated to 120 keV to measure their spin orientation by Mott scattering. A detailed description of the operation of the excitation source and the flow tube to obtain maximum polarization is given in Part I. A schematic of the entire apparatus including the Mott scattering analyzer is shown in Fig. 1 and a detail view of the electron extractor is given in Fig. 2. The basic result of Part I and II that concerns the present experiment is that, for pressures $\leq .15$ torr, electron densities on the order of 10^9 cm^{-3} can be obtained with a polarization of 30% which is independent of parameters such as the distance from the Penning gas injector to the extractor.

Figure 25: Schematic diagram of flow tube for measurement of spin exchange rate constant (not to scale).

Figure 26: Schematic diagram of apparatus for calibrating reactant gas flow rates.

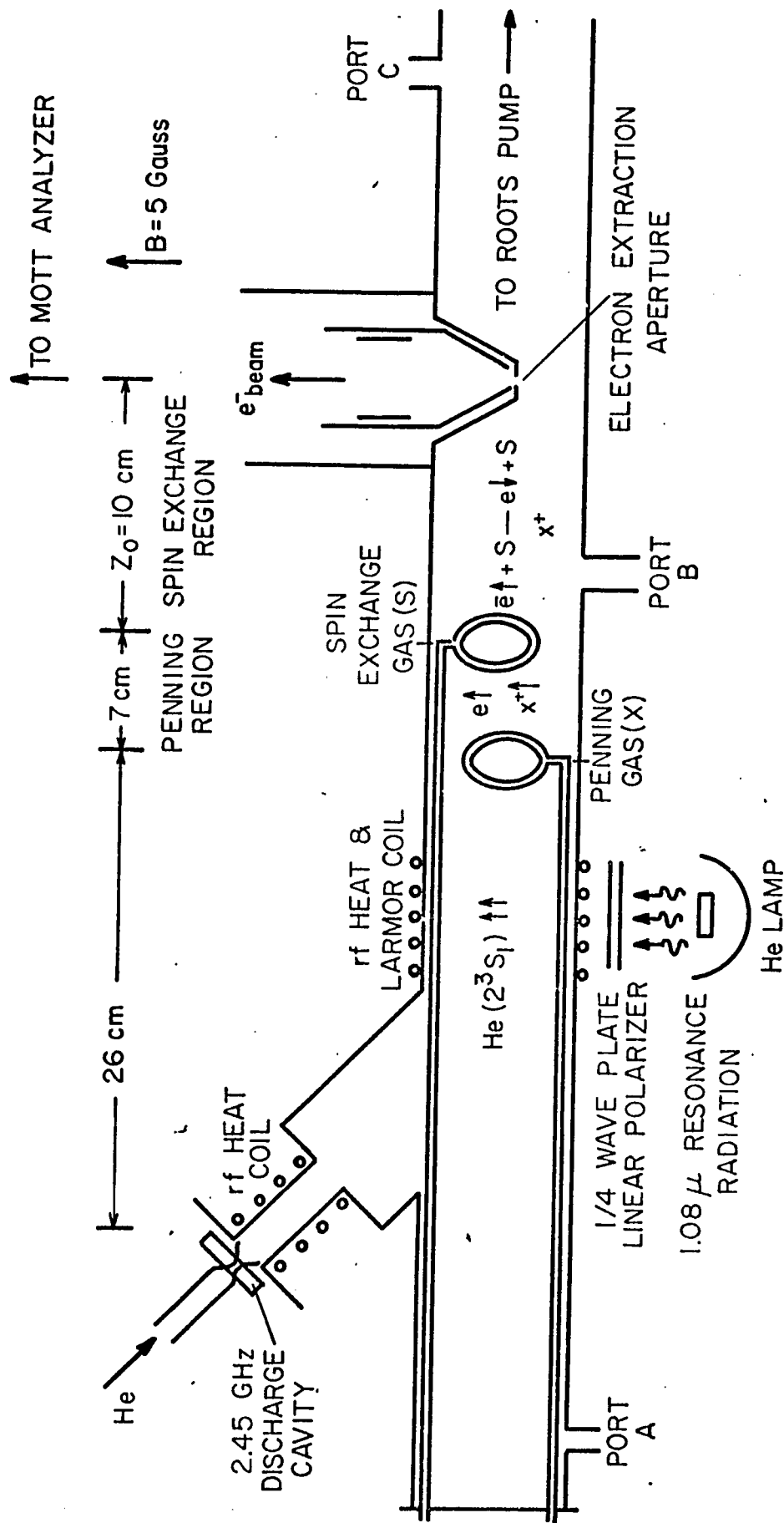


FIGURE 25

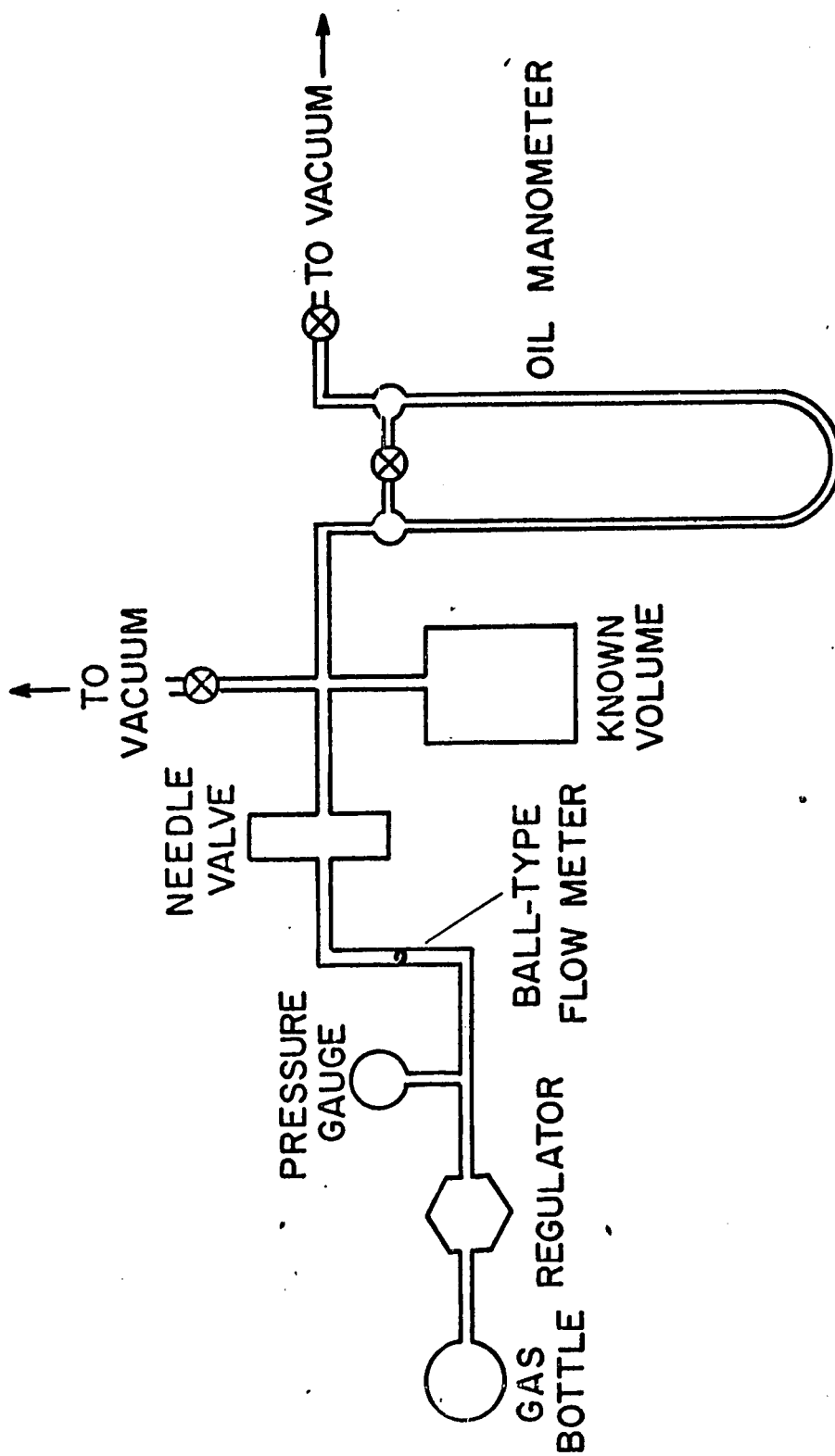


FIGURE 26

B. Calibrations

In order to calculate the rate for reaction (21) from the observed decrease in electron polarization, the average flow velocity, V_o , and the density of S, N_s , must be determined. These are in turn related to the pressure in the flow tube, p (torr), and the flow rates of the helium buffer gas Q_{He} and the sample gas Q_s (in units of torr liters/sec at 273°K) by

$$V_o = \frac{Q_{He}}{\pi a^2 p} \frac{T}{273} \quad \left(\frac{\text{cm}}{\text{sec}} \right) \quad (22)$$

and

$$N_s = 3.55 \times 10^{19} \frac{Q_s}{\pi a^2 V_o} \quad (\text{cm}^{-3}) \quad (23)$$

where a is the radius of the tube (cm) and T is the temperature in °K.

The flow tube pressure was monitored by thermocouple gauges TC_1 and TC_2 at ports "A" and "C" respectively shown in Fig. 25. (These gauges were not placed in the center of the reaction zone to avoid any possible electrical interference with the electron swarm prior to extraction.) The thermocouple gauges were calibrated under both static and flowing conditions by a McLeod gauge connected to port "C." The pressure indicated by TC_2 decreased .01 torr relative to the McLeod gauge from the static to flowing gas measurements. This is assumed to be due to a cooling effect of

the flowing gas on the thermocouple. The pressure drop between port B and C due to the gas flow was obtained by two methods: (a) measuring the pressure at B and C with the McLeod gauge for identical gas flow rates and (b) simultaneously measuring the pressure at B with the McLeod gauge and at C with TC₂ as calibrated above. Both methods indicate the pressure at B is .010 to .012 torr higher than at C over the pressure range of .07 to .170 torr. The pressure drop from A to C is .025 to .030 torr over this range and agrees with the calculated result for viscous flow given in Appendix A. The flow tube pressures quoted here are those determined for point B from the indicated pressure at TC₂ and the above calibration procedure. The absolute pressure is judged good to $\pm .010$ torr and is reproducible to $\pm .005$ torr.

The helium flow rate was monitored by a ball type flow meter and calibrated by a positive displacement gas meter which was in turn calibrated for us by the Carl Poe Co. against a standard "proving bell" accurate to $\pm 1\%$. The helium flow rate can be reproducibly set with the ball flow meter to $\pm 3\%$. The flow velocity calculated from equation (22) is given in Appendix A vs the flow tube pressure. At a pressure of .125 torr the helium flow rate is 38.2 torr liters/sec and the velocity is $4.3 \pm .1 \times 10^3$ cm/sec.

The flow rate of the sample gas, S, was calibrated by the "pressure rise" method described in Fig. 26. A low

pressure regulator maintains a constant pressure of 6 psig. at the input of a precision needle valve (Heraeus #173-17) which controls the flow rate and is reproducible to $\pm 2\%$. The flow rate is determined by the rate of pressure rise in an evacuated cylinder of known volume. In order to measure the flow rate to 2%, the total pressure rise in volume V must be less than 2% of the pressure drop across the needle valve (~ 6 psig) and this pressure rise must be in turn measured to better than 2%. This is feasible with an oil manometer. Two precautions are necessary when measuring high flow rates: 1) The low pressure side of the needle valve must be at the same pressure during the calibration that it is at during actual use. This can be as high as 100 torr depending on the conductance of the gas injector and its connecting tubing. 2) The conductance of the tubes connecting the known volume and the manometer must be large enough so that there is no significant pressure difference between them. With the above method and volumes of 0.5 and 10 liters, flow rates of .005 to 3.3 torr liter/sec have been measured to $\pm 2\%$.

The data analysis used here assumes that the density of S is given by Eq. (23) at all points after the gas injector, i.e. the gas is assumed to be injected in a plane with a radially uniform distribution. The ring injector used is a 1/16" OD stainless steel tube formed in a circle 4 mm in diameter and perforated with .010" holes, 12 on the

inside diameter and 28 on the outside diameter. The adequacy of this type of injector to approximate a planar distribution has been tested by several groups involved in flowing afterglow studies^{25,111}. This particular ratio of injector diameter to flow tube diameter (10 cm) produced the best results for injecting gases into an argon buffer gas which is the worst case due to its high viscosity¹¹². However the short reaction length of 10 cm used here borders on the limits of the above approximations due to some backstreaming of gas on the one hand and incomplete mixing at the position of the injector on the other. These two effects tend to cancel and the resulting effective reaction length is considered to be uncertain to $\pm 10\%$. This error in reaction length and the error in the absolute pressure are the major sources of error in determining the reaction rate.

C. Electron Extraction

In Part I we described in some detail various processes that degrade the electron polarization--particularly for pressures above .15 torr. Until some of these problems are solved, allowing the flow tube to be operated at higher pressures, the initial electron density is limited to 10^9 or 10^{10} cm^{-3} and the decay length due to ambipolar diffusion is on the order of 4 or 5 cm. The present configuration of the Mott scattering system requires about

10^{-10} A extracted from the afterglow to provide a usable current of 10^{-12} A in the Mott scattering chamber. All of these limitations necessitate a total path length in the flow tube from the Penning gas injector to the extractor of ≤ 17 cm. Even at this distance the extraction aperture had to be biased 10 V positive with respect to the flow tube to increase the extraction efficiency (see Part II). The Penning gas, X, was injected at a rate sufficient to de-excite 99% of the $\text{He}(2^3\text{S})$ atoms in 4 cm. The gas injector for the reactant gas S was placed 7 cm from the Penning gas injector to allow the electrons to thermalize and reach a spacial distribution characterized by the fundamental diffusion mode. Improvements in the above limitations on flow tube pressure and extracted current would allow more accurate measurements using 20 or 30 cm reaction lengths.

III. DATA ANALYSIS

In this section, we show that the rate equation for the decay of electron spin polarizations due to spin changing collisions with a reactant gas can be put in the same form with the same boundary conditions as those for ion-molecule reactions studied in flowing afterglows. Therefore the analysis used to relate the observed decay rate to the actual reaction rate in ion molecule reactions can be carried over completely and applied to spin exchange measurements. In Appendix A, a summary is given of the basic hydrodynamic properties of the flowing helium buffer gas and of the effects of the flowing system on diffusion losses of metastables and electrons. The basic difference between reactions in a static and flowing system is that, for viscous, laminar flow in a cylindrical tube, the flow velocity has a parabolic radial profile given by

$$v(r) = 2V_0 \left(1 - \left(\frac{r}{a}\right)^2\right) \quad (24)$$

where V_0 is the average or bulk flow velocity and a is the tube radius. As a result, the ions or electrons near the tube axis are transported down the tube faster than those near the tube walls and therefore those near the axis experience a slower apparent diffusion and reaction rate. Not only does this change the eigenmodes of diffusion for a cylindrical geometry, but introduces a coupling of reac-

tion and diffusion. There have been several detailed treatments of the data analysis for ion molecule reactions in flowings systems^{23-25,113-115} which are in excellent agreement even though the basic approaches to the problem have been quite different.

A. Rate Equations for Spin Polarization

If ambipolar diffusion is the only net loss mechanism of electron in the flow tube and the exchange reaction (21) is the only method of reversing the electron's spin then the rate equation describing the population of $m_s = \pm \frac{1}{2}$ states of the electrons scattering from unpolarized atoms or molecules, S, as a function of times is

$$\frac{dN_e^+}{dt} = - D_A \nabla^2 N_e^+ - k \frac{N_S}{2\beta} (N_e^+ - N_e^-) \quad (25)$$

and

$$\frac{dN_e^-}{dt} = - D_A \nabla^2 N_e^- + k \frac{N_S}{2\beta} (N_e^+ - N_e^-) \quad (26)$$

where N_e^\pm are the densities of the $m_s = \pm \frac{1}{2}$ states of the free electrons, D_A is the ambipolar diffusion coefficient, k is the rate constant for exchange, N_S is the number density of the S atoms or molecules, and $\frac{1}{2}\beta$ is a numerical factor arising from the definition of the spin exchange cross section. For the case of the particle S being a spin $\frac{1}{2}$ state, the rate constant, k , is defined for the reaction

$$e(m_s = \frac{1}{2}) + S(m_s = -\frac{1}{2}) \xrightarrow{k} e(m_s = -\frac{1}{2}) + S(m_s = \frac{1}{2}) \quad (27)$$

collisions of electrons and S both in the $m_s = +\frac{1}{2}$ or $-\frac{1}{2}$ states cannot lead to spin reversal. Since we assume the species S is unpolarized, the density of $S(m_s = +\frac{1}{2}, -\frac{1}{2})$ states is just $N_S/2$ so that $\beta = 1$. In the case of a triplet state (such as O_2) it can be shown¹³² that the cross sections for spin exchange between an electron in the $m_s = +\frac{1}{2}$ state and atoms in the $m_s = 0$ and -1 states are equal. Therefore, the effective density of S capable of spin exchange is $\frac{2}{3} N_S$ so that $\beta = 3/4$.

If N_e is the total electron density and P is the electron polarization as defined by Eq. (4) then $PN_e = N_e^+ - N_e^-$. Therefore from Eqs. (25) and (26)

$$\frac{d(PN_e)}{dt} = -D_A \nabla^2 (PN_e) - \frac{k}{\beta} N_S (PN_e) . \quad (28)$$

Transforming the time coordinate t to the spacial coordinate, z, by the relation $dz(r) = v(r,z)dt$ then Eq. (28) becomes

$$\frac{\partial[v(r,z)(PN_e)]}{\partial z} = -D_A \nabla^2 (PN_e) - \frac{k}{\beta} N_S (PN_e) . \quad (29)$$

(The dependence of $v(r,z)$ on z is introduced by the small pressure drop along the tube.) This equation has the same form as that for the ion concentration in an ion-molecule reaction in a flowing gas reactor. If, as will be shown below, the boundary conditions are the same and several

assumptions are equally valid in both cases, then the solution of Eq. (28) for the concentration PN_e on the tube axis ($r = 0$) at a point z is to a good approximation²³,

$$PN_e(r = 0, z) = PN_e(r = z = 0) \exp\left(-\frac{kcQ_s z}{\beta\alpha\pi a^2 V_o} - \frac{\lambda^2 D_a z}{a^2 V_o}\right) \quad (30)$$

where Q_s is the flow rate of S in torr liters/sec, c is a constant equal to 3.55×10^{19} atoms/torr liter, $\alpha = 1.6$ is a correction factor for the higher flow velocity on the tube axis (see reference 111 for a discussion of the value of α), and λ^2 is the character diffusion constant for the fundamental diffusion mode in a flowing cylindrical stream (see Appendix A). The spatial decay of the total electron density is determined by diffusion alone and is given by

$$N_e(r = 0, z) = N_e(r = 0, z = 0) \exp\left(-\frac{\lambda^2 D_a z}{a^2 V_o}\right) \quad (31)$$

therefore

$$P(r = 0, z) = P(r = 0, z = 0) \exp\left(-\frac{kcQz}{\beta\alpha\pi a^2 V_o}\right) \quad (32)$$

B. Assumptions and Boundary Conditions

The assumptions and boundary conditions that are common to ion molecule reactions in flowing systems and that are inherent in the above solution are:

- 1) Laminar flow exists in the tube producing a parabolic velocity profile.
- 2) The axial variation of the flow velocity due to the pressure gradient along the tube can be neglected if the velocity at the center of reaction region is used.
- 3) There is no source of primary ion (or PN_e in our case) in the reaction region, $z > 0$.
- 4) The initial radial density distribution of the ion (or PN_e) concentration is given by the fundamental diffusion mode.
- 5) There are no loss mechanisms for the ion (or PN_e) concentration other than diffusion and the bilinear reaction with S.
- 6) Transport of ions (or PN_e) down the tube by axial diffusion is much slower than by the convective flow.
- 7) The reactant S is injected in a radially uniform distribution at $z = 0$.
- 8) The density of S is a constant, independent of z for $z > 0$.

We will now briefly examine the validity of these conditions for the case of electron spin exchange.

- 1) Our flow tube is operated at .10 to .125 torr which is a factor of 2 below the lowest pressures commonly used in ion molecule studies. However, amount of slip flow

at the walls of the tube is still only 16% of the average flow velocity.

2) The pressure drop in our tube is typically .003 torr over the reaction length of 10 cm. Since the pressure is calibrated to be the pressure near the start of the reaction region, the maximum variation in V_0 is 3% over this region introducing a 6% variation in the reaction rate (proportional to V_0^2).

3) Sufficient Penning gas is injected to de-excite all He 2^3S metastables before the reaction region.

4) Even though the distance from the Penning gas injector to the start of the reaction region is only 7 cm, this still corresponds to 1.7 decay lengths for ambipolar diffusion. The next higher mode of diffusion decays approximately six times faster²⁴ so that we can assume the initial electron density does have approximately a fundamental diffusion mode distribution.

5) For the electron densities in this experiment of 10^9 to 10^{10} cm^{-3} , loss of PN_e by electron-ion recombination can be neglected. However in the case of O_2 on addition loss mechanism for the polarization P, does exist--spin exchange with the O_2^+ ions formed by charge transfer with the Penning ions. This is discussed in Section V.

6 and 7) At the highest flow rates for the reactant S, the polarization is reduced by a factor of 10 over the reaction length of 10 cm. The importance of axial diffusion

of the polarized electrons can be crudely estimated by comparing the characteristic time for diffusion over a distance z , $\tau = z^2/\lambda^2 D_A$ to the convective transport time $t = z/v_0$. At .1 torr D_A is typically $9000 \text{ cm}^2/\text{sec}$ so that for $z = 10 \text{ cm}$ $\tau \sim 3 \text{ msec}$ and $t = 1.5 \text{ msec}$. Since these are of the same order axial diffusion will tend to increase the polarization at $z = 10$. However, also at the highest flow rates the reactant gas tends to diffuse further upstream from the position of the injector making the effective reaction length longer and thereby lowering the polarization at the extractor. Thus these two effects tend to cancel each other. Within the error of our polarization measurement, no systematic deviation from a simple exponential is observed indicating these effects are small or nearly cancel.

8) Not only is the density of S a constant over the reaction region, its polarization remains zero since the density of reactant gas (10^{12} to 10^{14} cm^{-3}) is much larger than the electron density.

Two additional assumptions are worth noting. First, the solution for PN_e or P in Eqs. (30) and (32) is for the electrons on the flow tube axis. In the present configuration, with the electron extractor protruding radially into the afterglow and a substantial bias potential applied to increase the extraction efficiency, a sizeable volume of the flow tube may be contributing to the measured polarization. While the importance of this effect is probably small,

it is the type of systematic error that should be investigated if more accurate results are desired. Second, we have assumed that the electrons have come to thermal equilibrium with the background gas in a distance of 7 cm. A simple calculation shows that electrons will thermalize from 1 eV to .025 eV by elastic collisions with helium in about 10^4 collisions corresponding to .4 msec at a pressure of .1 torr. Although the time interval corresponds to a flow distance of 1.6 cm, the correspondence is not very meaningful when the distance is on the same order as the mean free path which is .6 cm at .1 torr. The presence of a molecular gas used for the Penning ionization of the helium metastables provides much more efficient thermalization via vibrational and rotational excitation. For example the fractional energy loss per collision of an electron with CO_2 is approximately 5%⁸⁴ requiring only 60 collisions to thermalize an electron from an initial energy of 1 eV. This is reflected in the very narrow energy spreads measured for electrons extracted from the afterglow (see Part II). The best evidence that the electrons are thermalized in the present experiment is the near equality of the rate constants measured when Ar, N_2 , and CO_2 were used as Penning gases. For more accurate results the electron temperature can be determined from measurements of the rotational temperature of molecular impurities.

We conclude that the assumptions made in the derivation of Eq. (32) are approximately met in the conditions of this experiment within the limits of error due to uncertainty in the absolute pressure ($\pm 10\%$) and the reaction length ($\pm 10\%$). However the present use of a reaction length of only 10 cm is near the limits of validity of the reaction model assumed. The ability to increase this length to 20 or 30 cm would greatly improve the accuracy of the measurements and allow several assumptions to be tested.

IV. RESULTS

The measured decay of polarization for electron scattering from O_2 and NO is shown in Figs. 27 to 31 as a function of zQ in cm torr liter/sec. The error bars represent one standard deviation of eight polarization measurements for each point. The line drawn through the points is a least squares fit of a straight line to the data points. A summary of the results is given in Table III. The thermally averaged cross sections are calculated from the measured rate constants by dividing by the average electron velocity of 1.05×10^7 cm/sec. The random error quoted is the standard deviation of the least squares fit to the data points. The systematic error is due to the uncertainty in the flow velocity (which enters as v_o^2) and the effective reaction length.

There are not sufficient data to determine whether the difference in the results for O_2 obtained at pressures of .10 and .125 torr is due to a pressure effect or to a difference in the Penning gases used. The data points in Fig. 27 taken as a function of reaction length with a fixed flow rate of O_2 are not unreasonable considering the failure of the basic assumptions for reaction lengths as short as 3 cm. These points were not included in the least squares fit or the calculation of the reaction rate.

Figures 27 to 29: Electron polarization vs reaction length times flow rate of O_2 for several different Penning gases. Reaction length, z , is 10 cm except for points indicated on Fig. 27. These points were not used to fit the line through data point. Solid line is least squares fit to data points.

Figures 30 and 31: Electron polarization vs reaction length times flow rate Q of NO. Solid line is least squares fit to data points.

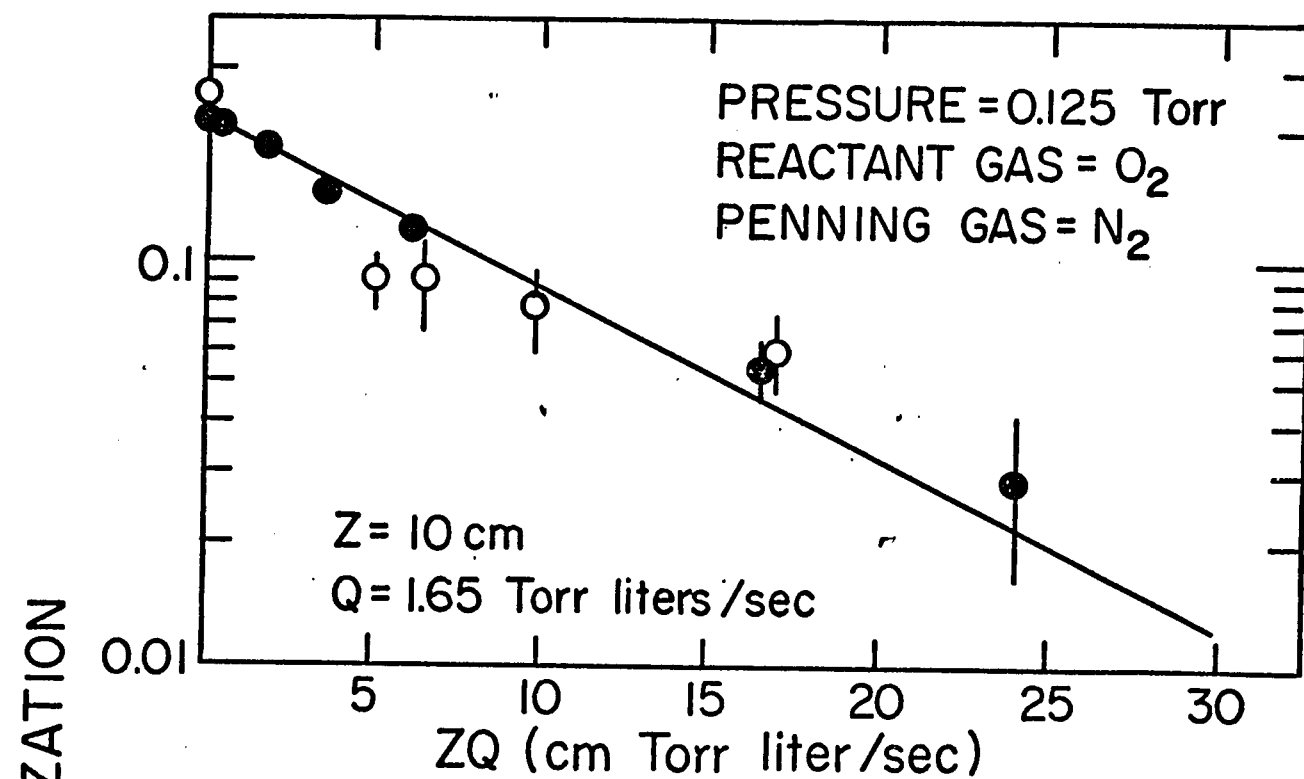


Figure 27

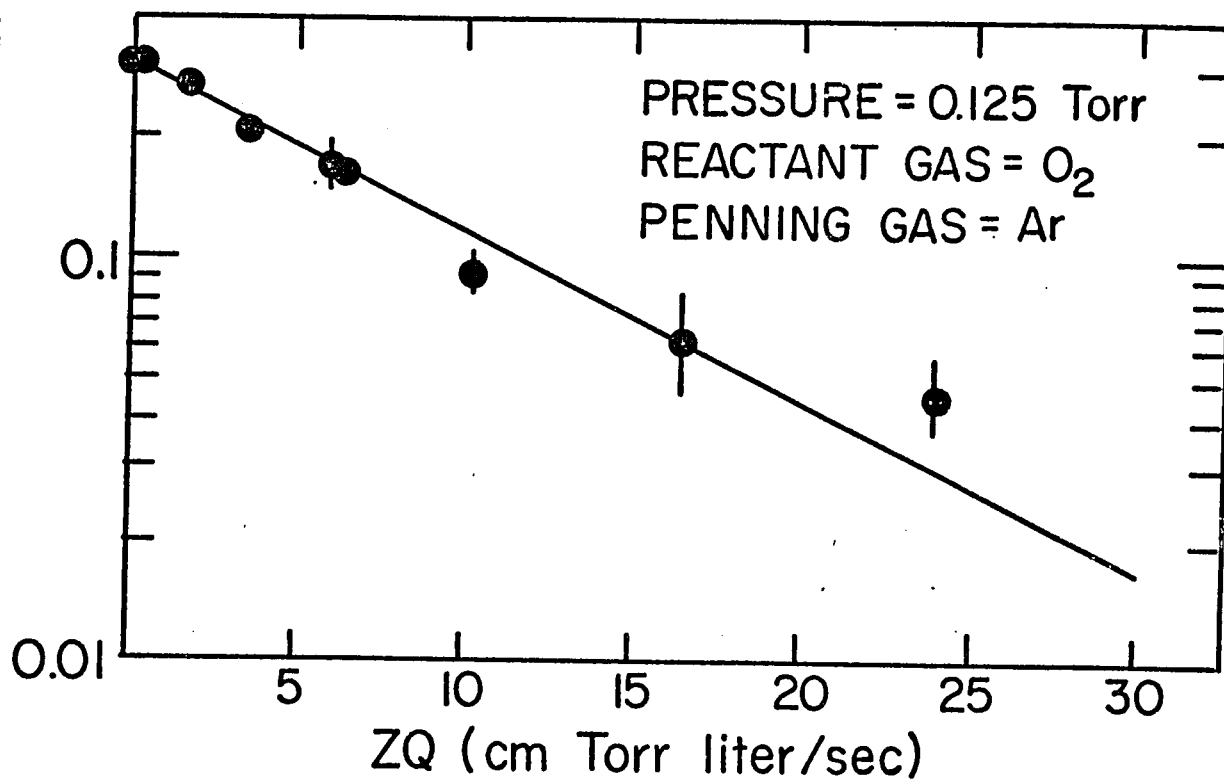


Figure 28

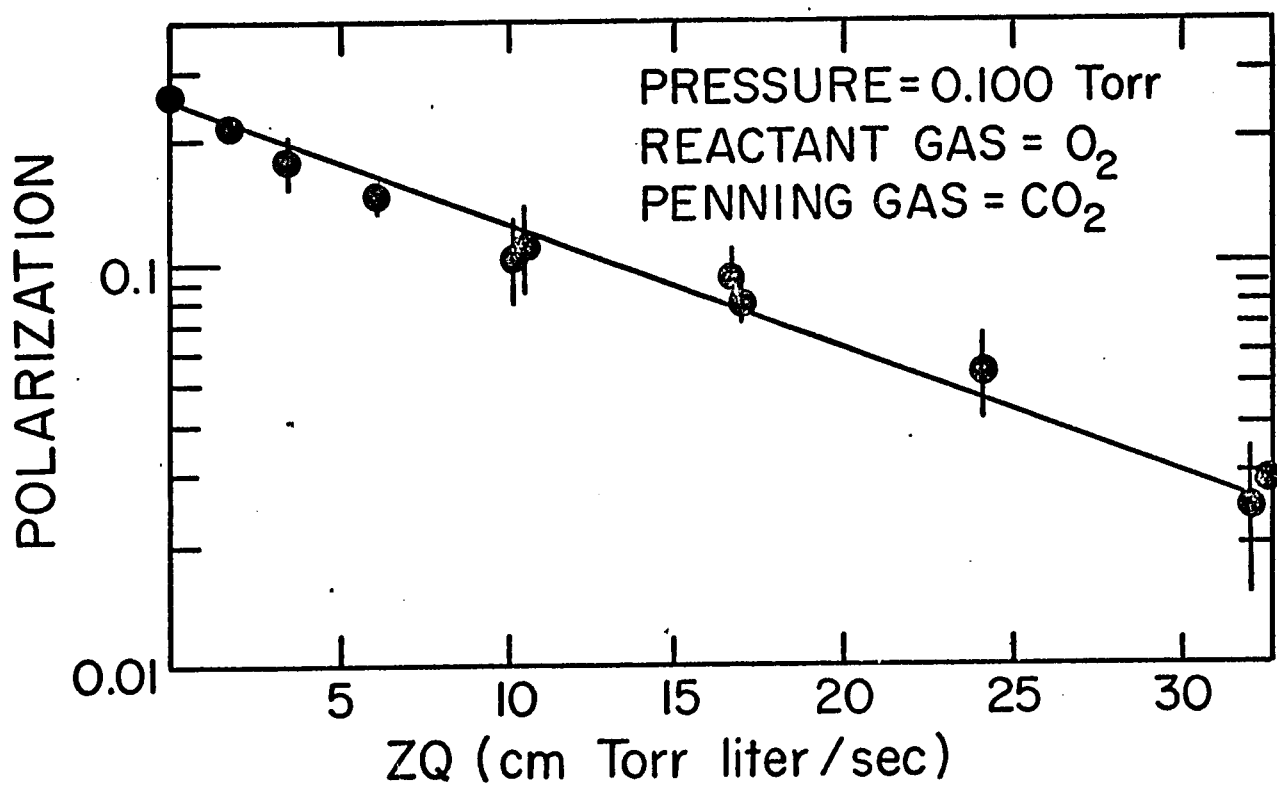


Figure 29

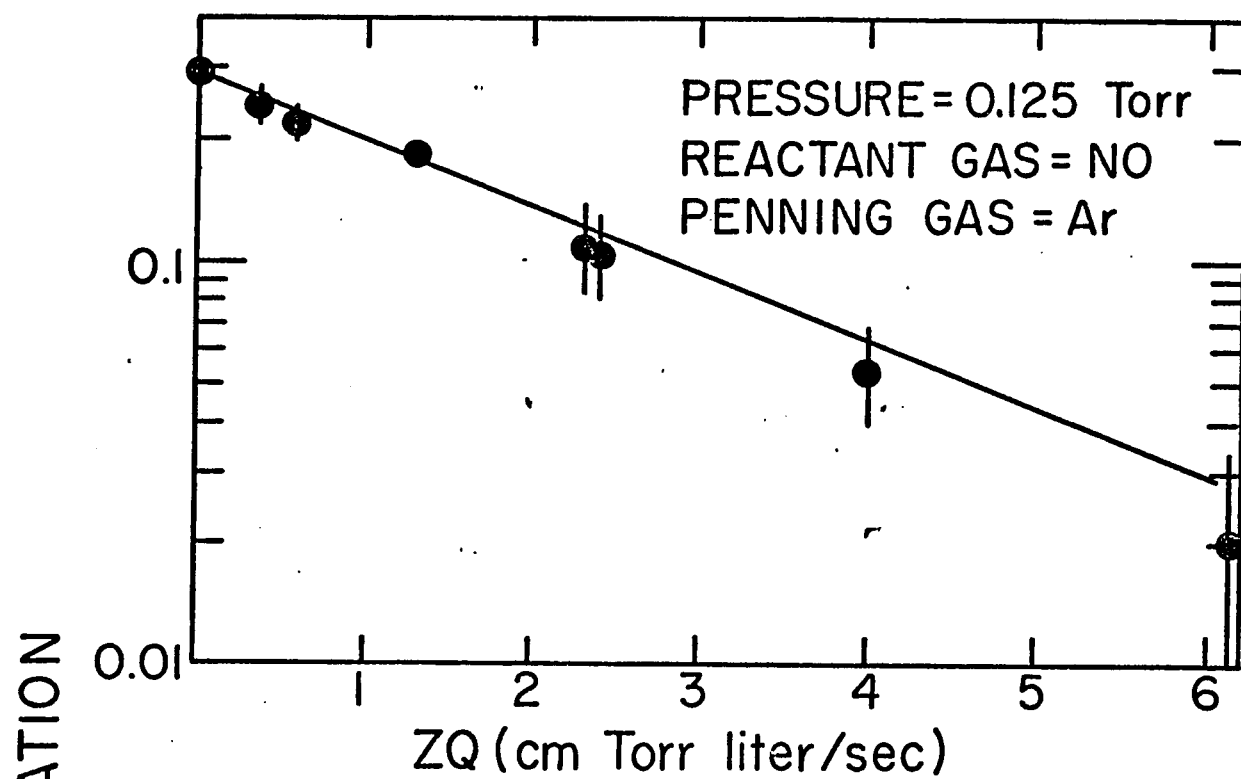


Figure 30

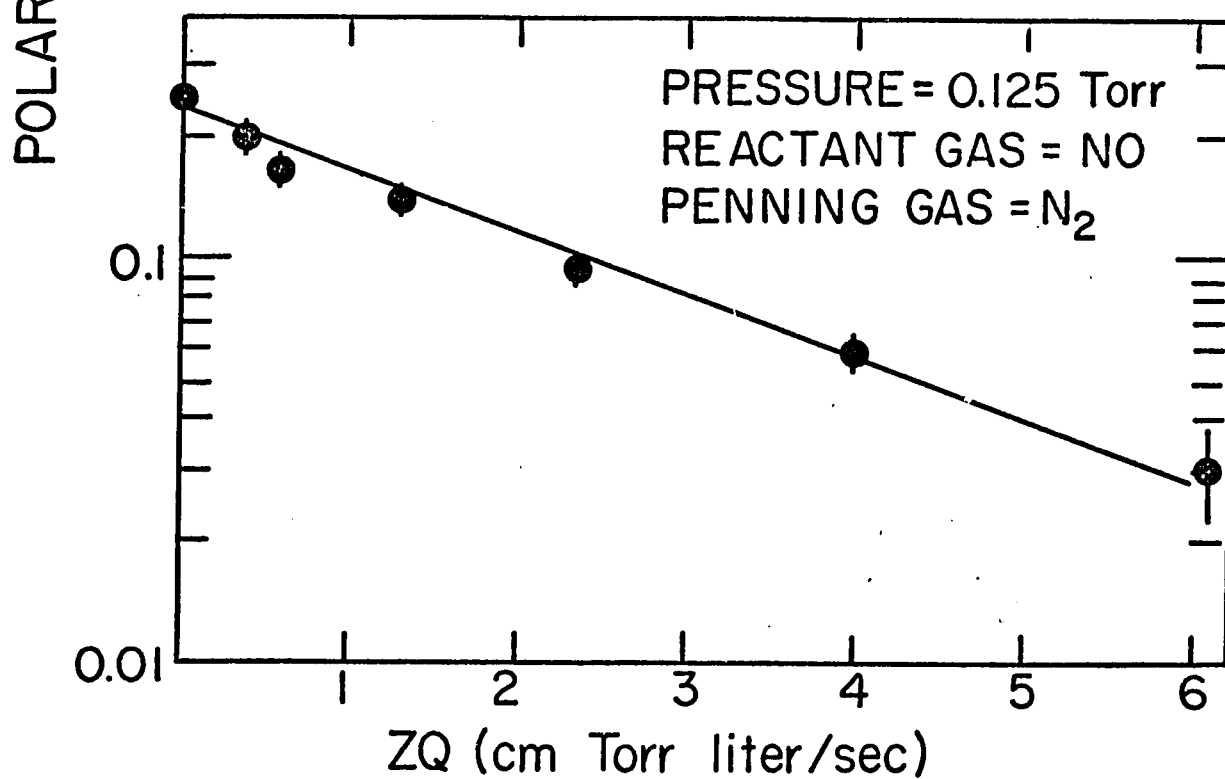


Figure 31

TABLE III

Thermal Spin Exchange Rates of Electrons with Molecules*

Spin Exchange Specie	Afterglow Pressure (torr)	Reaction Length (cm)	Penning Gas	Reaction Rate (cm ³ /sec)	Cross Section (cm ²)	Random Error	Systematic Error
O ₂	.125	10	N ₂	4.57x 10 ⁻¹²	4.35x 10 ⁻¹⁹	± 7%	± 25%
"	.125	10	Ar	4.5 x 10 ⁻¹²	4.28x 10 ⁻¹⁹	± 5%	± 25%
"	.100	10	CO ₂	3.15x 10 ⁻¹²	3.0 x 10 ⁻¹⁹	± 7%	± 25%
NO	.125	10	Ar	2.37 x 10 ⁻¹¹	2.26 x 10 ⁻¹⁸	± 10%	± 25%
"	.125	10	N ₂	2.14 x 10 ⁻¹¹	2.04 x 10 ⁻¹⁸	± 7%	± 25%

* The mechanism for the observed spin change in the scattered electron is electron exchange in the case of NO but this may not be true for O₂ (see Section V).

V. DISCUSSION

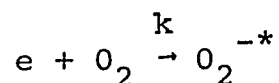
One obvious result of these measurements is that the probability of a spin reversal in the scattering of an electron from O_2 and NO is small. The momentum transfer cross section for both gases is about $3 \times 10^{-16} \text{ cm}^2$ ¹¹⁶. Therefore the probability per collision of a spin change is about .2% for O_2 and 1% for NO. However, before concluding that this spin change of the scattered electron is due to the mechanism of electron exchange, two other processes should be investigated: spin exchange with the molecular ions such as O_2^+ and the formation of temporary negative ions.

Both O_2^+ and NO^+ are rapidly formed by charge transfer with the Penning ions used ¹¹⁷ Ar^+ , N_2^+ , and (CO_2^+, CO^+) . The NO^+ ion is a $^1\Sigma$ state so that spin exchange cannot occur. However O_2^+ is a $^2\Pi_g$ state and must be considered. At an O_2 density of $2 \times 10^{13} \text{ cm}^{-3}$, corresponding to a flow rate of .176 torr liters/sec, the probability per msec for each Penning ion to undergo charge transfer with O_2 is ~ 2 for the ions Ar^+ and CO_2^+ and ~ 1 for N_2^+ . (It should also be noted that at the maximum O_2 density of $3.5 \times 10^{14} \text{ cm}^{-3}$, the probability of the reaction $N_2^+ + O_2 \rightarrow NO^+ + NO$ is less than .01 /msec.) ¹¹⁷ Therefore all the Penning ions are converted to O_2^+ ions even at low flow rates of O_2 . The cross section for spin exchange with O_2^+ ions necessary to explain the

observed decrease can be calculated from Eq. (13) which is an adaption of Eq. (32) assuming the ions are uniformly distributed across the tube and decay exponentially in a length d_A . Given an initial ion density of $3 \times 10^9 \text{ cm}^{-3}$ the required cross section is $\sim 10^{-13} \text{ cm}^2$. Although this is not unreasonably large for S state atomic ions^{81,82}, it is ten times larger than the maximum cross section estimated in Part I, Section VI for other molecular ions such as N_2^+ . It is therefore unlikely that exchange with O_2^+ contributes to the observed polarization decay, but the best way to test for this effect is to use a Penning gas such as NH_3 or C_2H_2 whose ions have insufficient energy to form O_2^+ . When longer reaction lengths and higher pressures are feasible, any contribution by ions can be detected by their dependence on reaction length or ion density.

The possible contribution to polarization loss by spin orbit coupling during the lifetime of a temporary negative ion is also limited to O_2 . Both O_2 and NO have negative ion resonances available at thermal energies but the lifetime of the NO^{-*} resonance is estimated at 10^{-14} sec ¹¹⁸ and should therefore not exhibit any appreciable spin flip during the resonance scattering¹⁸. The lifetime of the O_2^{-*} resonances however have been estimated by several authors^{119, 120, 121} to be 10^{-12} , 7×10^{-12} and $3 \times 10^{-10} \text{ sec}$. The spin orbit splitting in O_2^- has been measured by Land and Raith¹²² to be .022 eV corresponding to a spin

precession time of 2×10^{-13} sec. Therefore nearly every scattering via the negative ion resonance should result in the loss of spin orientation. The rate constant for this reaction,



has been shown to be greater than $2 \times 10^{-11} \text{ cm}^3 \text{ sec}^{-1}$ by Warman et al.¹²³ which agrees with estimates made by Herzenberg¹²¹. Since this is on the same order as the measured rate constant for spin reversal, it is possible that the observed decay of polarization for O_2 is due to spin orbit coupling in the resonant scattering and not to electron exchange. Unfortunately it is impossible to distinguish these processes in the present experiment. It would be interesting to obtain an estimate of the spin exchange cross section which can be done by the quantum defect method¹²⁴ assuming accurate spectra are available.

Note added in proof: Dissociative recombination is known to be rapid for many molecular ions with cross sections on the order of 10^{-13} to 10^{-14} cm^2 ¹³³. In this manner, additional non singlet atoms can be produced in the afterglow as in the case of NO^+ which results in $N + O^*$. Since this is a secondary reaction to the charge transfer process which forms NO^+ and O_2^+ , it is probably negligible in the present experiment and in fact no decrease in extracted current (and therefore electron density) was observed as a function of NO or O_2 density. However, this is another type of systematic error which should be accounted for.

VI. CONCLUSION

A preliminary measurement of the rate constant for spin changing collisions between thermal electrons and NO gives $k = 2.2 \pm .6 \times 10^{-11} \text{ cm}^3/\text{sec}$. This rate is assumed to be due to electron exchange during the collision. The corresponding rate for electron scattering from O_2 is $k = 4.1 \pm 1.1 \times 10^{-12} \text{ cm}^3/\text{sec}$. These rates have been calculated from Eq. (32) which assumes k is the rate constant for spin exchange. However it has not been determined whether the spin reversal in e-O_2 scattering is due to electron exchange or to spin orbit coupling in resonance scattering via the negative ion state of O_2^- . The method that has been described for measuring these spin reversal processes is quite general and can be applied to nearly any atom or molecule. In particular the quite basic measurement of the thermal energy, spin exchange rate for electrons scattering from atomic hydrogen is now possible.

APPENDIX A

MASS TRANSPORT IN A FLOWING SYSTEM

This appendix presents a summary of the basic mass transport properties in a flowing system of cylindrical geometry. Particular attention is paid to the results for helium gas flows in the pressure range of .04 to .2 torr since previous studies for ion-molecule reaction have been concerned only with pressures above .2 torr. Section A follows the treatment by Ferguson et al.²⁴ whereas Section B is derived from the work of Bolden et al.¹¹⁴ Many of the formulas can be found in Dushman and Lafferty¹²⁵.

A. Properties of the Bulk Flow

The simplest model of gas flow in a tube is the one dimensional model often referred to as "plug flow." From the conservation of mass, the flow velocity is

$$v_o = \frac{Q}{\pi a^2 P} \frac{T}{273} \quad (\text{cm/sec}) \quad (\text{A-1})$$

where Q is the flow rate of gas in torr liters/sec (at 273°K), a is the tube radius in cm, P is the pressure in torr, and T is the temperature on °K. In any realistic model in which the velocity is a function of the radial coordinate, r, Eq. (A-1) remains valid for the average or bulk flow velocity.

The actual flow characteristics depend mainly on the ratio of the mean free path L to the tube radius, L/a , which is called the Knudsen number. For $L/a < .01$ the flow is viscous and for $L/a > 1$ the flow is molecular being dominated by collisions with the walls rather than with other gas atoms. Values of L/a between .01 and 1.0 are considered the transition range. L is given by¹²⁵

$$L = (\sqrt{2} \pi N d^2)^{-1}$$

$$\text{or } L = 8.59 \eta \left(\frac{T}{M}\right)^{\frac{1}{2}} \frac{1}{P} \quad (\text{A-2})$$

where N is the number density, d is the atomic or molecular diameter, η is the viscosity in poise (for helium $\eta = 1.95 \times 10^{-4}$), and M is the molecular weight. At $P = .1$ torr, the mean free path in helium is .147 cm so that for $a = 5$ cm $L/a = .03$ which is nearly viscous flow.

For purely viscous flow the axial velocity at the wall is zero. If the flow is also laminar the radial velocity profile is parabolic given by

$$v(r) = 2V_0 (1 + (r/a)^2) \quad (\text{A-3})$$

which is also known as Poiseuille flow. The distance required to fully develop this profile is given by Dushman¹²⁵ as

$$d = 0.227 aR \quad (\text{A-4})$$

where

$$R = 1.85 \times 10^{-5} \frac{MQ}{a\eta}$$

R is called the Reynolds number . For our system at a pressure of .1 torr, the flow rate is 29 torr liters/sec so that $d = 2.5$ cm.

A small, non-zero velocity always exists at the walls which increases as molecular flow is approached. This is referred to as "slipping" of the gas over the walls of the tube and increases the conductance of the tube. Conductance, F , is defined as the ratio of the flow rate to the pressure difference over some length of tube. There is no adequate analytic description of the flow in the transition range so we rely on the empirical relation formulated by Knudsen for the conductance of a long tube of length ℓ

$$F = F_V + Z F_m , \quad (A-5)$$

where $F_V = \frac{\pi a^4 P_a}{8\eta \ell} = \text{viscous conductance},$

$$F_m = 30.48 \times \frac{a^3}{\ell} \left(\frac{T}{M}\right)^{1/2} = \text{molecular conductance},$$

Z is a pressure dependent number between .81 and 1.0 that is tabulated by Dushman and Lafferty¹²⁵, and P_a is the average pressure in the tube. From these definitions the pressure drop per unit length is

$$\frac{\Delta P}{\Delta Z} = \frac{Q}{\Delta Z F} = \frac{Q}{\frac{\pi a^4 P_a}{8\eta} + 30.48 a^3 \left(\frac{T}{M}\right)^{1/2} Z} . \quad (A-6)$$

Because the pressure is a function of distance along the tube, the average velocity becomes $V_o(z)$. To obtain the

radial dependence of the flow velocity, it is assumed that the contributions from slip and viscous flow act independently and are weighted according to their respective conductances; therefore

$$v(r, z) = v_o(z) \left[\frac{2F_v}{F} \left(1 - \frac{r^2}{a^2} \right) + z \frac{F_m}{F} \right] \quad (A-7)$$

In Table A1 we compare the measured pressure drop over 100 cm to that calculated from (A-6). The percent of slip flow is also given as calculated from (A-7) and from the formula used by Bolden et al.¹¹⁴

B. Diffusion and Reaction in a Flowing System

If an unstable species that is destroyed by wall collisions such as electrons or helium metastables is introduced into the flow tube, a characteristic radial distribution will be established that determines the rate of diffusion to the walls which in turn determines the axial dependence of the distribution. In this section we summarize the effects of a parabolic velocity profile, including corrections for slip flow and the axial pressure gradient, on the characteristic diffusion mode.

In a stationary gas or one that is transported down a tube at a radially uniform velocity (i.e. planar flow) the distribution of any specie that is subject only to diffusion losses can be determined analytically. The solution is²⁴

$$N(r, z) = N_0 J_0\left(\frac{\lambda r}{a}\right) \exp\left(-\frac{\lambda^2 D z}{a^2 V_0}\right) \quad (\text{A-8})$$

where N_0 is the density at $r = z = 0$, J_0 is the zero order Bessel function, λ is the first or fundamental root of J_0 and D is the diffusion coefficient for the particular specie. We have neglected all higher diffusion modes which correspond to the higher roots of J_0 since these decay much more rapidly than the fundamental mode. In the case of a parabolic velocity profile, the solution, which is found numerically, has nearly the same form but with different values of λ designated by γ

$$N(r, z) = N R(r) \exp\left(-\frac{\gamma^2 (DP) z}{a^2 PV_0}\right) \quad (\text{A-9})$$

where $R(r)$ is the radial distribution which is evaluated below. In Table A2 we list the values of λ^2 and γ^2 for the first five diffusion modes which were calculated by Ferguson et al.²⁴ The characteristic decay constants, γ^2 , for parabolic flow are smaller than the corresponding λ^2 's because the density of the diffusing specie is highest at $r = 0$ where they are transported down the tube at a velocity twice the average.

We will now discuss the effects of an axial pressure gradient and slip flow on diffusion. In the exponential term of Eq. (A-9) the explicit dependence of the diffusion coefficient on the pressures is shown, i.e. $(DP) = \text{const.}$

From Eq. (A-1) the product Pv_0 depends only on the flow rate Q . Therefore the exponential rate of decay down the tube characterized by the "decay length" $d = a^2 v_0 P / \gamma^2 (DP)$ is independent of any pressure gradient. This is strictly true as long as the pressure drop is not large enough to substantially increase the amount of slip flow. As the pressure in the tube is reduced and slip flow becomes important, the radial velocity profile approaches planar flow so that the density distribution $R(r)$ approaches $J_0(\frac{\lambda r}{a})$ and the attenuation constants γ^2 approach λ^2 . To calculate $R(r)$ and γ^2 is a function of pressure we have used the method of Bolden et al.¹¹⁴ and in the following paragraphs we have used their notation.

The flow velocity is given by

$$v(r, z) = w \bar{v}(z) \left(b - \left(\frac{r}{a} \right)^2 \right) \quad (A-10)$$

where

$$b = 1 + \frac{2s}{a}$$

$$w = \frac{2}{1 + 4s/a}$$

$$s = 1.38 L_1 / P$$

where s is a slip parameter derived empirically, L_1 is the mean free path at 1 torr, P is the pressure in torr, and $\bar{v}(z)$ is velocity at a point z averaged over the tube's cross section. The average velocity over the whole tube will be designated by \bar{v}_{av} such that $P_{av} \bar{v}_{av} = P(z) \bar{v}(z)$.

If Eq. (A-10) is put in the same form as (A-7), it becomes

$$v(r, z) = \bar{v} \frac{P_{av}}{P(z)} \left(\frac{2(1 - (\frac{r}{a})^2) + 4s/a}{1 + 4s/a} \right) \quad (A-11)$$

so that the fraction of slip flow is given by $(4s/a)(1+4s/a)^{-1}$. In Table A1 we have compared the percent of slip flow from this expression to that given by the molecular conductance. They agree to within 25%.

If $N(r, z)$ is the density of a species subject to diffusion and a bilinear reaction with a reactant gas injected into the flow at a rate of Q atom/sec then the $N(r, z)$ is determined by

$$\frac{\partial [v(r, z)N(r, z)]}{\partial z} = -D \nabla^2 N(r, z) - \frac{kQN(r, z)}{\pi a^2 \bar{v}(z)^2} \quad (A-12)$$

A solution for $N(r, z)$ is obtained with the assumption that $\bar{v}(z)^2$ in the reaction term can be replaced by \bar{v}_{av}^2 and that the $\partial^2/\partial z^2$ term of the Laplacian can be neglected, i.e. axial diffusion is ignored. However the solution by Bolden et al. does include the full effects of an axial pressure gradient and slip flow. Their result is

$$N(r, z) = N_0 R(r) \frac{\bar{v}(0)}{\bar{v}(z)} \exp\left(-\frac{\Delta D P(z) z}{a^2 P_{av} \bar{v}_{av}} - \frac{\Gamma k Q z}{\pi a^2 \bar{v}_{av}^2}\right) \quad (A-13)$$

where $R(r) \approx \alpha(1 - (\frac{r}{a})^2) + \beta(1 - (\frac{r}{a})^2)^2$, $\alpha + \beta = 1$ and N_0 is the density at $r = z = 0$, Δ is the pressure dependent diffusion attenuation constant corresponding to λ^2 or

γ^2 in the planar or parabolic limits, and Γ is the correction factor corresponding to $1/\alpha$ that appears in Eq. (30) in Part III.

Before treating the pressure dependence of Δ , we will simply point out the results of Bolden et al. for $\alpha = 1/\Gamma$. In the pure viscous limit $\alpha = 1.59$; for pressures between 1.0 and .2 torr α decreases from 1.59 to 1.53. However Howard et al.¹¹¹ point out that the effects of axial diffusion which is ignored in the above treatment tend to cancel the effect of slip flow so that α remains near 1.59. We have not attempted to evaluate these effects for the lower pressures of .1 torr at which the present experiment is conducted but within our systematic error of $\pm 25\%$ for the results of Part III, the assumption that $\alpha = 1.6$ appears justified.

In the absence of any reaction, it is easy to calculate the attenuation coefficient Δ at pressure below .2 torr which was the lower limit of Bolden et al. Again slip flow but not axial diffusion is included. Therefore these results for Δ are upper limits since axial diffusion will tend to propagate atoms down the tube faster and thus decrease wall collisions.

In the case of no reaction losses Δ is defined as K_0^2/w for the fundamental diffusion mode. K_0^2 is obtained by the solution of

$$\alpha[2 + K_o^2(.1 - .25b)] + 4 - K_o^2(.75b - .15) = 0$$

and $\alpha K_o^2(.05 - .15b) + 4 - K_o^2(.6b - .10) = 0$

where α and b are defined in Eq. (A-10). The results for Δ and α are shown in Table A3. Also given are the measured decay lengths for the He 2^3S metastables and the calculated decay length based on the attenuation constants λ^2 , γ^2 , and Δ . It can be seen that the effects of slip flow are still small at pressures as low as .08 torr.

Figure A1: Average flow velocity vs flow tube
pressure. Pressure calibrated at
part "B" of Fig. 25.

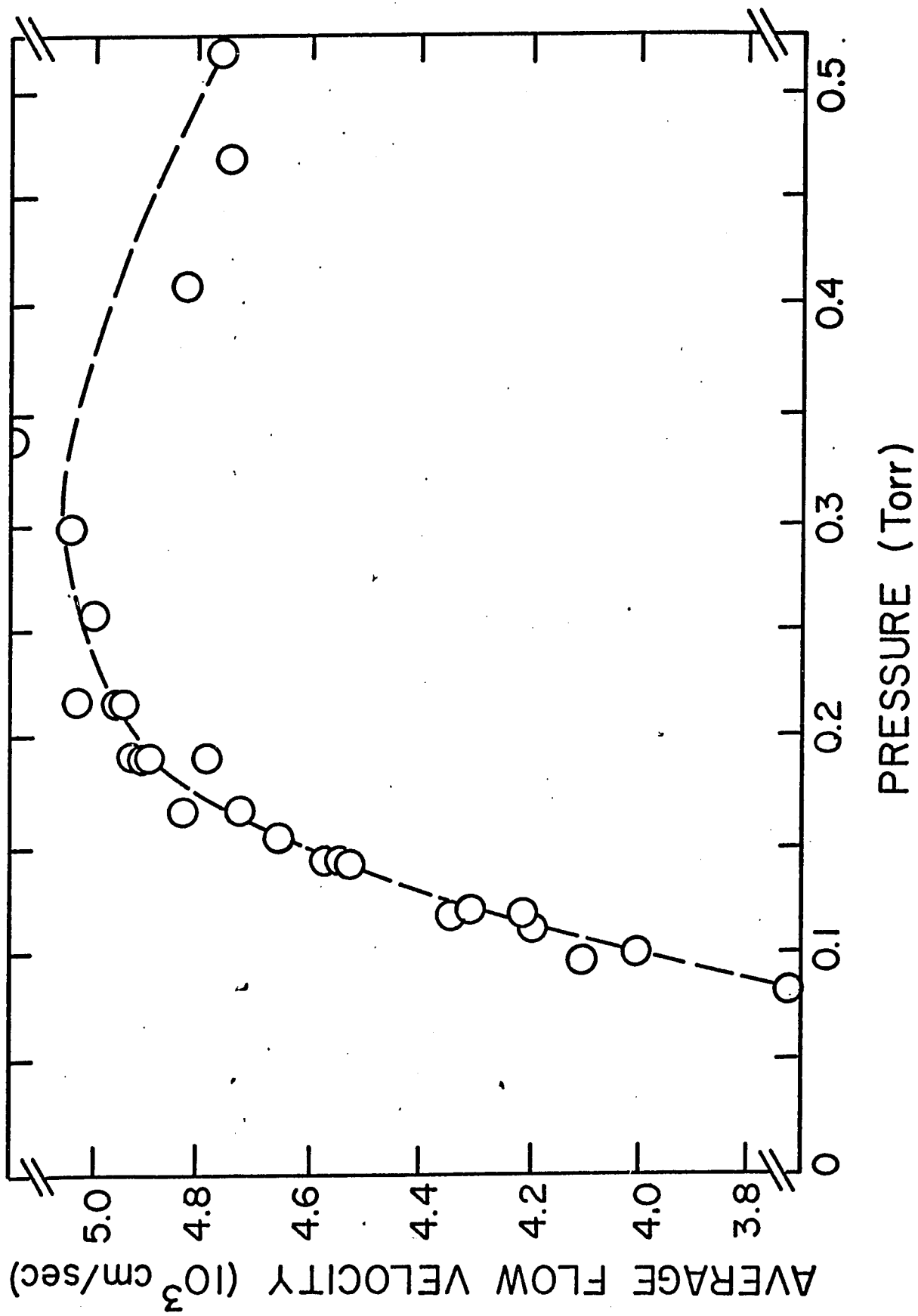


Figure A1

Table A1
Properties of He Gas Flow

Flow Tube Pressure (mtorr)	Flow Rate of Helium (torr $\frac{\text{liters}}{\text{sec}}$)	Pressure Drop per Meter (mtorr/m)		Percent of Slip Flow Calculated from	
		Calculated	Measured	Eq. (A-7)	Eq. (A-11)
60	14	13	20	26.4	21
80	21.2	16	20	21.2	16.7
100	29.2	19	24	17.7	13.8
125	38.2	20	24	14.7	11.3
150	49.0	22	24	12.5	9.6
175	59.0	24	24	10.9	8.4
200	70.	25		9.6	7.4

Table A2
Diffusion Attenuation Constants*

Mode	γ^2	λ^2
	(parabolic flow)	(planar flow)
1	3.66	5.78
2	22.30	30.47
3	56.96	74.89
4	107.59	139.03
5	174.20	222.93

*From Ferguson et al.²⁴

Table A3

Diffusion Decay Lengths

Pressure (torr)	Δ^*	$3 V_0$ (10^3 cm/sec)	α'	Diffusion Decay Lengths for He (2^3 S) \neq $d = \left(\frac{\Delta(DP)}{2} \right)^{-1} \text{ (cm)},$ $a^2 PV_0$			
				Planar Flow	Parabolic Flow with Slip**	Parabolic Flow	Measured
.06	3.98	3.55	.471	1.96	2.8	3.1	
.08	3.91	3.7	.466	2.72	4.05	4.3	4.4 \pm .2
.10	3.87	4.0	.463	3.68	5.5	5.8	5.5 \pm .3
.125	3.83	4.3	.461	4.95	7.5	7.8	6.7 \pm .3
.15	3.81	4.6	.459	6.35	9.65	10.0	8.4 \pm .3
.17	3.78	4.8	.458	7.5	11.5	11.9	9.9 \pm .3
.21	3.71	4.9	.456	9.5	14.6	15.0	14.0 \pm 1.0

* For planar (molecular) flow $\Delta = \lambda^2 = 5.78$

For parabolic (viscous) flow $\Delta = \gamma^2 = 3.66$

\neq α is the radial distribution parameter, defined by Eq. (A-13).

\neq For He(2 S) DP = $470 \pm 25 \text{ cm}^2/\text{sec}^{55}$.

**Calculated from Eq. (A-14).

APPENDIX B

In this appendix we have compiled the results of several authors on the cross sections and branching ratios for the chemiionization by $\text{He}(2^1\text{S}, 2^3\text{S})$ of the various gases studied in the present experiments. It should be noted that effective temperature of the reactions in crossed atomic beam machines can be as high as 600°K . whereas the reactions in our flowing afterglow are at 300°K . Recent unpublished data of Ferguson et al. show that the reaction rate for the $\text{He}(2^3\text{S})$ with many gases is strongly temperature dependent and explains the apparent disagreement between the published cross section from cross beam experiments and flowing afterglow experiments. The branching ratios that describe the distribution of final products of the reaction appear to be much less sensitive to temperature as can be seen in the results for argon. Therefore branching ratios measured by West⁶⁸ at a temperature of 600°K should be approximately correct for the afterglow.

Table B2
Total Chemiionization Cross Sections for He (2^1S)
(10^{-16} cm^2)

Target	Flowing Afterglow	Crossed Beam	
	300°K Schmeltekopf and Fehsenfeld ^a	420 Sholette and Mushlitz ^b	600° Riola <u>et al.</u> ^c
Ar	16.4±30%	7.6±.5	{27±35%*} 23±20% }
Kr	28.2 "	9±2	33.4±20%
Xe	36.4 "	12±3	34.1 "
H ₂	2.3 "	1.7±.5	3.0 "
N ₂	12.5 "	7±1	20.9±25%
O ₂	44.6 "	14±1	42.9 "
NO	32.6 "		37.9 "
CO	23.7 "	7±1	28.7 "
CO ₂	84.6 "		58.6 "
N ₂ O	70.6 "		46.3 "
NH ₃	95.0 "		
CH ₄	26.8 "		32.6 "

* He 2^1S density calibrated by gas cell method.
Remainder done by cross beam method.

a reference 134

b reference 138

c reference 139

Table B3
Branching Ratios for Chemiionization by He(2^3S), (2^1S)

Target Ion	He(2^3S)			He(2^1S)		
	Hotop et al.	Hotop et al.	Muschlitz et al.	West	Hotop et al.	Muschlitz et al.
	90° *	320° *	420°	600°	90° *	320° * 420° 600°
Ar ⁺	.86 ^a	.87 ^a	.87 ^b	.88 ^d	.70 ^a	.83 ^a .91 ^b .96 ^d
ArHe ⁺	.14	.13	.13	.12	.30	.17 .09 .04
Kr ⁺	.81	.86	.88 ^c		.69	.88 .93 ^c
KrHe ⁺	.19	.14	.12		.31	.12 .07
Xe ⁺	.85	.90	>.95 ^c		.93	>.95 ^c
XeHe ⁺	.15	.10	<.05		.07	.02 <.05

* Rundel and Stebbings¹⁰ point out that the actual He* beam temperature is higher due to preferential scattering of slower atoms out of the beam during the excitation process.

a reference 77

b reference 140

c taken from reference 77

d reference 68

Table B4

Branching Ratios for Reactions with He(2^3s), (2^1s)

Target	Ion	He(2^3s)			He(2^1s)		
		Hotop <u>et al.</u>	Muschlitz <u>et al.</u>	West	Hotop <u>et al.</u>	Muschlitz <u>et al.</u>	West
		320°K	420°K	600°K	320°K	420°K	600°K
H ₂	H ₂ ⁺	.88* ^a	.88* ^d	.88 ^j			.85 ^j
	H+H ⁺			.021			.022
	H+HeH ⁺	.10	.10	.081			.10
	HeH ₂ ⁺	.02	.02	.015			.026
N ₂	N ₂ ⁺		(1.00) ^e				
	O ₂ ⁺		.94 ^f	.94	.86 ^f		.75
	O ₂ ⁺ ($0^- + 0^+$) ^k		.06	.06	.14		.25
	O+O*	(observed) ^g					
NO	NO ⁺	1.00* ^b		1.00			1.00
	HeNO ⁺	.0003					
CO	CO ⁺	(~1.0)					
	O+C*	(.04) ^h					
CO ₂	CO ₂ ⁺	.73 ^c		.69	.70 ^c		.68
	O+CO ⁺	.065		.045	.11		.09
	CO+O ⁺	.20		.27	.19		.23

Table B4
(continued)

Target	Ion	Hotop <u>et al.</u> 320°K	Muschlitz <u>et al.</u> 420°K	West 600°K	Hotop <u>et al.</u> 320°K	Muschlitz <u>et al.</u> 420°K	West 600°K
N ₂ O	N ₂ O ⁺			.47			.31
	O+NO ⁺			.51			.61
	NO+O ⁺			.024			.07
CH ₄	HeO ⁺						
	CH ₄ ⁺	.49 ^c	.47 ⁱ		.34 ^c	.38 ⁱ	
	CH ₃ ⁺	.46	.49		.59	.57	
	CH ₂ ⁺	.05	.04		.07	.05	

* mixed beam of He(2³s) and (2¹s)

a reference 141

b reference 142

c reference 77

d reference 143

e dissociative ionization energetically disallowed

f reference 140

g reference 144

h reference 80

i reference 145

j reference 68

k Bush et al. show that pair production of 0⁺+0⁻ accounts for all 0⁺ observed and that the cross section for production by He(2¹s) is 3.3 times that for He(2³s).

APPENDIX C

MEASUREMENT OF He 2^3S AND 2^1S DENSITY BY ABSORPTION
OF 1.08 μ AND 2.06 μ RESONANCE RADIATION

Accurate calculation of the net absorption of resonant radiation from a real light source is not easy due to at least four experimental uncertainties: 1) the width of the emission and absorption lines, 2) the relative intensity of several separate lines, 3) the effect of broad emission lines that overlap more than one absorption line, and 4) frequency shifts between the emission and absorption lines. We first summarize the treatment of Mitchell and Zemansky¹²⁷ for the absorption of a simple (single), unshifted resonance line assuming gaussian line shapes for emission and absorption lines with different widths. The presence of two well resolved components in (2^3S-2^3P) transition is easily incorporated into this formalism. Inclusion of effects 3 and 4 mentioned above was accomplished by numerical methods for the (2^3S-2^3P) transition by Byerly¹²⁸. We then review the available data on the pertinent line widths, relative intensities, and frequency shifts and present the results for several values of these parameters. Finally other experimental evidence is examined to check the consistency of the above calculations.

A. Theory: Absorption of a Simple Resonance Line

As described in detail by Mitchell and Zemansky¹²⁷ the intensity of light, $I(\nu, \ell)$, of frequency ν that is transmitted a distance ℓ through an absorbing medium is given by

$$I(\nu, \ell) = I(\nu, 0) \exp(-k(\nu) \ell) \quad (C-1)$$

where $I(\nu, 0)$ is the incident light intensity and $k(\nu)$ is the absorption coefficient. Assuming the incident light is distributed over a range of frequencies, then the net fractional absorption is defined as

$$\begin{aligned} A(\ell) &= \frac{\int [I(\nu, 0) - I(\nu, \ell)] d\nu}{\int I(\nu, 0) d\nu} \\ &= \frac{\int I(\nu, 0) (1 - \exp(-k(\nu) \ell)) d\nu}{\int I(\nu, 0) d\nu} \end{aligned} \quad (C-2)$$

The above expression is true in general. Its evaluation requires a knowledge of $I(\nu, 0)$ and $k(\nu)$. For the resonant absorption of light from a lower level (1) to an upper level (2) of an ensemble of atoms, the integral of the absorption coefficient is given by

$$\int k(\nu) d\nu = \frac{\lambda_o^2}{8\pi} \frac{g_2}{g_1} \frac{N_1}{\tau} \left(1 - \frac{g_1}{g_2} \frac{N_2}{N_1} \right) \quad (C-3)$$

where

λ_0 = the wave length of the line center

g_2, g_1 = statistical weight of the upper and lower states

N_2, N_1 = number density of atoms in the upper and lower states

τ = lifetime of the upper state against decay to the lower state.

Equation (C-3) is independent of whatever physical processes are responsible for the formation of the absorption line and therefore the right hand side of Eq. (C-3) is independent of the line shape. If the population of the upper state is due only to the absorption itself, then for conventional light sources the ratio N_2/N_1 is very small and is therefore neglected hereafter. If we assume a gaussian line shape of width $\Delta\nu_a$ (fwhm) for the absorbing atoms then

$$k(\nu) = k_0 e^{-\omega^2} \quad (C-4)$$

$$\text{where} \quad \omega = \frac{2(\nu - \nu_0)\sqrt{\ln 2}}{\Delta\nu_a}, \quad (C-5)$$

and ν_0 is the frequency of the line center. k_0 is evaluated by substituting Eq. (C-4) into (C-3) neglecting the N_2 term. The result is

$$\begin{aligned}
 k_o &= \frac{2}{\Delta v_a} \sqrt{\frac{\ell n^2}{\pi}} \frac{\lambda_o^2}{8\pi} \frac{g_2}{g_1} \frac{N}{\tau} \\
 &= .0374 \frac{\lambda_o^2}{\Delta v_a} \frac{g_2}{g_1} \frac{N}{\tau}
 \end{aligned}
 \tag{C-6}$$

where N is written for N_1 .

Finally if we assume the incident light is a single, unshifted emission line of gaussian shape with a width Δv_e then

$$I(v, o) = I_o e^{-\left(\frac{w}{\alpha}\right)^2} \tag{C-7}$$

where $\alpha = \Delta v_e / \Delta v_a$

I_o = absolute intensity at $v = v_o$

$A(\ell)$ can now be evaluated by substitution of (C-4) and (C-7) into (C-2) so that

$$\begin{aligned}
 A_\alpha &= \frac{\int_{-\infty}^{\infty} e^{-(w/\alpha)^2} \left(1 - e^{-k_o \ell e^{-w^2}}\right) dw}{\int_{-\infty}^{\infty} e^{-(w/\alpha)^2} dw} \\
 &= \frac{k_o \ell}{\sqrt{1+\alpha^2}} - \frac{(k_o \ell)^2}{2! \sqrt{1+2\alpha^2}} + \dots + (-1)^n \frac{(k_o \ell)^n}{n! \sqrt{1+n\alpha^2}}
 \end{aligned}
 \tag{C-8}$$

This integral is evaluated by Mitchell and Zemansky in their Appendix IV and their table is reproduced here in

Table C1. For any given value of α and $k_0 \ell$, the corresponding number density and fractional absorption can be calculated.

Note: In the above derivation we implied that N was a constant over the path length ℓ . For species such as the 2^3S and 2^1S metastables in the flow tube where this is not the case, a simple derivation shows that the absorption depends only on the average value of N , \bar{N} , over the path ℓ independent of the spacial distribution (as long as density of the upper state can be ignored). If N is a function of position x then $k(\nu)$ is also and can be written from (C-4) and (C-6) as

$$k(\nu, x) = c N(x) e^{-w}{}^2 \quad (C-9)$$

where c is a constant. Then the differential form of (C-1) is

$$\frac{dI(\nu, x)}{dx} = - I(\nu, x) c N(x) e^{-w}{}^2 \quad (C-10)$$

Therefore the light transmitted to $x = \ell$ is given by

$$\begin{aligned} I(\nu, \ell) &= I(\nu, 0) \exp\left(-c e^{-w} \int_0^{\ell} N(x) dx\right) \\ &= I(\nu, 0) \exp(-k(\nu, \bar{N}) \ell) \end{aligned} \quad (C-11)$$

where $\bar{N}l \equiv \int_0^l N(x)dx$ and the dependence of k on N is shown explicitly. This is the same form as (C-1) and does not change the calculation of A_α .

B. Numerical Methods: Absorption by Several Resonance Lines

The 2.06μ ($2^1S_0 - 2^1P_1$) line in He^4 is an example of a simple line having no fine or hyperfine structure. If we assume there is no frequency shift between the intense emission line from a high pressure lamp (10 torr) and the weak absorption line in the He afterglow (0.1 torr), then from the above formulas the fractional absorption for the singlet (s) line, A_s , can be applied directly. However for the 1.08μ ($2^3S_1 - 2^3P_{0,1,2}$) line, there are three fine structure components, denoted by D_0 , D_1 , D_2 respectively. As shown in the absorption spectrum by Fred et al.¹²⁹ (Fig. C1), the D_1 and D_2 lines are not resolved since the separation of their centers is $.079 \text{ cm}^{-1}$ which is on the same order as the doppler width at 300°K . Hence to a first approximation these two lines can be treated as a single line, denoted by D_3 , which is well separated from the D_0 line.

Method 1

If we approximate the 2^3S-2^3P transition as consisting of 2 separate lines, D_0 and D_3 , with no relative frequency shift between the emission and absorption spectra, then the fraction absorption of each line is computed separately according to (C-8) and the net absorption is given by

$$A_T = \frac{I_0 A_0 (\Delta\nu_{a0}, \alpha_0) + I_3 A_3 (\Delta\nu_{a3}, \alpha_3)}{I_0 + I_3} \quad (C-12)$$

where A_T = net fractional absorption for the triplet (T) line

A_0, A_3 = fractional absorption for the D_0 and D_3 components

I_0, I_3 = intensity of the D_0 and D_3 components.

The dependence of A_0 and A_3 on the absorption line width, $\Delta\nu_a$, and the ratio of emission to absorption width, α , have been shown explicitly because these parameters are not necessarily the same for both D_0 and D_3 components. The ratio of statistical weights for the D_0 line is $g_2/g_1 = 1/3$ and for the D_3 line it is the sum of the ratios for the D_1 and D_2 lines, $\frac{g_2}{g_1} = \frac{8}{3}$.

Method 2

The inclusion of pressure induced frequency shifts into the calculation of absorption was done by Byerly¹²⁸

for the 2^3S-2^3P transition. Since the widths of the emission lines are 3 or 4 times the absorption widths (see below) the D_1 and D_2 components are treated as a single emission line, D_3 , but as 2 separate absorption lines. For convenience the frequencies of absorption lines, D_0 , D_1 , and D_2 are assumed to be shifted by amounts S_0 , S_1 and S_2 relative to the center of their respective emission lines, ν_0 and ν_3 . This is accomplished by redefining the absorption coefficients so that (C-4), (C-5), and (C-6) become

$$k_0(\nu) = k_0 e^{-z_0^2} \quad (C-13)$$

$$z_0 = \frac{2(\nu - \nu_0 - S_0)\sqrt{\ln 2}}{\Delta\nu_a}$$

$$k_0 = \frac{2}{\Delta\nu_a} \sqrt{\frac{\ln 2}{\pi}} \frac{\lambda_0^2}{8\pi} \frac{N}{\tau} \left(\frac{g_2}{g_1}\right)_0$$

and

$$k_3(\nu) = k_1 e^{-z_1^2} + k_2 e^{-z_2^2} \quad (C-14)$$

$$z_1 = \frac{2(\nu - \nu_3 - S_1)\sqrt{\ln 2}}{\Delta\nu_a}$$

$$z_2 = \frac{2(\nu - \nu_3 - S_2)\sqrt{\ln 2}}{\Delta\nu_a}$$

$$\begin{Bmatrix} k_1 \\ k_2 \end{Bmatrix} = \frac{2}{\Delta\nu_a} \sqrt{\frac{\ln 2}{\pi}} \frac{\lambda_0^2}{8\pi} \frac{N}{\tau} \begin{Bmatrix} (g_2/g_1)_1 \\ (g_2/g_1)_2 \end{Bmatrix}$$

The fractional absorption for each emission line is computed separately by numerical integration of (C-2) and the net absorption is then given by (C-12). For the case of $S_0 = S_1 = S_2 = 0$ this method is identical to method 1. In his calculations, Byerly assumed the same $\Delta\nu_a$ and α for both D_0 and D_3 lines.

C. Data on Line Widths, Frequency Shifts, and Relative Intensity

Neither the absorption nor the emission line widths have been measured in our experiment, but approximate values can be estimated from other data. The absorption line width $\Delta\nu_a$ in a weak discharge has been measured by others^{129,130} to be nearly equal to the Doppler width $\Delta\nu_D$ and this is certainly true in the late afterglow. The Doppler width (fwhm) is given by¹²⁷

$$\Delta\nu_D = \frac{2\nu}{c} \sqrt{\frac{2\ln 2RT}{M}} = 7.16 \times 10^{-7} \nu \sqrt{T/M} \text{ (sec}^{-1}\text{)}$$

where R is the gas constant, c is the speed of light, T is the gas temperature in $^{\circ}\text{K}$, and M is the molecular weight. At 300°K , for the 1.08μ line, $\Delta\nu_D = .057 \text{ cm}^{-1}$ and for the 2.06μ line, $\Delta\nu_D = .030 \text{ cm}^{-1}$. Whenever the D_1 and D_2 lines are treated as one line, the effective

$\Delta\nu_a$ for this line may be twice as large as $\Delta\nu_D$ since the separation of the two lines is $.079 \text{ cm}^{-1}$ ¹²⁹. This perhaps explains the spectral data of Scheerer¹³¹ that shows the fractional absorption of the D_3 line is roughly 4 times that for the D_0 line. In the thin absorber limit from (C-8) $A \propto g_2(g_1 \Delta\nu_a \sqrt{1+\alpha^2})^{-1}$. If both $\Delta\nu_a$ and α were the same for both lines, then the absorption rate of the D_3 line should be 8 times that of the D_0 line based on their statistical weights.

The emission widths, $\Delta\nu_e$, are more difficult to estimate. Greenhow¹³⁰ measured $\Delta\nu_e \sim .2 \text{ cm}^{-1}$ for the 1.08μ line from his lamp while Fred et al.¹²⁹ obtained widths "severalfold" as large as the Doppler width for a variety of He lines. A rough estimate of $\alpha = \Delta\nu_e/\Delta\nu_a$ in the present experiment was obtained by measuring the fractional absorption vs pressure in a weak rf discharge lit in the afterglow tube. The absorption for both 1μ and 2μ light increased linearly with pressure up to 30% absorption at .100 torr. For pressures from .10 to .40 torr the increase in absorption was much smaller. This indicates $\alpha \approx 3$ or 4.

Estimates of the size of frequency shifts are also sketchy. From the data of Fred et al.¹²⁹, Byerly defined

the values of S for the unshifted absorption lines relative to emission lines as $S_0 = S_1 = 0$, $S_2 = -.075 \text{ cm}^{-1}$. (This value of S_2 is not due to a pressure shift but simply defines the D_2 line relative to the D_1 line.) From Table I of Fred et al. pressure shifts for several singlet and triplet lines were $\sim -.1 \text{ cm}^{-1}$ for $p = 10$ torr but the 1.08 and 2.06 μ lines were not observed. Spectral data of Schearer¹³¹ indicate a shift of the D_0 line of $-.07 \text{ cm}^{-1}$ for an absorber at .4 torr and a lamp at 4 torr. We can only conclude that frequency shifts on the order of two Doppler widths may be present.

The spectral data of Schearer¹³¹ indicate the relative intensity of the D_0 to D_3 lines is $I_0/I_3 = 1/2$. Colegrove found $I_0/I_3 = 1/2$ to $1/3$. Since most of the absorption is due to the D_3 line (4/5 based on Schearer's data, 8/9 based on statistical weights) the uncertainty in the ratio I_0/I_3 does not appreciably effect the net absorption.

D. Results

In order to evaluate the effects of the parameters $\Delta\nu_a$, α , I_0/I_3 , and $S_{0,1,2}$ that enter into the absorption calculation, we have computed, in the thin absorber limit,

the percent absorption per unit atom density, A/N , where the unit of density is 10^9 cm^{-3} . The absorption for the 2.06μ (2^1S-2^1P) line is denoted by A_S , and for the 1.08μ (2^3S-2^3P) line by A_T . According to method 1, the absorption of each simple line in the thin absorber limit is given by the first term of the expansion in (C-8) such that

$$A = \frac{k_o \ell}{\sqrt{1+\alpha^2}} = \frac{\lambda_o^2}{4\pi} \sqrt{\frac{\ell n 2}{\pi}} \frac{N \ell}{\tau} \frac{g_2}{g_1} \frac{1}{\sqrt{1+\alpha^2} \Delta \nu_a}$$

$$\text{Therefore} \quad \left(\frac{A}{N}\right)_S = \frac{10.3}{\sqrt{1+\alpha^2}} \left(\frac{\% \text{ Absorption}}{10^9 \text{ } 2^1S \text{ atoms}} \right) \quad (\text{C-15})$$

$$\begin{aligned} \text{where} \quad \lambda_o &= 2.058 \times 10^{-4} \text{ cm} \\ \tau &= 5.1 \times 10^{-7} \text{ sec} \\ \Delta \nu_D &= \Delta \nu_a = .90 \times 10^9 \text{ Hz} = .030 \text{ cm}^{-1} \\ g_2/g_1 &= 3 \\ \ell &= 10 \text{ cm.} \end{aligned}$$

and

$$\left(\frac{A}{N}\right)_T = \frac{I_o \left(\frac{A_o}{N}\right) + I_3 \left(\frac{A_3}{N}\right)}{I_o + I_3} \left(\frac{\% \text{ Absorption}}{10^9 \text{ } 2^3S \text{ atoms}} \right) \quad (\text{C-16})$$

$$\left(\frac{A}{N}\right)_T = \frac{.1392}{I_o + I_3} \left[I_o \left(\frac{1}{\Delta \nu_a \sqrt{1+\alpha^2}} \frac{g_2}{g_1} \right)_o + I_3 \left(\frac{1}{\Delta \nu_a \sqrt{1+\alpha^2}} \frac{g_2}{g_1} \right)_3 \right]$$

$$\begin{aligned} \text{where} \quad \lambda_o &= 1.083 \times 10^{-4} \text{ cm} \\ \tau &= 1.05 \times 10^{-7} \text{ sec} \end{aligned}$$

$$\Delta\nu_D = 1.72 \times 10^9 \text{ Hz} = .0575 \text{ cm}^{-1}$$

$$l = 10 \text{ cm}$$

The calculations by method 2 that include frequency shifts were originally computed for $l = 4.8$ and $\Delta\nu_a = .067 \text{ cm}^{-1}$. These calculations have not been redone but the results have been scaled for the new values of l and $\Delta\nu_a$ according to (C-16). This correction is exact in the thin absorber limit for the dependence on l . For non-zero shifts, the correction for $\Delta\nu_a$ is not exact but the error should be very small if the shifts are stated in units of $\Delta\nu_a$. The results for methods 1 and 2 are given in Table C2. The values of $(A/N)_T$ range from .5 to 1.7 over the expected range of the four parameters. This indicates the experimental uncertainty in the absolute metastable densities determined by absorption measurements.

The ratio of the singlet to triplet absorption probabilities, $\left(\frac{A}{N}\right)_S \left(\frac{A}{N}\right)_T^{-1}$, is probably better known than the absolute values of A/N . Two reasonable assumptions are: 1) The effects of frequency shifts on the absorption probability are nearly the same for both lines. (Recall that Fred et al.¹²⁹ found nearly equal shifts for several singlet and triplet lines.) 2) The ratio α is the same for both lines. It was noted above that the percent

absorption of both the 1.08 μ and 2.06 μ lines indicated saturation at 30% in an active discharge. Given these two assumptions, the singlet to triplet ratio depends mainly on the assumed absorption width for the D_3 line and to a lesser extent on the D_0 to D_3 intensity ratio, I_0/I_3 . In the lower part of Table C2 the ratio $\left(\frac{A}{N}\right)_S \left(\frac{A}{N}\right)_T^{-1}$ is given for $(\Delta\nu_a)_3 = .1 \text{ cm}^{-1}$ and $.057 \text{ cm}^{-1}$ assuming $\alpha = 3$ and no frequency shifts. We conclude that the true ratio is between 2 and 4. This is consistent with the result that in an active discharge the measured absorptions A_s and A_t are nearly equal. If the electron temperature in the discharge is much larger than that corresponding to the 0.8 eV energy difference between the 2^1S and 2^3S states, then the population of these states is expected to be proportional to their statistical weights, or $N_t = 3N_s$. Hence if $A_s = A_t$, then $\left(\frac{A}{N}\right)_S \left(\frac{A}{N}\right)_T^{-1} = 3$.

In Fig. C2 we have plotted the densities N_S and N_T as a function of percent absorption of the 2.06 μ and 1.08 μ lines respectively. These curves were calculated by method 1 assuming $\alpha = 3$ for both lines, and $I_0/I_3 = 1/2$ for the 1.08 μ line. The curves labelled 1 and 2 were used to calculate the 2^1S and 2^3S densities in the body of this thesis. Thus we have assumed $\left(\frac{A}{N}\right)_S \cdot \left(\frac{A}{N}\right)_T^{-1} = 2.24$

in the thin absorber limit. It should be noted that if the above methods are used to calculate the absorption probability in an active discharge, some consideration must be given to increasing to absorption line width above the Doppler width for very intense discharges.

Figure C1: Absorption profile of $2^3\text{S}-2^3\text{P}$ transition from Fred et al.

Figure C2: $\text{He}(2^3\text{S})$ and $\text{He}(2^1\text{S})$ density vs percent absorption of $1.08\ \mu$ and $2.06\ \mu$ resonant radiation respectively. Curve 1 is $\text{He}(2^1\text{S})$ density for $\alpha = 3$. Curve 2 is $\text{He}(2^3\text{S})$ density for $\alpha = 3$, $I_0/I_3 = .5$ and $(\Delta\nu_a)_0 = (\Delta\nu_a)_3 = .057$. Curve 3 is same as curve 2 except $(\Delta\nu_a)_0 = .057$, $(\Delta\nu_a)_3 = .10$. All curves calculated by method 1. In the thin absorber limit
 $N_S = 3.07 \times 10^8 A_S$; curve 2,
 $N_T = 6.85 \times 10^8 A_T$; curve 3,
 $N_T = 1.16 \times 10^9 A_T$.

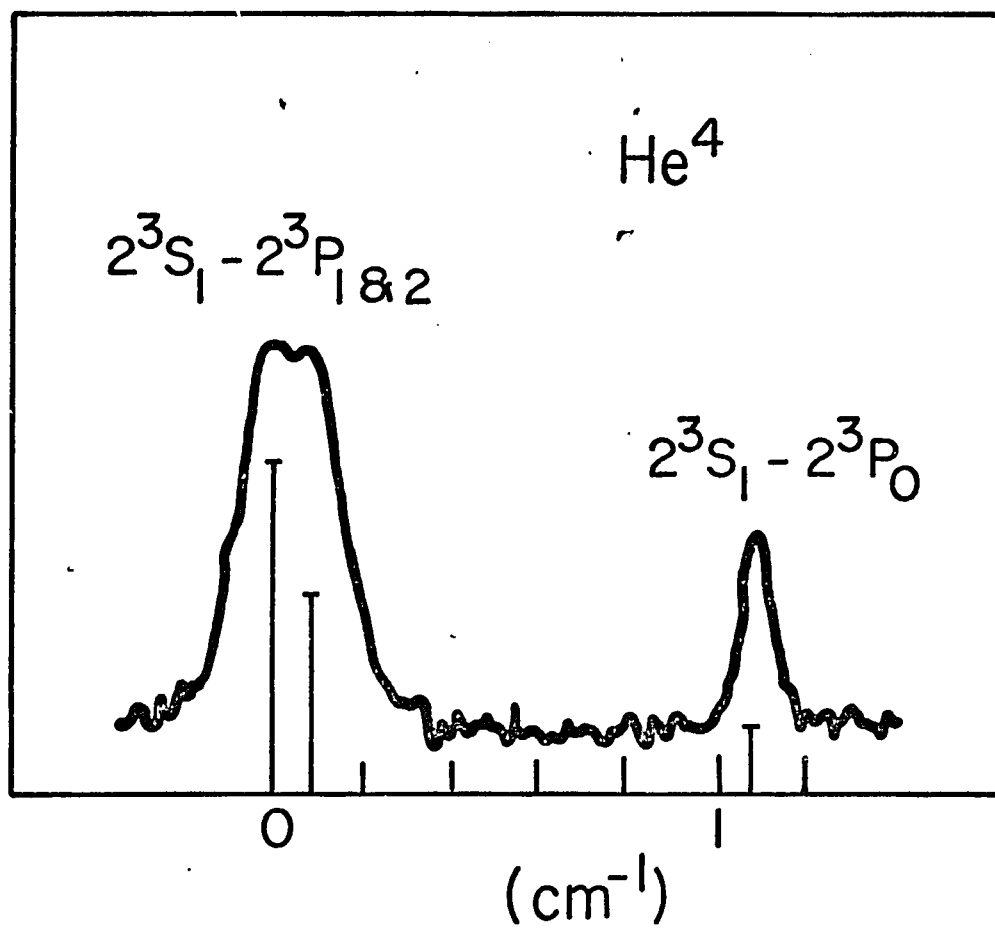
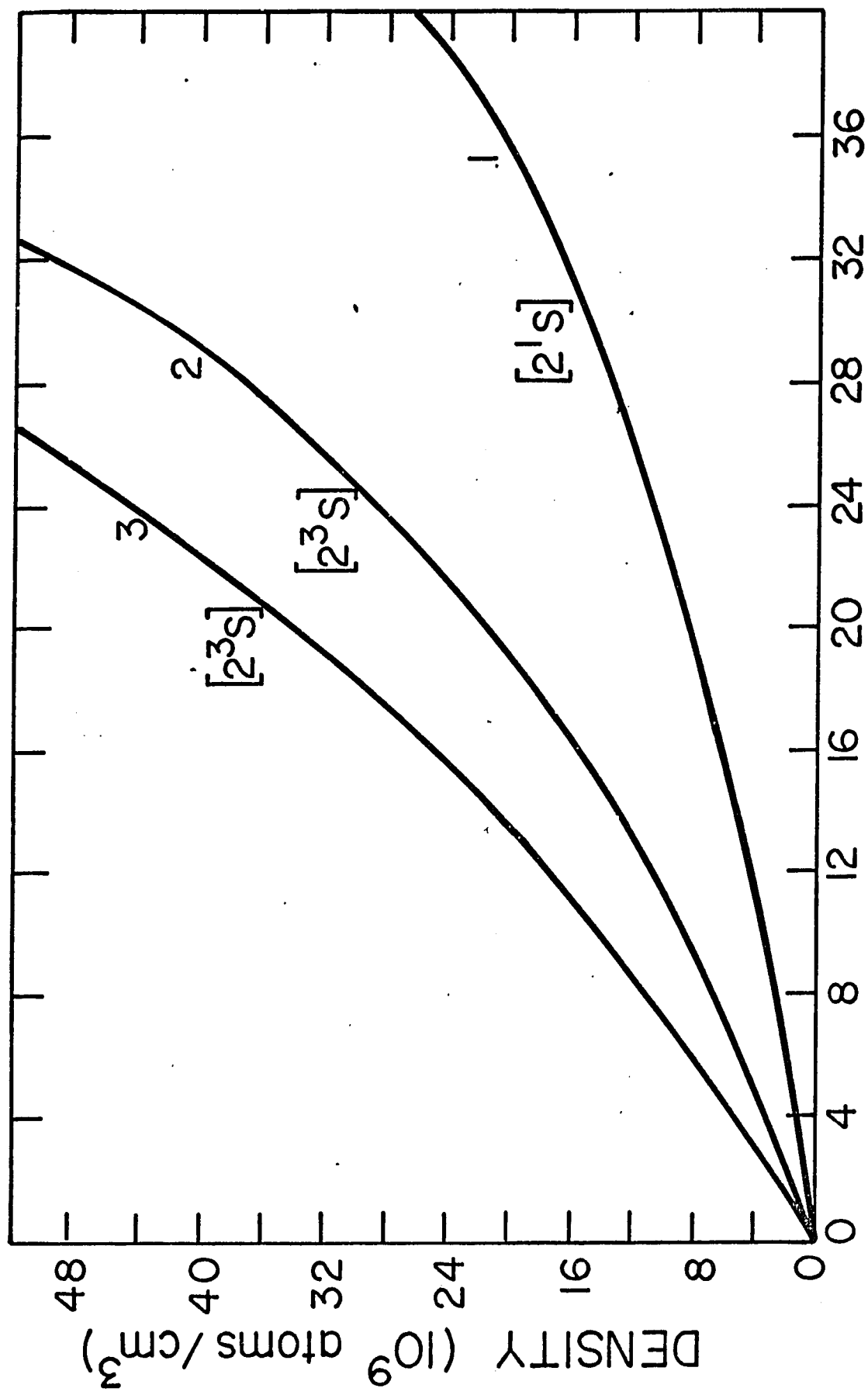


FIGURE C1



% ABSORPTION

FIGURE C2

Table C1
The Absorption A_{α}^*

$\frac{\Delta v_e}{\Delta v_a} =$	0	.5	1.0	1.5	2.0	2.5	3.0	3.5	4.0	4.5	5.0	5.5
$k_O \ell$												
.25	.221	.200	.160	.126	.102	.085	.072	.063	.056	.050	.045	.041
.50	.393	.359	.291	.231	.187	.156	.133	.116	.102	.091	.083	.075
1.0	.632	.587	.486	.390	.318	.266	.227	.198	.175	.157	.142	.128
1.5	.777	.733	.619	.502	.412	.345	.245	.257	.228	.204	.185	.169
2.0	.865	.826	.711	.582	.480	.403	.346	.302	.267	.240	.217	.198
2.5	.918	.886	.774	.641	.531	.447	.384	.335	.297	.266	.241	.220
3.0	.950	.925	.820	.684	.570	.481	.414	.361	.321	.288	.261	.238
3.5	.970	.950	.853	.718	.600	.508	.437	.382	.339	.304	.276	.252
4.0	.982	.966	.878	.744	.624	.529	.456	.400	.355	.318	.289	.264
4.5	.989	.977	.896	.765	.644	.547	.472	.414	.367	.330	.299	.273
5.0	.993	.984	.910	.762	.660	.562	.486	.426	.378	.340	.308	.282
6.0	.998	.992	.930	.807	.686	.586	.507	.445	.396	.356	.323	.295
7.0	.999	.996	.943	.826	.705	.604	.524	.460	.410	.368	.334	.306

* A_{α} was calculated according to the power series expansion of Eq. (C-8).

TABLE C2

Percent Absorption Per Unit Metastable Density: $\frac{A}{N}^*$

Absorption of 1.08 μ Light by He(2 ³ S)									
$(\Delta\nu)_O$ (cm ⁻¹)	$(\Delta\nu)_a$ (cm ⁻¹)	$\alpha_O = \alpha_3$	S_O	S_1	S_2	$\frac{A_O}{N}$	$\frac{A_3}{N}$	$I_O/I_3 = .5$	$(\frac{A}{N})_T$
(unit = $\Delta\nu_a$)									
(Method 1)									
.057	.10	3	0	0	0	.26	1.17	.86	.94
↓	↓	4	↓	↓	↓	.20	.90	.66	.72
↓	↓	5	↓	↓	↓	.16	.72	.53	.58
.057	.057	3	↓	↓	↓	.26	2.06	1.46	1.61
↓	↓	4	↓	↓	↓	.20	1.58	1.12	1.23
↓	↓	5	↓	↓	↓	.16	1.28	.91	1.00
(Method 2)									
.057	.057	2	0	0	-1.18	.36	1.96	1.42	1.57
↓	↓	3	↓	↓	↓	.25	1.67	1.20	1.33
↓	↓	4	↓	↓	↓	.19	1.40	1.00	1.10
↓	↓	5	↓	↓	↓	.16	1.18	.84	.94
↓	↓	3	-1	-1	-2.18	.19	.94	.69	.75
↓	↓	↓	0	0	0	.25	2.08	1.46	1.63
↓	↓	↓	-.5	-.5	-.5	.24	1.95	1.37	1.52
↓	↓	↓	-1	-1	-1	.19	1.57	1.11	1.22
↓	↓	↓	-1.5	-1.5	-1.5	.13	1.11	.79	.88
↓	↓	↓	-2	-2	-2	.078	.68	.48	.54
↓	↓	↓	↓	↓	↓	↓	↓	↓	↓

* Unit Metastable Density = 10⁹ cm⁻³

APPENDIX D

PROPERTIES OF THE OPTICAL SIGNAL

The 1.08 μ pumping light actually consists of three fine structure components from the transition $2^3S-2^3P_{0,1,2}$ which are labelled respectively D_0 , D_1 , and D_2 . The P_1 and P_2 transitions however are not resolved in either emission or absorption. The precise intensity of these lines in the pumping radiation relative to their corresponding absorption lines is not well known as described in Appendix C; therefore the parameters K and L are introduced so that the intensities of pumping radiation exciting D_0 , D_1 and D_2 transitions are in the ratio K:L:1.

The optical signal that is observed is actually the sum of the signals from each of the three pumping transition so that

$$\frac{\Delta I}{I_0} = \sum_{j=0}^2 \frac{\Delta I^{(j)}}{I_0} = \sum_{j=0}^2 (I^{(j)} - I_0^{(j)}) / I_0$$

where $I^{(j)}$ and $I_0^{(j)}$ represent the total light absorbed by the D_j component in the pumped and unpumped conditions, respectively, and $I_0 = \sum_j I_0^{(j)}$. It was shown by McCusker et al.² that

$$\frac{\Delta I^{(0)}}{I_0} = \frac{9K}{5+3L+K} \left(\frac{N_-}{3} - \frac{1}{9} \right)$$

$$\frac{\Delta I^{(1)}}{I_0} = \frac{9L}{5+3L+K} \left(\frac{N_0 + N_-}{2} - \frac{1}{3} \right)$$

$$\frac{\Delta I^{(2)}}{I_0} = \frac{9}{5+3L+K} \left(N_+ + \frac{N_0}{2} + \frac{N_-}{6} - \frac{5}{9} \right)$$

$$\frac{\Delta I}{I_0} = \frac{9}{5+3L+K} \left(\frac{N_0}{2} (L-1) + \frac{N_-}{6} (3L+2K-5) \right)$$

where N_+ , N_0 , and N_- are the relative populations of the 2^3S sublevels in the optically pumped condition such that $N_+ + N_0 + N_- = 1$. Note that $\Delta I/I_0$ cannot uniquely determine both the N_0 and N_- . This relation must be obtained by the optical pumping model referred to above. It can be shown the pumping with right circularly polarized light always decreases the populations N_0 and N_- below their values of $\frac{1}{3}$ in the unpumped condition. Therefore the signals $\Delta I^{(0)}/I_0$ and $\Delta I^{(1)}/I_0$ can be seen to be always less than zero and $\Delta I^{(2)}/I_0$ is always greater than zero. Since the value of L is near 1 and K near .4, the total signal that is actually observed is then the small difference between large quantities and is very sensitive to the values of K and L .

This sensitivity to K and L has two important results. First, since the D_0 , D_1 and D_2 lines are absorbed at different rates through the sample, changing the relative values of K and L, the signal changes polarity from negative to positive as the percent of absorption is decreased. This was first observed by Scheerer⁹. (It should be noted that the label on his figures 4 and 5 is in error and should read $\Delta I = \bar{I} - I$ since he defined I as the transmitted light instead of the light absorbed as done here.) The position of the inversion is not precise but generally occurs between 10 and 20% absorption. Therefore it cannot be determined whether the increase in the optical signal with decreasing 2^3S density as shown in Fig. 5a is due simply to this dependence on percent absorption or actually represents an increase in the 2^3S polarization. Second, due to the uncertainty in our knowledge of K and L even in the thin absorber limit, the values of the predicted 2^3S polarization based on $\Delta I/I_0$ vary so widely that they are not very useful. In Fig. 5b the 2^3S polarization is calculated for the simple model of the optical signal which assumes an optically thin sample, i.e. K and L independent of position. The measured electron polarizations from the chemiionization of N_2 are also given as a function of the measured optical signal. It was argued in Section VI that these measured electron polarizations are nearly equal to the 2^3S polarization. The data points do not even follow the same linear dependence

indicating that the thin absorber approximation is not valid for absorption as low as 3%.

We note here that the expression given by McCusker et al.² for $\Delta I/I_0$ in their Eq. (16) is actually the expression for $\Delta I^{(0)}/I_0$ which is not sensitive to K and L. The resulting polarizations predicted by their expression for $\Delta I^{(0)}/I_0$ are likewise not sensitive to K and L. This approximation was apparently made because their values of the measured optical signal were negative and spectral data of Scheerer⁸ show that except for very thin absorbers the total signal $\Delta I/I_0$ is almost entirely due to $\Delta I^{(0)}/I_0$. However the validity of using a thin absorber approximation to derive $\Delta I^{(0)}/I_0$ is questionable. It can also be shown that the value of L for a true thin absorber must be less than 1.2 to produce large positive values of $\Delta I/I_0$ contrary to the effective value of $L = 1.3 \pm .2$ assumed for the thick absorber condition studied by McCusker et al.

It can be seen from Eq. (10) above that $\Delta I^{(0)}/I_0$ depends only on K, L, and N_- . An even simpler expression results if I_0 is replaced by $I_0^{(0)}$ namely $\Delta I^{(0)}/I_0^{(0)} = 3N_- - 1$. Therefore if the D_0 line, which is separated from the D_1 and D_2 lines by 1 \AA , can be isolated by a monochromator so that only $\Delta I^{(0)}/I_0^{(0)}$ is measured, then the relative population of the $m_s = -1$ level is determined directly and is independent of all the approximations made in the usual optical pumping model. If the intensity of this D_0 beam is

small enough so as only to probe the 2^3S sublevels without doing any pumping itself, then reversing its polarization to left circularly polarized light will measure $(3N_+-1)$. Therefore the 2^3S sublevel populations and polarization are uniquely defined.

Needless to say this is a difficult measurement. On the other hand Scheerer's method of measuring the polarization of radiation emitted by excited ions produced in a chemiionization reaction is a simple but not absolute method of monitoring the 2^3S polarization. If the method is "calibrated" by the above absolute measurement of the 2^3S polarization, it could provide a versatile diagnostic technique for investigating spin dependent processes in the afterglow as well as the limitation to the 2^3S polarization discussed below.

REFERENCES

1. J. C. Hill, L. L. Hatfield, N. D. Stockwell, and G. K. Walters, *Phys. Rev. A* 5, 189 (1972).
2. M. V. McCusker, L. L. Hatfield, and G. K. Walters, *Phys. Rev. A* 5, 177 (1972).
3. M. V. McCusker, L. L. Hatfield, and G. K. Walters, *Phys. Rev. Letters* 22, 817 (1969).
4. M. V. McCusker, Ph.D. Thesis, Rice University, 1969 (unpublished).
5. L. D. Schearer, *Atomic Physics*, Ed. P.G.H. Sandars (Plenum Press, London, 1970) p. 87.
6. L. D. Schearer and L. A. Riseberg, *Phys. Rev. Letters* 26, 599 (1971).
7. N. D. Stockwell, Ph.D. Thesis, Rice University, 1967 (unpublished).
8. L. D. Schearer, *Phys. Rev.* 160, 76 (1967).
9. L. D. Schearer, *Advances in Quantum Electronics*, ed. J. R. Singer (Columbia Univ. Press, New York, 1961) 239-251.
10. R. D. Rundel and R. E. Stebbings, *Case Studies in Atomic Collision Physics*, Ed. E. W. McDaniel and M.R.C. McDowell (North Holland Publishing Co., Amsterdam, 1972) Vol. 2, Chap. 8.
11. F. W. Lampe, *Ion-Molecule Reactions*, Ed. J. L. Franklin (Plenum Press, New York, 1972), Vol. 2, Chap. 13, p. 601.
12. R. S. Berry, *Molecular Beams and Reaction Kinetics*, Ed. C. H. Schlier (Academic Press, New York, 1970) p.
13. A. Niehaus, *Ber. Bunsenges. Phys. Chem.* 77, 623 (1973).
14. J. S. Cohen and N. F. Lane, *J. Phys. B: Atom. Molec. Phys.* 6, L113 (1973).
15. W. H. Miller, C. A. Slocumb, and H. F. Schaefer, *J. Chem. Phys.* 56, 1347 (1972).
16. W. H. Miller, *J. Chem. Phys.* 59, 3193 (1973).

17. H. Hotop and A. Niehaus, Z. Physik 228, 68 (1969).
18. The probability of a spin flip due to a magnetic dipole interaction during a simple electron-atom scattering can be estimated by $\text{prob} = (\gamma H \tau)^2$ where γ is the electron gyromagnetic ratio, H is the magnetic field at the electron due to the atomic electrons, and τ is the collision time. If H is approximated by the dipole field of one Bohr magneton at a distance of 10^{-8} cm then $H = \mu_B / r^3 \sim 10^4$ gauss. Given $\gamma = 2 \times 10^7$ then $\text{Prob} = (2 \times 10^{11} \tau)^2$. Therefore τ must be $\geq 10^{-12}$ sec for a significant probability of a spin flip whereas the gas kinetic collision time is $\sim a_0 / v \approx 10^{-13}$ sec.
19. L. D. Schearer and L. A. Riseberg, Phys. Letters 33A, 325 (1970).
20. In this and the following reference, the general formalism for this method is worked out. W. F. Parks and L. D. Schearer, Phys. Rev. Letters 29, 531 (1972).
21. G. F. Drukarev, V. D. OB'Edkov, and R. K. Janev, Phys. Letters 42A, 213 (1972).
22. L. D. Schearer and L. A. Riseberg, Phys. Lett. (1971)
23. R. W. Huggins and J. H. Cahn, J. Appl. Phys. 38, 180 (1967).
24. E. E. Ferguson, F. C. Fehsenfeld, and A. L. Schmeltekopf, Advances in Atomic and Molecular Physics, Ed. D. R. Bates and I. Esterman (Academic Press, New York, 1969) Vol. 5, p. 1.
25. A. L. Farragher, Trans. Faraday Soc. 66, 1411 (1970).
26. H. D. Hagstrum, Phys. Rev. 96, 336 (1954).
27. L. J. Varnerin, Phys. Rev. 91, 859 (1953).
28. D. A. MacLennan, Phys. Rev. 148, 218 (1966).
29. F. B. Dunning and A.C.H. Smith, J. Phys. B: Atom. Molec. Phys. 4, 1696 (1971).
30. T. A. Delchar, D. A. MacLennan, and A. M. Landers, J. Chem. Phys. 50, 1779 (1968).
31. H. D. Hagstrum and C. D'Amico, J. Appl. Phys. 31, 715 (1960).
32. H. D. Hagstrum, Phys. Rev. 104, 1516 (1956).

33. F. M. Propst and E. Luscher, Phys. Rev. 132, 1037 (1963).
34. Y. Takeishi and H. D. Hagstrum, Phys. Rev. 137, A641 (1965).
35. H. D. Hagstrum, J. Appl. Phys. 31, 897 (1960).
36. H. C. Hayden and N. G. Utterback, Phys. Rev. 135, A 1575 (1964).
37. S. N. Ghosh and W. F. Sheridan, J. Chem. Phys. 26, 480 (1957).
38. F. B. Dunning, A.C.H. Smith, and R. F. Stebbings, J. Phys. B: Atom. Molec. Phys. 4, 1683 (1971).
39. R. D. Rundel, F. B. Dunning, J. S. Howard, J. P. Riola, and R. F. Stebbings, Rev. Sci. Instr. 44, 60 (1973).
40. W. Allison, F. B. Dunning, and A.C.H. Smith, J. Phys. B: Atom. Molec. Phys. 5, 1175 (1972).
41. B. L. Donnally, R. Faber, J. Gates, and C. Volk, Bull. Am. Phys. Soc. 18, 141 (1973).
42. F. C. Fehsenfeld, K. M. Evenson, and H. P. Broida, Rev. Sci. Instr. 36, 294 (1965). The cavity used in this experiment is #5 tested by these authors.
43. For a discussion of the generation of off-resonant photons by microwave cavities in flowing systems, see reference 24.
44. J. A. Simpson and L. Marton, Rev. Sci. Instr. 32, 802 (1961).
45. J. Kessler and H. Lindner, Z. f. angew. Physik 18, 7 (1964).
46. N. F. Mott, Proc. Roy. Soc. (London) A124, 425 (1929).
47. H. A. Tolhoek, Rev. Mod. Phys. 28, 277 (1956).
48. G. Holzworth and H. J. Meister, Nucl. Phys. 59, 56 (1964).
49. S. R. Lin, Phys. Rev. 133, A965 (1964).
50. L. Mikaelyan, A. Borovoi, and E. Denisov, Nucl. Phys. 47, 328 (1963).
51. J. Van Klinken, Nucl. Phys. 75, 161 (1966).

52. J. Kessler, private communication.
53. The 2^1S density is further reduced by quenching in the optical pumping region due to absorption of 2.06μ (2^1S-2^1P) photons and subsequent 584 \AA radiation to the ground state. However, at these pressures, most of the 584 \AA photons are trapped, reverting back to the 2^1S state after $\sim 10^3$ absorptions and re-emissions. The net quenching is measured to be $\sim 15\%$.
54. E. C. Beaty and P. L. Patterson, Phys. Rev. 137, A346 (1965).
55. A. V. Phelps, Phys. Rev. 99, 1307 (1955).
56. H. J. Oskam and V. R. Mittelstadt, Phys. Rev. 132, 1435 (1963). They report their results as an "effective" mobility. $u_{\text{eff}} = \frac{7.63}{P} D_a P_0$ where P_0 is the pressure reduced to 273°K . They report an unexplained increase in $D_a P_0$ for pressures below .3 torr. This effect, if present in the afterglow would further increase the loss rate of electrons relative to metastables.
57. The diffusion time in a cylindrical tube with parabolic flow is given by $\tau = a^2 P / (3.66 D P)$ where a is the tube radius, D is the diffusion coefficient and P is the pressure in torr, for $P = .1$ torr, $D P = 460 \text{ cm}^2 \text{ torr/sec}$ $\tau = 1.5 \times 10^{-3}$ sec. The time for an electron to thermalize from 1 ev to .025 ev in helium at $P = .1$ torr $= 4 \times 10^{-4}$ sec assuming the fractional energy loss per collision is $\frac{2m}{M}$ where m and M are the electron and atomic masses and that the mean free path is .61 cm independent of energy.
58. If the rf heating is applied within a few cm of the extractor, a 10% decrease in I_s is observed at all pressures presumably due to heating of electrons in the extractor itself.
59. E. W. McDaniel and E. A. Mason, The Mobility and Diffusion of Ions in Gases (John Wiley, New York, 1973).
60. For a general review of metastable impact on surfaces, see M. Kaminsky, Atomic and Ionic Impact Phenomena on Metal Surfaces (Academic Press, New York, 1965). For rare gas ions on clean surfaces see references 33, 34, 61 and 62. For rare gas ions on dirty surfaces see references 31-37. For other ions including N_2^+ , H_2^+ , O_2^+ and several hydrocarbon ions, see references 32, 33, 37, 63 as well as N. G. Utterback and G. H. Miller, Rev. Sci. Instr. 32, 1101 (1961); J. H. Parker, Jr., Phys. Rev. 93, 1148 (1954).

61. H. D. Hagstrum, Phys. Rev. 96, 325 (1954) and 104, 317 (1956).
62. H. D. Hagstrum, Phys. Rev. 104, 672 (1956).
63. D. W. Vance, Phys. Rev. 164, 372 (1967).
64. R. Byerly, Ph.D. Thesis, Rice University, 1967 (unpublished).
65. L. D. Schearer, Phys. Rev. 166, 30 (1968).
66. J. M. Daniels and R. S. Timsit, Can. J. Phys. 49, 525 (1971) and 49, 545 (1971).
67. This is a common assumption for $\text{He}(2^1\text{S}, 2^3\text{S})$, but not strictly true. For example 10% of He^* destructions by O_2 results in $\text{O}^+ + \text{O}^- + \text{He}$ (Bush et al., J. Chem. Phys. 57, 4501 (1972)) and another $\sim 2\%$ results in $\text{O}^* + \text{O} + \text{He}$ (see reference 75b); $\sim 4\%$ of He^* destructions by CO produce $\text{C}^* + \text{O} + \text{He}$ (see reference 80). Since the production of neutral atoms in their ground state is difficult to detect, significant non-ionizing destruction of He^* may exist of other species. However destruction cross sections and ionization cross section agree fairly well indicating that the major loss of He^* is by ionization.
68. P. West, M.A. Thesis, Rice University, 1974 (unpublished).
69. It is possible for spin-orbit perturbations in elastic scattering to produce a "spin flip" of the scattered electron. Although this is usually a negligible effect for low Z atoms and at low energies, 5 and 10% effects have been observed in the differential scattering of electrons from neon and argon at 40 ev. See K. Schackert, Zeitschrift fur Physik 213, 316 (1968) and J. Mehr, Zeitschrift fur Physik 198, 351 (1967).
70. A. V. Phelps and J. P. Molnar, Phys. Rev. 89, 1202 (1953).
71. H. Hotop and A. Niehaus, Z. Physik 238, 452 (1970).
72. H. Hotop and A. Niehaus. (a) Int. J. Mass Spectrom. Ion Phys. 5, 415 (1970). (b) Chem. Phys. Letters 3, 687 (1969).
73. H. Hotop, Advances in Mass Spectrometry 5, 116 (1971).
74. W. W. Robertson, J. Chem. Phys. 44, 2456 (1966).

75. W. C. Richardson and D. W. Setser. (a) Chem. Phys. Letters 12, 349 (1971). (b) J. Chem. Phys. 58, 1809 (1973).
76. H. Hotop and A. Niehaus, Chem. Phys. Letters 8, 497 (1971).
77. H. Hotop, A. Niehaus, and A. L. Schmeltekopf, Z. Physik 229, 1 (1969).
78. G. M. Begun and L. Landau, J. Chem. Phys. 35, 547 (1961) and 36, 1083 (1962).
79. P. Natalis and J. E. Collin, Inter. J. Mass. Spec. Ion. Phys. 2, 221 (1969).
80. W. B. Hurt and W. C. Grable, J. Chem. Phys. 57, 734 (1972).
81. H. Goldwire, Ph.D. Thesis, Rice University (unpublished).
82. E. W. Weber, H. Ackermann, N. S. Laulainen, and G. zu Putlitz, Bull. Am. Phys. Soc. 19, 164 (1974).
83. H.S.W. Massey and E.H.S. Burhop, Electronic and Ionic Impact Phenomena (Clarendon Press, Oxford, 1969) Vol. I, p. 357.
84. Ibid., Vol. II, Chap. 11.
85. P. S. Farago, Reports Prog. Phys. 34, 1055 (1971).
86. D. Hils, M. V. McCusker, H. Kleinpoppen, and S. J. Smith, Phys. Rev. Letters 29, 398 (1972).
87. R. E. Collins, B. Bederson, and M. Goldstein. (a) Phys. Rev. A 3, 1976 (1971). (b) A. Kasdan, T. M. Miller, and B. Bederson, Proceeding of the Eighth International Conference on the Physics of Electronic and Atomic Collisions, Abstracts of Papers, Beograd, Yugoslavia, 1973, p. 255.
88. K. Rubin, B. Bederson, M. Goldstein, and R. E. Collins, Phys. Rev. 182, 201 (1969).
89. H. Kleinpoppen, Phys. Rev. A 3, 2015 (1971).
90. P. G. Burke and J.F.B. Mitchel, J. Phys. B: Atom. Mol. Phys. 7, 214 (1974).
91. E. Karule, J. Phys. B: Atom. Molec. Phys. 5, 2051 (1972); D. L. Moores and D. W. Norcross, J. Phys. B: Atom. Molec. Phys. 5, 1482 (1972).

92. J. Kessler, Rev. Mod. Phys. 41, 3 (1969).
93. W. Franzen and R. Gupta, Phys. Rev. Letters 15, 819 (1965); T. Heindorff, J. Hoffft, and E. Reichert, Proceeding of the Eighth International Conference on the Physics of Electronic and Atomic Collisions, Abstracts of Papers, Beograd, Yugoslavia, 1973, p. 484.
94. P. J. Jennings, Surface Science 26, 509 (1971); P. J. Jennings and B. K. Sim, Surface Science 33, 1 (1972); R. Feder, Phys. Stat. Sol. (b) 49, 699 (1972).
95. P. S. Farago, (a) Advances in Electronics and Electron Physics (Ed. L. Marton, Academic Press, N. Y., 1965) p. 1. (b) W. Raith, Atomic Physics (Plenum Press, 1969) p. 389; Physics of the One- and Two-Electron Atoms Ed. F. Bopp and H. Kleinpoppen (North Holland Amsterdam, 1969) p. 727. (c) J. Kessler, Atomic Physics 3, Ed. S. J. Smith, G. K. Walters, (Plenum Press, N. Y., 1973) p. 523. (d) K. Jost and H. D. Zeman, Stanford HEPL 590, 1971.
96. J. Kessler and J. Lorenz, Phys. Rev. Letters 24, 87 (1970); U. Heinzmann, J. Kessler, and J. Lorenz, Z. Physik 240, 42 (1970).
97. N. Muller, W. Eckstein, W. Heiland, and W. Zinn, Phys. Rev. Letters 29, 1651 (1972).
98. G. Busch, M. Campagna, and H. C. Siegmann, J. Appl. Phys. 41, 1044 (1970), 42, 1781 (1971); G. Busch, M. Campagna, P. Cotti, and H. C. Siegmann, Phys. Rev. Letters 22, 597 (1969); U. Banninger, G. Busch, M. Campagna, and H. C. Siegmann, Phys. Rev. Letters 25, 585 (1970).
99. M. Wilmers, R. Haug, and H. Deichsel, Z. angew Physik 27, 204 (1969); H. D. Zeman, K. Jost, and S. Gilad, Proceedings of the Seventh International Conference on the Physics of Electronic and Atomic Collisions, Abstract of Papers, Amsterdam, 1971 (North Holland, Amsterdam, 1971) p. 1005. See also reference 92.
100. V. W. Hughes, R. L. Long, Jr., M. S. Lubell, M. Posner, and W. Raith, Phys. Rev. A 5, 195 (1972).
101. A. J. Simpson, Methods of Experimental Physics (ed. by L. Marton, V. W. Hughes, and H. Schultz, Academic Press, New York, 1967) Vol. 4A, p. 84.
102. R. L. Gamblin and T. R. Carver, Phys. Rev. 138, A946 (1965).

103. A. Gilardini, Low Energy Electron Collisions in Gases: Swarm and Plasma Methods Applied to Their Study (John Wiley & Sons, New York, 1972).
104. At pressures above .2 torr or extraction voltages above 700 volts arcing occurs between the floating afterglow and the grounded mechanical pump.
105. J. A. Simpson, Rev. Sci. Instr. 32, 1283 (1961).
106. V. Cermak, J. Chem. Phys. 44, 3781 (1966).
107. See reference 83, p. 357.
108. W. Happer, Rev. of Mod. Phys. 44, 169 (1972).
109. B. Bederson, Atomic Physics 3, Ed. by S. J. Smith and G. K. Walters (Plenum Press, New York, 1973) p. 401.
110. H.S.W. Massey and E.H.S. Burhop, loc. cit. p. 522; P. G. Burke and H. M. Schey, Phys. Rev. 126, 163 (1962).
111. C. J. Howard, H. W. Rundel, and F. Kaufman, J. Chem. Phys. 53, 3745 (1970).
112. C. J. Howard, Ph.D. Thesis, University of Pittsburgh, 1971 (unpublished).
113. F. Kaufman, Progr. Reaction Kinetics 1, 12 (1961).
114. R. C. Bolden, R. S. Hemsworth, M. J. Shaw, and N. D. Twiddy, J. Phys. B: Atom. Molec. Phys. 3, 45 (1970).
115. H.M.P. Stock, J. Phys. B: Atom. Molec. Phys. 6, L86 (1973).
116. See reference 103, pp.392 and 433.
117. E. W. McDaniel, V. Cermak, A. Dalgarno, E. E. Ferguson, and L. F. Friedman, Ion-Molecule Reactions (John Wiley & Sons, New York, 1970) p. 321.
118. D. Spence and G. J. Schulz, Phys. Rev. A 3, 1968 (1971).
119. F. Linder and H. Schmidt, Z. Naturforsch, 26a, 1617 (1971).
120. R. D. Hake and A. V. Phelps, Phys. Rev. 158, 70 (1967).
121. A. Herzenberg, J. Chem. Phys. 51, 4942 (1969).
122. J. E. Land and W. Raith, Atomic Physics 3, Ed. S. J. Smith and G. K. Walters (Plenum Press, New York, 1973) p. 553.

123. J. M. Warman, K. M. Bansal, and R. W. Fessenden, Chem. Phys. Letters 12, 211 (1971).
124. Burgess and M. J. Seaton, Mon. Not. R. Astron. Soc. 120, 123 (1960).
125. E. N. Fortson, Bull. Am. Phys. Soc. 19, 544 (1974).
126. S. Dushman and J. M. Lafferty, Scientific Foundations of Vacuum Technique (2nd ed., John Wiley, New York, 1962).
127. A.C.G. Mitchell and M. W. Zemansky, Resonance Radiation and Excited Atoms (University Press, Cambridge, 1971).
128. R. Byerly, private communication.
129. M. Fred, F. S. Tomkins, J. K. Brady, and M. Hamermesh, Phys. Rev. 82, 406 (1951).
130. R. C. Greenhow, Phys. Rev. 136, A660 (1964).
131. L. D. Schearer, private communication.
132. N. F. Lane, private communication. See also A. E. Glassgold, Phys. Rev. 132, 2144 (1953).
133. See reference 12 and E.W.M. Daniel, Collision Phenomena in Ionized Gases (John Wiley & Sons, New York, 1964) p. 610.
134. A. L. Schmeltekopf and F. C. Fehsenfeld, J. Chem. Phys. 53, 3173 (1970).
135. R. C. Bolden, R. S. Hermsworth, M. J. Shaw, and N. D. Twiddy, J. Phys. B: Atom. Molec. Phys. 3, 61 (1970).
136. M. Cher and C. S. Hollingsworth, J. Chem. Phys. 50, 4942 (1969).
137. E. E. Benton, E. E. Ferguson, F. A. Matsen, and W. W. Robertson, Phys. Rev. 128, 206 (1962).
138. W. P. Sholette and E. E. Muschlitz, J. Chem. Phys. 36, 3368 (1962).
139. J. P. Riola, J. S. Howard, R. D. Rundel, and R. F. Stebbings, J. Phys. B: Atom. Molec. Phys. 7, 376 (1974); 6, L109 (1973) and Phys. Rev. Lett. 29, 321 (1972).
140. J. A. Herce, K. D. Foster, and E. E. Muschlitz, Bull. Am. Phys. Soc. 13, 206 (1968).

- 141. H. Hotop and A. Niehaus, Z. Physik 215, 395 (1968).
- 142. H. Hotop, Diplom-Thesis, Albert-Ludwigs Universitat, Freiburg, Germany, 1967 (unpublished).
- 143. J. R. Penton and E. E. Muschlitz, J. Chem. Phys. 49, 5083 (1968).
- 144. W. B. Hurt and W. C. Grable, Bull. Am. Phys. Soc. 15, 219 (1970).
- 145. J. A. Herce, J. R. Penton, R. J. Cross, and E. E. Muschlitz, J. Chem. Phys. 49, 958 (1968).